FACULTEIT GENEESKUNDE
BIOMEDISCHE WETENSCHAPPEN

Skeletspier weefsel engineering: *in vivo* evaluatie van een prevascularisatie strategie en verkennen van nieuwe synthetische draagstructuren

Skeletal muscle tissue engineering: *in vivo* evaluation of a prevascularization strategy and exploration of novel synthetic scaffolds

Masterproef voorgedragen tot het behalen van de graad van Master in de biomedische wetenschappen door

Lisanne Terrie

Promotor: Prof. Dr. Ir. Lieven Thorrez
Begeleidster: Drs. Dacha Gholobova

Leuven, 2017-2018

KU LEUVEN

FACULTEIT GENEESKUNDE
BIOMEDISCHE WETENSCHAPPEN

FACULTEIT GENEESKUNDE
BIOMEDISCHE WETENSCHAPPEN

Skeletspier weefsel engineering: *in vivo* evaluatie van een prevascularisatie strategie en verkennen van nieuwe synthetische draagstructuren

Skeletal muscle tissue engineering: *in vivo* evaluation of a prevascularization strategy and exploration of novel synthetic scaffolds

Masterproef voorgedragen tot het behalen van de graad van Master in de biomedische wetenschappen door

Lisanne Terrie

Promotor: Prof. Dr. Ir. Lieven Thorrez
Begeleidster: Drs. Dacha Gholobova

Leuven, 2017-2018

1 PREFACE

Terugblikkend op de afgelopen 5 jaar met als spreekwoordelijke kers op de taart mijn thesisjaar, besef ik dat veel mensen een belangrijke rol hebben gespeeld hierin. Een woord van dank is daarom zeker op zijn plaats.

In de eerste plaats wil ik **Prof. dr. ir. Lieven Thorrez** bedanken. Professor, bedankt voor het vertrouwen dat ik van u kreeg het afgelopen jaar. De hiermee gepaard gaande vrijheid heeft mijn leerproces alleen maar versterkt. Bedankt voor uw input en toegankelijkheid, deze waren van onschatbare waarde.

Ook bedankt aan mijn begeleidster **Dacha.** Hoewel het gezien je eigen drukke agenda en vele verantwoordelijkheden niet altijd evident was, stond je toch telkens voor me klaar. Ik waardeerde iedere input dan ook enorm. Jouw positieve ingesteldheid maakte de sfeer in het labo nog aangenamer, waardoor ik steeds met veel plezier naar het labo kwam. Ik wens je dan ook alleen maar het beste toe nu ook jouw werk in het labo bijna kan afgerond worden.

Ook wens ik mijn juryleden, **dr. Maarten Mees** en **dr. Robin Duelen**, te bedanken voor het werpen van hun kritische blik op mijn thesis.

Vervolgens wil ik ook heel wat mensen in de bloemetjes zetten die het voorbije jaar (of de voorbije jaren), elk op hun manier (op de voor- of achtergrond), hun bijdrage hebben geleverd om mij tot dit punt te brengen.

Bedankt **dr**. **Mélanie Gérard en Linda** om steeds mijn onderzoek te ondersteunen door mijn talrijke vragen te beantwoorden en me te voorzien van een klare uitleg. Bedankt **Petra** voor de hulp bij het aanleren van het nemen van mijn talrijke ‘beeldjes’ en hulp bij *troubleshooting*. Verder wil ik ook heel wat van mijn kulak-collega’s bedanken die ik mocht leren kennen het afgelopen jaar. Bedankt **Elise, Faes en Vincent** voor de lunchloopkes, maar vooral bedankt voor jullie raad en het delen van ervaring wanneer ik weer eens aan het twijfelen sloeg. Bedankt **Joke** voor het beantwoorden van mijn vele deurklopkes bedoeld aan Dacha. Bedankt ook voor jouw hulp bij het ontrafelen van nieuwe programma’s of artikels. Bedankt **Sandrine** om jouw kritische blik te werpen op mijn thesis en presentaties, maar vooral bedankt voor je hulpvaardigheid. Bedankt **Stijn** voor het overnemen van kleine taakjes wanneer ik in Leuven zat en bedankt om de laatste maanden mee kleur te geven. Bedankt ook aan **Dr. Eva Dewasch** om me de kneepjes van het hechten aan te leren. Tenslotte, bedankt **Prof. Evie**

Vereecke voor je steunbetuiging tijdens mijn laatste blokperiode en me te laten meevolgen bij biopsies en autopsies.

Vervolgens wil ik ook **Josephine** bedanken. Bedankt om er steeds voor me te zijn. We hebben nog veel koffiepauzes te goed, maar de paar die we hadden boden de nodige stimulans om te blijven gaan.

Tenslotte wil ik mijn dankwoord richten aan een aantal mensen in mijn dichte omgeving. Lieve **papa en Malika**, bedankt voor de kansen die jullie me gegeven hebben. Natuurlijk zou ik hier nu niet staan zonder jullie. Jullie hebben me gemaakt tot wie ik ben, een doorzetter. Bedankt surrogaatmama en zus **Delphine**, jij moet wel mijn grootste fan zijn. Jouw onvoorwaardelijke steun en luisterend oor hebben me door heel wat zware momenten gesleurd. Bedankt ook **Mathieu**: Bedankt voor je luisterend oor en je steunende woorden wanneer je 'ukkietje' weer eens begon te twijfelen. Bedankt aan **Gaby,** een heel grote bijdrage is weggelegd voor jou. Je moet zowat de enige persoon zijn die me echt kan oppeppen wanneer ik het niet meer zie zitten. Waar een wil is, is een weg, maar als ik de weg even kwijt ben breng jij me steeds terug op pad. Bedankt ook aan **Anita en Riquet**: vaak onbewust hebben jullie sterk bijgedragen aan deze verwezenlijking. De verwachtingen waren hoog en de lat lager leggen was geen optie, maar bedankt om me te pushen zodat ik het maximale uit mijn studies zou halen. Een extra woord van dank voor jullie steun tijdens mijn blokperiode en kotperiode mogen ook niet ontbreken, dus bedankt voor de goede zorgen en het ondersteunen op alle mogelijke manieren. Vervolgens ook bedankt aan **Carmen**: bedankt voor je oprechte interesse en het brengen van rust wanneer mijn doemdenken de bovenhand nam. Je voelsprieten stonden altijd op actief waardoor ieder sluimerend dipje gauw de kop werd ingedrukt met een '*yes you can'* berichtje.

En als laatste maar belangrijkste persoon, wiens bijdrage zich op alle vlakken liet gelden: mijn vriend **Riquet.** Belangeloos stond je telkens voor me klaar, geklaag mocht je telkens weer aanhoren. Je geloofde echter als geen ander in mijn kunnen en wist dat ik ondanks beklag me toch telkens volop zou inzetten. Mijn studies namen merendeel van de tijd in, maar nooit heb je me hierin geremd. Jouw onvoorwaardelijke steun vertaalde zich op onnoemelijk veel vlakken, maar je grootste bijdrage bij het bereiken van dit punt is de kalmte die je telkens tot me bracht.

Bedankt allemaal! Jullie geloofden meer in me dan ik vaak zelf deed en woorden schieten te kort om mijn dank hiervoor te betuigen.

2 TABLE OF CONTENTS

3 LIST OF ABBREVIATIONS

2D	2-Dimensional
3D	3-Dimensional
ADSCs	Adipose-derived stem cells
ANOVA	Analysis of variance
BAM	Bio-artificial muscle
BM-MSCs	Bone marrow-derived mesenchymal stem cells
BSA	Bovine serum albumin
DAPI	4',6-diamidino-2-phenylindole
DMEM	Dulbecco's modified Eagle's medium
DPBS	Dulbecco's phoshate-buffered saline
ECM	Extracellular matrix
EGM	Endothelial growth medium
ESCs	Embryonic stem cells
FBS	Foetal bovine serum
GFP	Green fluorescent protein
HBSS	Hank's balanced salt solution
HUVEC	Human umbilical vein derived endothelial cell
IGF	Insulin-like growth factor
iPSCs	Induced pluripotent stem cells
SkGM	Skeletal muscle growth medium
MRF4	Myogenic regulatory factor 4
MSC	Mesenchymal stem cell
MV	Microvascular
Myf5	Myogenic factor 5
MyoD1	Myogenic differentation 1
NOD/SCID	Non-obese diabetic severe combined immunodeficiency
NS	Not significant
Nu/Nu	*Foxn1nu*
P/S	Penicillin/Streptomycin
Pax7	Paired box 7
PBS	Phosphate buffer saline
PCL	Polycaprolactone
PDO	Polydiaxanone
PFA	Paraformaldehyde
PGA	Poly(glycolic acid)
PGS	Poly(glycerol sebacate)
PGSC	Poly(glycerol sebacate citrate)
PLA	Poly(lactic acid)
PLGA	Poly(lactic-co-glycolic acid)
PSC	Pluripotent stem cell
PXS	Poly(xylitol sebacate)
PXSC	Poly(xylitol sebacate citrate)
RFP	Red fluorescent protein
RT	Room temperature

SkFM	Skeletal muscle fusion medium
SkMVEC	Skeletal muscle microvascular endothelial cell
SMTE	Skeletal muscle tissue engineering
TA	Tranexamic acid
UC-MSC	Umbilical cord mesenchymal stem cell
UEA-I	Ulex europaeus agglutinine-I
VEGF	Vascular endothelial growth factor
W/V	Weight/volume

4 ABSTRACT

Tissue-engineered bio-artificial muscles (BAMs) resemble skeletal muscle because they contain parallel, fused myofibers. However, they still differ from real skeletal muscle in several aspects, which limits applications. In this thesis, we explored ways to address some of the current limitations. First, a limitation due to the lack of perfusion is the size of the BAMs. Prior to this thesis, an approach to generate endothelial networks in the BAMs had been developed, based on 3D co-culture of human muscle and endothelial (HUVEC) cells. In this thesis, we investigated the behaviour of these networks *in vivo*. BAMs were implanted for 2 weeks in mice and rats from several strains. In immunodeficient mice, we demonstrated connection of the BAM endothelial networks with host vessels. However, no human myofibers were retrieved, indicating a need for further maturation of the BAM *in vitro*. In parallel, we explored the use of skeletal muscle microvascular endothelial cells. Improved myofiber formation was observed compared to the previous HUVEC co-culture. We also further evaluated culture media which best supported differentiation of both myofibers and HUVECs and found a medium which improved both myofibers and endothelial networks. Second, we explored two classes of synthetic biomaterials as scaffolds to support cell fusion and formation of long muscle fibers. Differentiation of human myoblasts on a polycarbonate biomaterial decreased in the proximity of the scaffold due to impaired cell survival. In contrast, human myoblasts were biocompatible with poly(glycerol sebacate) and differentiated well to myofibers on this scaffold.

5 INTRODUCTION

5.1 TISSUE ENGINEERING

Tissue engineering is a rapidly growing scientific field which aims at creating biological tissue *in vitro* (1). The field was introduced in the late 1980s and requires synergistic insights from medicine, material sciences and engineering (1). It is an interdisciplinary field which aids in deeper fundamental understanding of mammalian tissue function and structure both in normal and pathological conditions.

The loss or failure of an organ or tissue is a main problem in human healthcare. The lack of suitable transplant organs is also an important cause of death; 20 people die each day waiting for a transplant **(Figure 1)** (1–3). Tissue engineering organs therefore seems a promising path to explore. To develop, repair or even replace tissues and organs *in vitro*, a combination of cells, biomaterials and/or biologically active molecules is required. In addition, after implantation the engineered tissues must have functionality and the ability to become integrated into the body. To obtain biomimetic tissues, the principles that occur during embryonic development are used as a blueprint. Therefore, collaborations between developmental biologists, clinicians and engineers are essential to further advance the field.

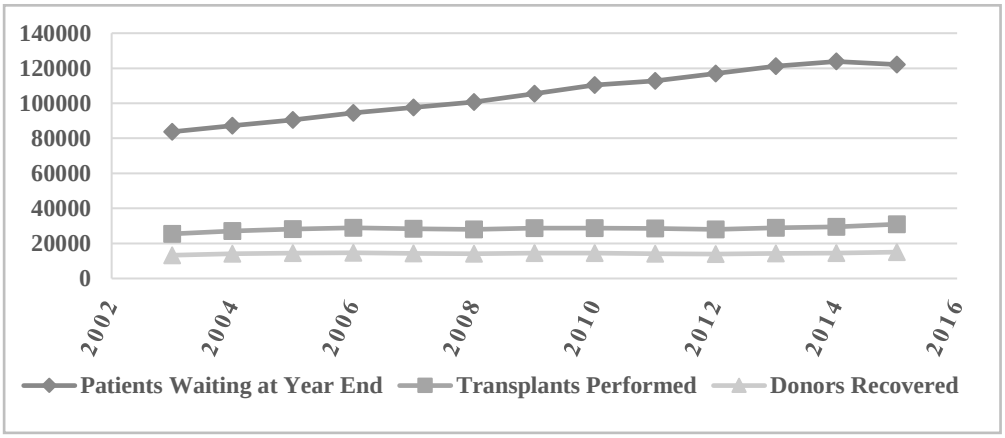

Figure 1 *The organ shortage continues (figure adapted from* (3)*).*

Currently, there are several hurdles impeding clinical applications of tissue engineering. These include (i) the identification of an appropriate matrix material, (ii) the vascularization of engineered tissue and (iii) the transfer from laboratory-scale to clinical-scale production (1).

5.2 SKELETAL MUSCLE TISSUE ENGINEERING

5.2.1 Skeletal muscle

Skeletal muscle comprises 30% of the human body and is of high clinical importance due to its role in metabolism and movement (4). Skeletal muscle is surrounded by a strong and thick sheath of connective tissue, called the epimysium and is composed of muscle bundles (5). Muscle bundles are surrounded by a layer of connective tissue called the perimysium and in turn are composed of muscle fibers (myofibers) **(Figure 2)**. Muscle fibers have a cylindrical shape with a diameter of 10-100 µm and can reach a length of several centimetres (6). They are wrapped in a thin connective tissue layer of collagen and reticular fibers, the endomysium (7).

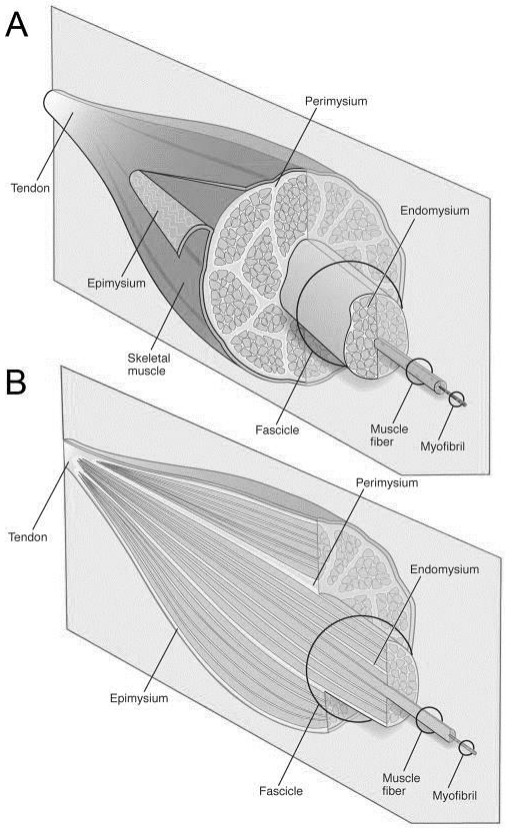

***Figure 2**. Structure of skeletal muscle (figure taken from (7)).*

The contractile unit of the myofibers is composed of myofibrils arranged in sarcomeres and located in the sarcoplasm. Each myofibril is composed of thick and thin filaments, myosin and actin respectively, which results in striations which are characteristic of skeletal muscle (**Figure 3**). Furthermore, the sarcoplasm contains the T-tubule which is crucial for the excitation-contraction coupling as it conducts the electrical signals.

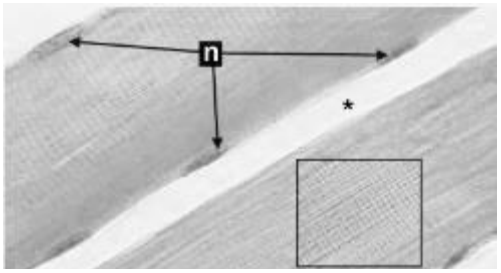

***Figure 3**. High magnification image of native histology of striated skeletal muscle with n referring to muscle cell nuclei and * indicating the endomysium (image taken from (12)).*

Until the middle of the 19th century, it was believed that muscles did not regenerate. Nowadays, the regenerative capacity of skeletal muscle is known and divided into five interrelated and time-dependent phases: degeneration (necrosis), inflammation, regeneration, remodelling, and maturation/functional repair (8). The central role in muscle regeneration is played by the muscle stem cells known as satellite cells.

5.2.1.1 Satellite cells

Adult skeletal muscle contains tissue specific adult stem cells called satellite cells (9) with Paired box 7 (Pax7) as its most widely used molecular marker (10). They are positioned under the basal lamina of myofibers, are at rest in normal conditions and possess myogenic differentiation capacity (11). It is a heterogeneous population of stem and progenitor cells involved in the growth, maintenance and regeneration of skeletal muscle (12). Necrosis of damaged muscle fibers following exercise, injury or disease results in an inflammatory response which eventually gives rise to the phagocytosis of injured myofibers (5). As satellite cells are readily responsive to molecular triggers, these events result in the activation of this normally quiescent population into active myoblasts. These myoblasts are in turn able to fuse with the damaged myofibers or with each other into newly formed myofibers **(Figure 4)**(12).

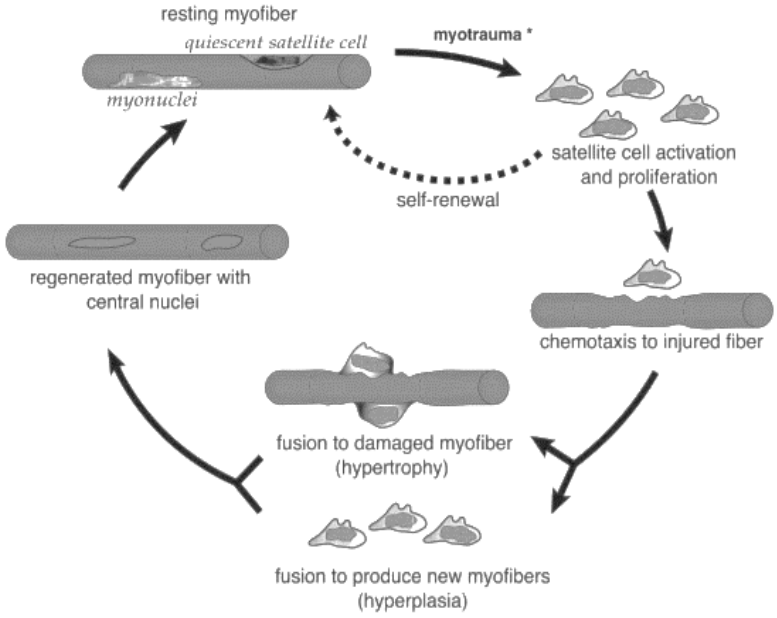

Figure 4*. Satellite cell response to skeletal muscle trauma or injury (myotrauma) (figure taken from* (18)).

Experiments in which damage was induced to muscle showed that genetic ablation of the satellite cells resulted in impaired muscle regeneration (13). Satellite cells recapitulate, to a certain extent, the embryonic skeletal muscle development through analogous mechanisms in response to injury.

The activation of quiescent $Pax7^{+}$ myogenic precursors is a highly orchestrated process with different stimuli being proposed as initiators of satellite cell activation. At the site of injury many growth factors are released and some e.g. hepatocyte growth factor (14) and insulin-like growth factor (IGF)(15) are able to activate satellite cells. Invading inflammatory cells, especially macrophages, are important for the resolution of necrosis but may also support satellite cell survival and induce muscle regeneration (16,17). Next to growth factors, proteins

involved in muscle embryogenesis like Notch, sonic hedgehog, and Wnt may also be involved in satellite cell activation and postnatal muscle regeneration (18,19).

Once they are activated, they start to proliferate and give rise to myoblasts. This commitment to a myoblastic lineage is characterized by the expression of myogenic differentiation 1 (MyoD1) which induces together with myogenic factor 5 (Myf5) the Myogenin expression. This induction phase further coincides with cell cycle exit and commitment to differentiation resulting into elongated myoblasts, called myocytes (20). Post-mitotic myocytes display a shift in gene expression which enables their fusion into multinucleated myotubes characterized by myogenin and myogenic regulatory factor 4 (MRF4) expression. Terminal differentiation of the myotubes post-fusion into muscle fibers results in the abundant expression of genes such as myosin and actin **(Figure 5)**(21).

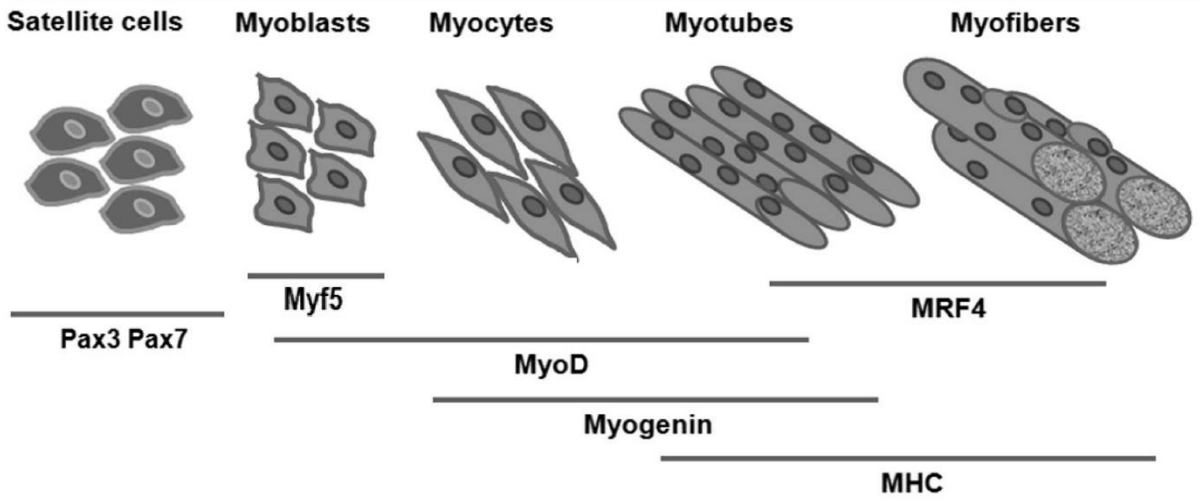

Figure 5*. Stages of myogenesis tightly regulated by a network of transcription factors (figure adapted from (24)).*

The expansion of the satellite cells during this regeneration either results in the replenishment of the satellite cell pool by symmetric expansion or in two distinct cell fates as a result of asymmetric division (22). The latter gives rise to one daughter cell contributing to the regeneration while the other daughter cell remains attached to the basal lamina, where it retains the satellite stem cell identity.

5.3 BIO-ARTIFICIAL MUSCLE

5.3.1 Cell sources

Use of satellite cells for skeletal muscle tissue engineering (SMTE) is a logical choice but satellite cells have significant limitations. Satellite cells can be isolated by single fiber explant culture (23) or enzymatic digestion (24). Both methods have their limitations, respectively low

yield and lower purity (24). Based on the higher yield, enzymatic digestion is the most commonly used isolation method. Purification methods such as fluorescent or magnetic activated cell sorting can be applied after isolation (25), but there is no consensus as to whether pure cell populations are advantageous for tissue engineering. An additional issue is that only limited amounts of skeletal muscle tissue can be biopsied. Therefore, satellite cell expansion *in vitro* is essential for further tissue engineering. Although expansions through 20 doublings are described (26), senescence can occur already at early passages due to karyotype alterations (27). This limited expansion capacity hampers their use for tissue engineering. Because of these issues, alternative stem cell sources are being considered, discussed below.

5.3.1.1 Adipose-Derived Stem Cells (ADSCs)

ADSCs have attracted attention as they are easily and abundantly isolated from lipoaspirate. ADSCs are a class of mesenchymal stem cells (MSC) which can differentiate into mesodermal lineage tissues including cartilage, bone, adipose tissue and skeletal muscle (28). Their abundance and multipotency compared to satellite cells makes them attractive to tissue engineers. Moreover, their lack of major histocompatibility complex (MHC) class II expression might allow the use of ADSCs from allogeneic or xenogeneic donors without immunosuppression (29). Furthermore, ADSCs secrete paracrine factors which have anti-apoptotic or neovascularization properties (30). These features offer significant advantages over satellite cells.

A subpopulation of ADSCs have inherent myogenic potential as they are able to respond to natural myogenic cues (31). ADSC induction to myoblasts remains the critical step for SMTE. Several different methods such as using myogenic media, co-culturing with myoblasts (31), biophysical stimuli (32) or genetical manipulation (33) have been described but lack efficiency. This results in the differentiation to other cell types and a heterogenous population.

5.3.1.2 Bone Marrow-Derived Mesenchymal Stem Cells (BM-MSCs)

BM-MSCs are known to participate in skeletal muscle regeneration (34) and have myogenic potential comparable to ADSCs (35). BM-MSCs were used to treat skeletal muscle injuries by either direct injection (36) or after seeding on a muscle derived extracellular matrix (ECM) (37). However, it was not proven that the transplanted cells differentiated into myofibers suggesting an indirect action of these BM-MSCs (36)(38).

5.3.1.3 Umbilical Cord Mesenchymal Stem Cells (UC-MSCs)

UC-MSCs are derived from the cord-placenta. Their high tolerability in transplantations due to the lack of expression of MHC class I and II antigens makes them a promising alternative source for regenerative medicine (39). UC-MSCs have been studied in the context of muscular dystrophy therapy, but results concerning differentiation into skeletal muscle *in vivo* were contradictory (40,41). Successful myogenic induction by means of myogenic media (42) or MyoD1 transfection (43) indicate that these cells might serve as an alternative source in the future.

5.3.1.4 Pericytes

Pericytes are perivascular stellate cells positioned in the microvascular walls of virtually all vascularized organs, including skeletal muscle (44). They share similar features with MSCs such as mesodermal differentiation potential and expression of markers (e.g. CD90, CD44, CD105 and CD73)(45). Pericytes contribute to myogenesis during postnatal growth and regeneration of skeletal muscle by fusion with developing myofibers and entering the satellite cell compartment (46). *In vitro* differentiation, by using a combination of co-culture techniques and the use of myogenic differentiation medium, indicates a high skeletal myogenic potential (47). Pericytes also contribute to structural recovery after engraftment in dystrophic muscle fibers (47). Based on both the myogenic and vasculogenic differentiation capacity, pericytes are considered as a suitable cell source for investigations in the field of tissue regeneration (48). Finally, they are well accessible since they are present in a variety of tissues. Their accessibility, ease of *in vitro* expansion and ability to differentiate into skeletal muscle cells with high efficiency indicates that these cells are another alternative cell source. However, to date pericytes have not been used in SMTE.

5.3.1.5 Pluripotent stem cells (PSCs)

Pluripotent stem cells could theoretically provide unlimited quantities of any human cell type as they are characterized by endless self-renewal and pluripotency. Pluripotent stem cells include human embryonic stem cells and induced pluripotent stem cells. Embryonic stem cells (ESCs) are derived from the inner cell mass from blastocyst-stage embryos (49). Isolation protocols need further optimization as isolation is inefficient whilst requiring high specialization, training and expertise (50).Despite the potential for regenerative medicine, ESC derivation leads to ethical concerns as isolation requires embryo destruction (51).

The generation of induced pluripotent stem cells (iPSC) was an important impetus for research (52). IPSCs are generated by reprogramming somatic cells to an embryonic stem cell-like state using transcription factor overexpression and/or small molecules. Because autologous tissue can be used for reprogramming cells into different tissues, an immune rejection can be avoided. IPSCs therefore show great potential for cell-based therapy. However, reports on genomic and epigenomic changes resulting from the reprogramming process raise concerns (53), so iPSC technology must be scrutinized before clinical application.

We can conclude that, although alternatives exist for satellite cells as a cell source for muscle tissue engineering, their need for differentiation into myogenic lineages poses an important risk. The differentiation may not be perfect, giving rise to an unwanted heterogenic cell population or even cancerous tissue. To date, this differentiation withholds the widespread application of these cells. Further improvements and understanding of the differentiation protocols are expected to increase the use of alternative cell sources for tissue engineering applications.

5.3.2 Co-cultures

As using only one cell type does not resemble the *in vivo* cell heterotypic communication, attempts have been made to investigate the impact of co-cultures on maturation and functionality of the engineered tissues. One such approach has been to stimulate muscle cell differentiation and myotube maturation by combining skeletal muscle cell lines with fibroblasts (54). This co-culturing resulted in prolonged myotube survival and maturation. These results can be explained by fibroblast secretion of extracellular matrix components and growth factors which contributes to survival and differentiation (55).

Other studies have used co-cultures of skeletal muscle cells and endothelial cells to develop vascularized constructs since the provision of oxygen and nutrients to cells deep within a thick construct remains a major challenge. The formation of capillary-like networks in tissue-engineered constructs before implantation could overcome the limitations of simple diffusion in avascular tissues and is needed for increasing the size of engineered tissue constructs. Pre-vascularization is based on *de novo* blood vessel formation known as vasculogenesis. From a primary network of endothelial cells, new blood vessels arise through vasculogenesis during which endothelial sprouts elongate and fuse to form new vascular loops (56). Vasculogenic processes have been examined through *in vitro* two-dimensional (2D) and three-dimensional (3D) models using endothelial cells from different species and different matrices to obtain self-

assembled vascular networks (57–59). More complex models focus on endothelial-pericyte interactions to develop a layer of supporting pericytes which subsequently secretes basal membrane (60–62). Other efforts focus on perfusion of lumenised vessels through microfluidic devices to further mimic the complex *in vivo* tissue microenvironment (63,64). In the field of SMTE, different approaches are being explored to obtain pre-vascularized constructs. One approach sandwiches blood vessel cells between myoblast sheets to prepare pre-vascularized dense tissue constructs (65). Our lab has developed another approach combining endothelial cells and myoblasts resulting in a co-culture bio-artificial muscle (BAM) which consists of human aligned myofibers with interspersed endothelial networks (66).

Combining the aforementioned cells in a tri-culture (myoblasts, fibroblasts and endothelial cells) mimics the normal *in vivo* muscle composition even more closely. This approach showed more advanced myofiber maturation and morphology together with improved pre-organization of a capillary network, resulting in faster replacement of graft vessels by host vessels after implantation (67). The increase and stabilisation of the capillary network was explained by the observed increase of vascular endothelial growth factor when comparing the tri-culture to myoblast-endothelial co-culture (67).

Co-cultures of neural cells with myoblasts are being developed to study neuromuscular junction formation. In these so-called neuromuscular co-cultures, muscle-induced neuronal differentiation of the cultured primary neurons has been observed as a result of stimulated expression of neuronal acetylcholinesterase via a cyclic adenosine monophosphate dependent signalling pathway (68). Neuromuscular junction development would allow stimulation through nerves and further myofiber maturation. Furthermore, this would serve as a model for the treatment of neuromuscular diseases.

Although co-culturing may aid in getting a step closer to resembling native skeletal muscle tissue, this approach presents additional hurdles. Combining different cell types in one construct is difficult as each cell types has its own optimal culture conditions. Therefore, a trade-off needs to be found between the different cell types in terms of optimal culturing and differentiation conditions.

5.3.3 Tissue engineering of bio-artificial muscle

Relatively small muscle composed of aligned myofibers can already be created by tissue engineering. This engineered skeletal muscle has neonatal characteristics in terms of strength, tissue organization and gene expression (69). In order to create more mature muscle constructs,

scaffold-based approaches are developed next to the scaffold-free approach. Biomaterial scaffolds are made of synthetic or natural materials providing an artificial extracellular matrix (ECM). This attempt to mimic the ECM properties of the skeletal muscle tissue is driven by insights on the key role of the ECM molecules in the proliferation of muscle progenitor cells and subsequent stages of differentiation (69). The ECM can be mimicked in several ways, which are divided in scaffold-free and scaffold-based technologies.

5.3.3.1 Scaffold-free technology

BAMs can be created from self-organizing myofibers resulting in a soft tissue by using a hydrogel, mimicking the ECM. This hydrogel is mixed with cells and cast in molds with attachment posts (70). During cell-gel contraction, passive tension forces myoblasts to align parallel to each other along the length axis of the BAM. Differentiation, induced by switching to a culture medium containing low serum concentrations, results in parallel contractile fibers (71).

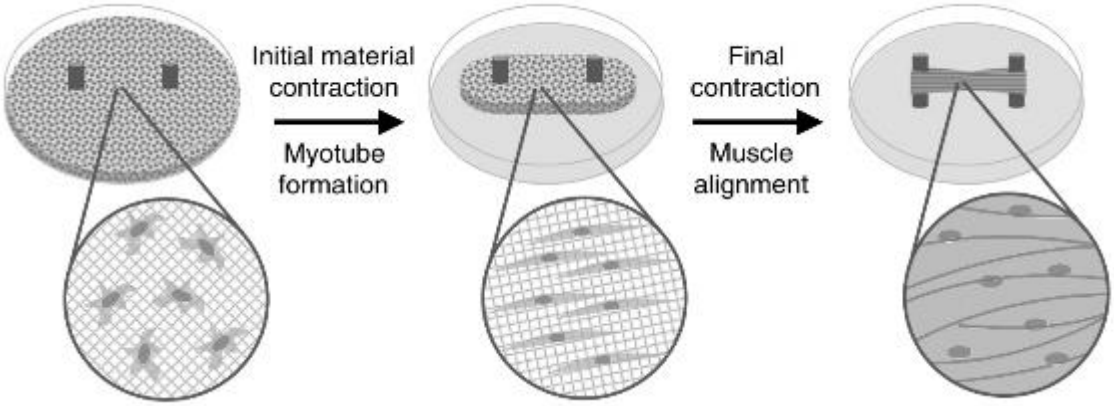

***Figure 6**. Bio-artificial muscle (BAM) formation; scaffold-free SMTE technology (Figure taken from (79)).*

5.3.3.2 Scaffold-based technology

This approach is based on the use of scaffolds which provide a physical support structure for the seeded myogenic cells. Scaffolds can be classified according to their composition, being either synthetic polymers or naturally derived biomaterials. With current lawsuits concerning mesh implantations in mind (72), the preference nowadays is to use naturally derived biomaterials to avoid sustained inflammatory reactions. However, biological polymers often suffer from poor mechanical properties (73).

Scaffolds play a pivotal role in the proliferation of cells, providing structure for new tissue formation and can prevent cavitation *in vivo*, which might result from massive tissue loss (74).

A SMTE scaffold should have following characteristics: biodegradability, mechanical properties similar to the target host tissue, adhesiveness for cells, biocompatibility and good suturability to ensure secure implantation (75).

5.4 SCAFFOLDS

5.4.1 Natural biomaterials

ECM molecules are required within the skeletal muscle differentiation process, since many of the cellular events that occur during skeletal muscle formation require cell-ECM interaction (76). Collagen is the most logical choice as a natural biomaterial since it is an important component (1 - 15% of total dry weight (77)) of skeletal muscle. Collagen is readily available: a matrix can be obtained by decellularization or it can be prepared through extraction from animal sources (78). Several collagen-based scaffolds are currently available on the market, such as Helistat (Integra LifeSciences), Instat Fibrillar (Johnson & Johnson) and Biobrane (UDL Laboratories) (78). The major drawback of this biomaterial is its intrinsic low mechanical properties. Therefore, cross-linking strategies are used to control the rate of degradation *in vitro* (79).

Gelatin is another source of a natural biomaterial, obtained by controlled hydrolysis of collagen. It is one of the most widely used protein-based polymers with a variety of applications in the food and pharmaceutical industry (80). Gelatin is produced in massive quantities at low cost, is biocompatible and biodegradable. Nonetheless, gelatin suffers from the same drawback as collagen namely its mechanical weakness resulting in the need for cross-linking or combination with other polymers (81).

Elastin is also found in the native ECM of connective tissues where total elastin content varies from 0.6 to 3.7 % (82). Its use as a biomaterial is limited as there are several drawbacks associated with this structural protein. Its tendency to calcify after implantation remains the biggest hurdle for its use as a scaffold in tissue engineering approaches. The use of elastin scaffolds showed the presence of glycation and oxidation products, associated with matrix crosslinking and stiffening, which ultimately led to inflammation and calcification (83). The complex purification process combined with the need for control of degradation via cross-linking further limits it use. Despite the many drawbacks, elastin is still being examined as a scaffold material in the field of cardiovascular tissue engineering due to its high elasticity

coupled with its low stiffness (73). It is often combined with collagen in an attempt to improve the viscoelasticity of collagen scaffolds without resorting to synthetic polymers (84).

Fibrinogen is a protein with an established role in wound healing, where after polymerization into fibrin fibers, it serves as a provisional matrix for tissue repair. Therefore the use of fibrinogen as a scaffold material for tissue engineering approaches is assumed to replicate the same support as during wound healing. Fibrinogen is known for its pro-inflammatory features, however there is a paradigm shift in the use of materials from avoiding the immune response towards modulating inflammation (85). The high capacity of fibrinogen to bind growth factors makes it an interesting polymer for use as a scaffold (86). Furthermore, fibrinogen has consistently demonstrated excellent bioactivity together with favourable cell migration (87). Fibrin clots are soft and degrade within a few days *in vivo*, but different cross-linking approaches with transglutaminase, glutaraldehyde, genipin or heterobifunctional carbodiimides are being examined to overcome this (86).

Finally, silk derivatives are used in medicine, for example in wound dressings, vascular prostheses and suture materials (88). Depending on the silk source, differences in composition, structure and properties may be observed but currently silkworm is the only source being used commercially (89). Due to the slow proteolytic degradation, silk is often misclassified as nondegradable, however it is slowly absorbed as biocompatible amino acids (79). In response to findings of allergic reactions when using silk meshes, the outer sericin coat is removed which enhances the bioresorption *in vivo* and promotes the biocompatibility (90). Although the tensile strength of silk is comparable to synthetic fibers like Kevlar, silk meshes are easily handled without being too rigid (90). So silk-based biomaterials with high elasticity and high structural strength are a promising scaffold biomaterial for tissue engineering (91).

5.4.2 Synthetic biomaterials

Poly(glycolic acid) (PGA) scaffolds are currently used in a variety of medical applications of which the most well known are surgical sutures which have been commercially available since 1970 (92,93). PGA has already been widely used in the field of tissue engineering (94,95). PGA polymers are biodegradable which allows transient support for the tissue engineered constructs until sufficient neo-matrix is secreted by the embedded cells. Because of its limited mechanical support and rigidity, it is especially suitable for applications where a fast-degrading material (6-8 weeks) is desired (96). However, the degradation via non-enzymatic hydrolysis leads to acidic by-products. This ultimately leads to reduced pH and accelerated degradation of

the supporting structure and might interfere with cell survival (97). However, since scaffolds used in tissue engineering applications have highly porous structures, the mass of polymer per unit volume remains relatively low. On the other hand, the by-products themselves are non-toxic for the body and are eliminated as carbon dioxide and water (98).

Poly(lactic acid) (PLA)-based scaffold displayed good integration into the host tissue with a decreased inflammatory response, indicative of constructive remodelling (99). Although the mode of degradation is the same as for PGA, PLA degrades at a much slower rate. The degradation typically takes around 30-35 weeks and is accompanied by the production of lactic acid which is naturally present and metabolized in the body excluding by-product toxicity (1,100). Moreover, PLA has good mechanical versatility which makes it suitable for diverse clinical applications, each with their required scaffold shape. On the other hand, one drawback restricting its widespread application in the field of tissue engineering is the crystallinity of degradation fragments which might cause inflammatory reactions in the body (101).

Scaffolds composed of both PGA and PLA, referred to as poly(lactic-co-glycolic acid) (PLGA), provide another approach for designing appropriate scaffold material. The ratios of each component might differ. For example, the commercially available woven Vicryl™ mesh is composed of a 90:10 ratio of glycolic acid and lactic acid respectively. Because of its flexibility and thin profile it is often utilised for meniscal repair. Due to its structural similarity to native bone it has been explored for orthopedic surgery as well (102). This copolymer degrades by bulk ester hydrolysis within a time period of 1-12 months depending on the relative ratios of both components (79). Moreover, the use of these scaffolds has not been linked to the presence of post-operation scars (103).

Polydioxanone (PDO) is another biodegradable polyester which has gained increasing interest in the medical field due to its biocompatibility and its shape memory. Shape memory refers to the ability of the material to return to its original shape after being deformed by an external stimulus. Shape memory limits application of PDO as a suture because knot retention is more difficult, but may be a desirable feature for SMTE. However, because of natural biodegradability with limited inflammation, PDO monofilaments have been used as suture material for several decades (104). This long-term use in the clinic guarantees its safety in humans. The degradation rate varies between 6-12 months with no acute or toxic effects upon implantation (79). Currently, PDO scaffolds are being used also in plastic surgery, drug delivery and bone repair (1,105).

For delayed regeneration processes, slowly degrading scaffold materials are required to give sufficient support throughout the regeneration process. This requirement makes polycaprolactone (PCL), with its typical degradation rates of 1-3 years, very promising. The degradation of this polyester occurs by bulk or surface hydrolysis of the ester linkages (1). Furthermore, PCL has favourable mechanical properties such as good elasticity and flexibility accompanied by an excellent biocompatibility (106). PCL scaffolds may be valuable in the field of tissue engineering and have been proposed to engineer bone tissue (107).

Compatibility of a biomaterial also refers to matching the mechanical properties to those of the host tissue. Elasticity, which implies recovery from deformation, is of particular importance in the context of dynamic tissues like muscle and tendon. Elastomers date back to the mid-1890s, but only emerged in the late 1990s in the field of tissue engineering (108). Elastomers can be divided into two categories: physically crosslinked elastomers, also referred to as thermoplastic elastomers, and chemically crosslinked elastomers. The latter will be further discussed. In chemically crosslinked elastomers, flexible polymer chains arising from reacting multifunctional monomers arrange in a 3D network through chemical bonds which are introduced during a curing process (108). This crosslinking, where at least three linkages with neighbouring molecules need to be attained, can be initiated thermally or by radiation. Poly(polyol sebacate) (PPS) is a family of crosslinked polyester elastomers developed by Langer's group in 2002 (109). PPS are synthesized from an alcohol containing multiple hydroxyl groups (polyol) and the dicarboxylic acid sebacic acid through polycondensation (esterification) (108). Subclasses of polyols arise from using different sugar alcohols like glycerol, xylitol and sorbitol (110). PPSs generally has little toxicity to the body tissues as they are composed of nontoxic monomers which degrade into metabolizable products (111,112). Poly(glycerol sebacate) (PGS) and poly(xylitol sebacate) (PXS) have been best studied. *In vivo* evaluation carried out for PGS and PXS showed mild acute inflammatory responses but no chronic inflammation (111,112). The biodegradation of PPSs through hydrolysis of the ester bonds with gradual loss of mechanical strength spans a period of several weeks (112,113). This surface erosion is the preferred way of degradation for regenerative purposes. Importantly, the physical characteristics can be tuned to match specific properties of biological tissues by altering processing methods (114) or using different monomer ratios (115,116). Furthermore, citric acid with hydroxyl and carboxyl functional groups can act as an additional cross-linker in PPS (117).

Finally, polycarbonate is known for its rubber-like properties, biocompatibility and biodegradability (118). The enzymatic degradation is mainly facilitated by surface erosion and an erosion rate of 6.7 micrometer per day has been reported (119). Due to its mechanical strength it is suitable for biomedical and pharmaceutical applications such as drug delivery systems, suture materials and in this context scaffold materials for supporting tissue engineered constructs (120). Polycarbonate is often studied as a composite biomaterial with polyurethane (121).

5.4.3 Patterned scaffolds for cell guidance

Obtaining aligned muscle fibers in bio-artificial muscle which are further assembled into organized muscle bundles is a key feature of engineering functional skeletal muscle tissue. To achieve this well-organized composition, micropatterned scaffolds have been fabricated to guide alignment of myoblasts which further fuse into aligned myotubes. Several methods such as electrospinning, photolithography or contact printing have been explored to achieve micropatterned surfaces (122). However, 2D patterned surfaces are limited in use because of their fixed thickness, making three-dimensional (3D) micropatterned scaffolds more promising, especially for tissue repair.

5.5 APPLICATIONS OF BIO-ARTIFICIAL MUSCLE

Differentiated myotubes serve as a model to study cellular mechanisms under controlled conditions *in vitro* (123). However, as two-dimensional culture on plastics does not mimic the native cellular microenvironment, there is growing interest in the use of 3D bio-artificial muscle models (124). 3D models in general constitute a promising and versatile *in vitro* model by mimicking normal cell physiology and function which strongly relies on cell-cell and cell-ECM interactions (125–128)h The use of human cells to create human muscle tissue increases the relevance to study human muscular diseases and evaluation of therapeutics. Also for basic science studies related to muscle physiology, innervation and development novel insights can be gathered based on these functional *in vitro* models.

Another application is the use of human tissue engineered muscle constructs for high-content drug screening. Tissues better predict the physiological activity of a screened compound compared to the traditional 2D screening technologies in which it is more difficult to predict the functional activity of a compound *in vivo* (129). Bioengineered human myobundles can serve as an *in vitro* system for testing novel muscle disorder therapeutics and aid in toxicology screening (130). Vandenburgh et al. described a tissue-based drug-screening platform for

compounds that affect muscle strength by measuring contractility changes upon drug administration in the medium (131). Furthermore, this application of tissue-engineered muscles can aid in reducing time, cost and number of animals needed for *in vivo* studies (132).

Intramuscular drug delivery systems have gained significant momentum in pharmaceutical industry during the past decades, as intramuscular drugs are cost effective, pharmacologically efficient and induce reduced side effects (133). Providing new strategies for testing intramuscular compounds by developing bio-artificial muscle may reduce animal testing.

In addition, SMTE is being explored as a 'clean' alternative for meat production. Meat production has an important impact on global warming as animals produce the greenhouse gas methane. According to the Food and Agriculture Organization of the United Nations, the demand for meat will increase 73 % towards 2050 (134). Therefore, alternative meat production sources are being explored. Culturing beef *in vitro* is based on the same SMTE principles as for clinical applications. However, as 20000 muscle strips were needed to create an 85 g hamburger it is doubtful that this approach will be either cost effective or technically feasible on a large scale (135).

The last application is in regenerative medicine, further discussed below. This may be the most promising but at the same time also the most challenging. Clinical situations where muscles are damaged, like traumatic injuries, tumour ablation or prolonged denervation seem attractive for bio-artificial muscle applications (79).

5.5.1 Regenerative medicine

The ultimate, but long-term goal of SMTE is its use in regenerative medicine for treating damaged or diseased muscle tissue. Skeletal muscle has a good regenerative capacity as compared to many other organs. However, the damage can be too extensive for normal healing to cope with the muscle loss. This can occur due to tissue ischemia, advanced age, severe injuries, surgery or genetic defects. Therefore, development of regeneration strategies for damaged muscle is important,

Direct injection of isolated cells aims at migration to the damaged site and support of regeneration of damaged tissue. However, the long-term goal to recover the contractile function is often not reached due to non-selective migration and death of the majority of injected cells. To tackle this problem cell transplantation approaches using biomaterials are being explored. In this context, the biomaterials act as a synthetic niche to mimic the natural satellite cell microenvironment which may improve the survival, engraftment and fate control of the seeded

cells (136). Still, this approach differs from the aforementioned scaffold based SMTE as this approach aims at using single cells with a scaffold as vehicle.

The use of autologous and allogeneic grafts is the most commonly used treatment but both options have intrinsic limitations. As autologous refers to patient's own grafts, this is the preferred material for replacement strategies. However, these tissues exist in limited quantities, necessitate a second operation to obtain the tissue and risk morbidity at the donor site (137). An example of this grafting approach is the treatment of invasive jaw cancer which uses the pectoralis muscle to replace jaw muscle that had been removed as part of the surgical procedure to treat this kind of cancers (52). Allogeneic grafts are typically derived from cadavers and have some serious drawbacks such as the risk of disease transmission and host inflammatory response. This again underscores the potential for tissue engineering alternatives.

A last approach in regenerative medicine is therapeutic drug delivery. Therapeutic drug delivery is explored for damaged or diseased skeletal muscle or for attenuation of wasting processes seen in (i) chronic diseases, (ii) disuse conditions such as denervation and (iii) aging (sarcopenia) (138). Localized delivery is preferred since systemic delivery can cause complications. An example of a complication, hypoglycemia, is seen when administering IGF-1 systemically for treating muscle wasting based on enhancing the intrinsic regenerative capacity (139). Bolus drug delivery often results in the loss of bioactivity and the delivered drugs being rapidly degraded due to the inflammatory environment created by the damaged tissue (140). This has triggered the development of *ex vivo* genetically engineered postmitotic myofibers for chronic local delivery of therapeutic agents (141,142). This approach might provide a safer alternative than other drug delivery approaches since postmitotic myofibers are non-migratory.

5.6 STIMULATION TO PROMOTE ENGINEERING OF SKELETAL MUSCLE

The ultimate aim of SMTE is to obtain functional muscle which exhibits functional contractility comparable to native muscle. Although traditional tissue engineering strategies are evolving rapidly, there are still shortcomings concerning the maturity of the resulting myofibers (143). To further promote the functional output and development of the bio-artificial muscle, several approaches are being examined. As exercise results in hypertrophy and fiber thickening, simulating exercise by the use of electrical or mechanical stimulation is an active area of research for promoting maturation of tissue engineered muscle constructs. Besides mechanical

and electrical stimulation, medium perfusion is also being applied to improve the functional myogenesis *in vitro* (144).

5.6.1 Mechanical stimulation

Mimicking mechanical stimulation of myofibers is an appealing way to stimulate myofiber maturation in SMTE. Mechanical stimulation of skeletal muscle by altered load shows hypertrophy, whereas a lack of adequate load results in atrophy. Mechanical stimulation *in vitro* has already been applied in other fields of tissue engineering such as in the field of cartilage tissue engineering and cardiac muscle tissue engineering (145,146).

One of the pioneers in the field of SMTE, Herman Vandenburgh, described in 1989 a computerized mechanical cell stimulator device for tissue cultured cells. These induced mechanical forces caused the myoblasts to fuse into parallel arrays of myotubes which were significantly longer than myotubes that arise from static culture conditions. Furthermore, intermittent stretch caused increased protein synthesis ultimately leading to the observed hypertrophic response (147). The tetanic and twitch contractile responses of tissue constructs implanted onto the latissimus dorsi muscle of mice also increased significantly after *in vitro* cyclic mechanical stimulation (148).

These show that the biochemical processes which occur upon muscle hypertrophy *in vivo* can be translated into *in vitro* applications as well. Current regimens exert cyclic and uniaxial forces to the engineered muscle constructs with an amplitude of stretch ranging between 6.7-20% with frequencies of 0.1-1 Hz for a period between 30 min and 10 days (149). The direction of the induced stretch needs to be considered thoroughly as it has been demonstrated that specific types of mechanical stretch activate distinct signalling pathways through mechanotransduction (150). In addition, the effect of mechanical stress on muscle tissue seems to be broader than hypertrophy as proangiogenic factors, including vascular endothelial growth factor (VEGF), were also upregulated in response to mechanical stimulation (151).

5.6.2 Electrical stimulation

Electrical stimulation of cells has become an active field of research since endogenous electric fields were reported to occur at wounds and around vasculature (152). Electrical stimulation has gained most attention in the field of regeneration in the central nervous system as applying an external electric current was shown to generate action potentials in damaged nerves, which ultimately led to muscular contractions (153). Currently, several rehabilitative

techniques based on electrical stimulation are in use to promote regeneration of neurites in injured nerve fibers (154).

Electrical stimulation is also examined in the field of SMTE, to mimic the transition from primary myotubes to secondary as seen during development. For example electrical stimulation of three-dimensional C2C12 myoblast cultures has been investigated showing enhanced sarcomere formation which intensifies the contractile force generation (155). Besides the enhanced sarcomere assembly, one effect of electrical stimulation is the upregulation of late muscle maturation marker MRF4, indicating accelerated skeletal muscle cell maturation upon electrical stimulation (156).

In contradiction to previous studies, a negative impact of electrical stimulation upon myogenic differentiation has been shown as well. Upon electrical stimulation of chick neonatal muscle tissue, downregulation of MyoD, myogenin and acetylcholine receptor was observed (157). These contradictory results indicate a limited understanding of the effects of electrical stimulation on myogenic differentiation.

Several methods and devices have been proposed to enable electrical stimulation for tissue engineering applications. As electrical stimulation is of interest for a variety of biological applications, the array of potential applications is expected to further expand. However, as the use of simple electrodes can be accompanied by several side-effects such as hydrolysis of the culture medium, heating of the medium or contamination of the culture medium due to electrode corrosion, the field is currently tending towards contactless electrodes to electrically stimulate engineered muscle tissue (144).

5.6.3 Medium perfusion

Bioreactors mimic the physiologic delivery of oxygen, nutrients and chemical signals which *in vivo* are achieved by blood flow. Besides creating a biomimetic cell culture environment with supply of fresh nutrients and growth factors accompanied by draining of metabolic waste products, they also allow the control of sterility and operating conditions such as pH and/or temperature. Different kinds of perfusion bioreactors are being used ranging from simple stirred flasks to perfusion bioreactors allowing continuous flow of culture medium (144).

The importance of fluid flow and its associated shear stress is well established in vasculogenesis (158–160), remodelling of immature vessels (161), and maintaining blood vessels (162). For the remodelling in particular, differences in blood flow between vessels in a branch point are suggested to be an important regulator of blood vessel pruning (163). Flow

was also found to be a regulator of arterial-venous differentiation in chick embryo yolk sac by changing the global patterning of the arteries and veins (163). Accordingly, this differentiation is associated with regulated changes in arterial and venous marker expression.

In vitro shear stress was associated with improved endothelial cell retention of prosthetic vascular grafts (164) and shear stress-induced transient reorganization of cytoskeletal and adherens junction proteins (165,166). Therefore medium perfusion is believed to accelerate vascular tissue morphogenesis which can ultimately enhance the development of thicker tissue constructs. In addition, bioreactors also promote the viability and long-term maintenance *in vitro* (167). Nonetheless, high shear stress as a result of perfusion may have an negative impact on the viability since striated muscles in general are known to be shear-sensitive (144). Ultimately, bioreactor based 3D culture systems still represent a promising approach to increase tissue functionality and are expected to further expand in coming years.

6 OBJECTIVES

This study aims at further development of a human bio-artificial skeletal muscle tissue engineering technology. The approach existing thus far is based on contraction and differentiation of myoblasts in a hydrogel, leading to formation of myofibers oriented in parallel. The resulting tissue has neonatal characteristics in terms of strength and gene expression, and is limited in size due to the lack of a proper vascular network.

In this work, we aim to progress along 2 frontiers. The Thorrez lab had recently described a new *in vitro* vasculogenesis approach (66). However, this vasculogenesis approach had never been evaluated *in vivo*. Second, we aim at the evaluation of new scaffold compositions next to the current scaffold-free approach. The rationale being that scaffolds could provide initial strength to the developing tissue and may even guide cell differentiation.

Objective 1: *In vivo* evaluation of endothelial cell-myoblast co-culture human bio-artificial muscle (BAM)

Since our BAMs are created with human cells, animals are likely to generate immune responses to the BAM. Therefore, we aim at determining the best animal model and implantation site where it is surgically feasible to implant the BAMs, where they survive best and where perhaps evidence can be found for anastomosis of the engineered endothelial networks with host blood vessels.

Objective 2: Use of synthetic biomaterials as a scaffold for myogenic cell attachment and differentiation

The objective of this study is to evaluate different polymer scaffolds in skeletal muscle tissue engineering. The aim is to evaluate whether human myoblasts within an extracellular matrix hydrogel can adhere and proliferate in the presence of different synthetic polymer scaffold. Furthermore the effect of contact guidance for myoblast elongation and alignment are determined.

7 MATERIALS & METHODS

7.1 ISOLATION AND CELL CULTURE OF HUMAN SKELETAL MUSCLE CELLS

Human skeletal muscle cells were isolated from fresh human muscle tissue biopsies obtained from the Human Body Donation programme of KU Leuven University (Prof. E. Vereecke). Briefly, tissue was stored on chilled Dulbecco's modified eagle's medium (DMEM; high glucose with Glutamax and pyruvate; Life Technologies; #331966-021) supplemented with 1% penicillin/streptomycin (P/S) (Life Technologies; #15070-063) at 4°C and isolation was performed within 48 hours after obtaining the muscle biopsy. Excess connective tissue and fat was removed from the tissue sample. Strips of approximately 2 mm x 10 mm were cut using sterile forceps and scalpel. Before isolation of cells, muscle strips were pinned under tension with stainless steel insect pins (Vermandel; #20.051) into sylgard coated 6-well plate wells to maintain cell survival while avoiding muscle atrophy. 48 hours after pinning the strips, enzymatic digestion was performed by incubating the muscle strips at 37°C for 1 hour in DMEM high glucose with Glutamax and pyruvate supplemented with 0.1% collagenase, type II (Sigma; #C6885) and 4 mg/ml dispase II (Roche Diagnostics; #165859). After the incubation, isolated cells were collected by filtering through a 100 µm cell strainer (FALCON) and fragments were incubated again to digest the whole tissue. Isolated cells were pooled, centrifuged for 5 min at 200 x g and resuspended in Ultroser based skeletal muscle growth medium (SkGM) ([SkGM]: DMEM high glucose with Glutamax and pyruvate supplemented with 10% FBS (Thermo Fischer; #105000-064), 50 µg/ml gentamicin (Life Technologies; #15750-37) and 1% Ultroser solution (Pall corporation; #15950-017)). Cells were cultivated on a Poly-L-Lysine coated T25 flask (Corning) in a humidified 5% CO_2-containing atmosphere at 37°C. Characterization of the isolated cells was performed when approximately 75-80% confluency was reached.

7.2 HUMAN BIOPSY CHARACTERIZATION: IMMUNOCYTOCHEMISTRY

Immunocytochemistry was performed to determine (i) the amount of myoblasts in the cell population and (ii) the fusion index of the myoblasts. Isolated muscle cells populations should meet following minimum requirements (i) minimal myoblast percentage in the isolated muscle cell population of 60 % (ii) minimal fusion index of 60 %. For the former, isolated muscle cells were cultured in SkGM in 24-well dishes (5.000 cells / well) for 2–3 days until 60–70 % confluent. To determine the fusion index, cells were cultured to 80 % confluence in SkGM in

12-well dishes (50.000 cells / well), and then switched to skeletal muscle fusion medium (SkFM) ([SkFM]: DMEM high glucose with Glutamax and pyruvate supplemented with 10 ng/ml animal-free recombinant human epidermal growth factor (Peprotech; #AF-100-15), 50 µg/ml bovine serum albumin (BSA; Sigma-Aldrich; #A2153), 10 µg/ml insulin and 50 µg/ml Gentamicin for 4 days to induce fusion into myofibers. Fixation was performed in a 1:1 methanol–acetone mix at -20°C for 10 min for desmin staining and in 4% formaldehyde freshly prepared from paraformaldehyde (PFA; Merck; #1040031000) solution weight/volume (w/v) at room temperature (RT) for 10 min followed by methanol fixation at -20°C for 10 minutes for tropomyosin staining. Next, fixed cells were blocked and permeabilized in blocking buffer containing 1x phosphate buffer saline (PBS), 1% BSA and 0.2% Triton X-100 (Sigma; #X100). Subsequently, cells were incubated for 2 hours at RT with a monoclonal mouse antibody against desmin (Sigma; D1033; 1:200 in blocking buffer) or tropomyosin (Sigma; T9283; 1:100 in blocking buffer) to determine the myoblast percentage and the fusion index, respectively. Cells were labelled with a polyclonal rabbit anti-mouse secondary antibody (Alexa Fluor 488; #A11059; Invitrogen) for 30 minutes in the dark and subsequently incubated with 4′,6-diamidino-2-phenylindole (DAPI; 0.1 µg/mL in PBS; Life Technologies) for 1 hour. Images were acquired with Zeiss Zen software by an AxioCam ICc 1 camera mounted on a Zeiss Axiovert 10 microscope. The percentage of myoblasts in a muscle cell population was defined as the ratio of desmin-positive cells to the total amount of cells (identified by the DAPI-stained nuclei). Fusion index was defined as the ratio of tropomyosin-positive cells to the total amount of myoblasts in the population.

7.3 CELL CULTURE

Murine C2C12 myoblasts were purchapsed from Sigma and were cultured in DMEM high glucose with Glutamax and pyruvate containing 10% foetal bovine serum (FBS), supplemented with 1 % P/S. Human umbilical vein endothelial cells (HUVECs) that constitutively express green fluorescent protein (GFP) were purchased from Angioproteomie and cultured in endothelial growth medium (EGM-2 with bullet kit; Lonza; #CC-4176). Human primary skeletal muscle microvascular endothelial cells (SkMVEC) were purchased from Cellbiologics and were cultured in EGM-microvascular (EGM-MV with bullet kit; Lonza; #CC-4147). Aforementioned isolated human muscle cells were expanded in culture in SkGM. For myoblast cultures, tissue culture flasks were uncoated. Endothelial cell cultures were cultured on gelatin-coated culture flasks (0.1% gelatin; Milipore; #46-000-CV). All cells were cultured at minimal seeding densities of 4.000 cells/cm^2 at 37 °C and 5 % CO2 and media was changed every 2

days. Human muscle cells were split at 60-70 % confluence and used in experiment at 14 doublings. Murine C2C12 myoblasts were split at 90 % confluence and used in experiment until 20 doublings. HUVEC and SkMVEC were split at 90 % confluence and used at passage 7.

7.4 3D TISSUE CONSTRUCT

BAMs were constructed into 25-mm-long custom silicone molds containing metal end attachment sites and a total casting volume of 1 ml. Two million muscle cells were mixed with 500 µL thrombin (4 U/ml [working solution] obtained by diluting 1000 U/ml [stock solution] (Bio Phar Laboratories LLC; #SKU 93-050) in DPBS with Ca^{2+} and Mg^{2+} (Gibco; #14040-083), and cast into the molds. Then, 500 mL fibrinogen (2 mg/mL [working solution] obtained by diluting 1000 U/ml [stock solution] (Merck Chemicals; #341576) in DPBS with Ca^{2+} and Mg^{2+} was added and the cell–gel mix was mixed by pipetting up and down to form a fibrin gel (1 mg/mL) containing the muscle cells. Following 3 hours of incubation at 37 °C, SkGM supplemented with fibrinolysis inhibitors, aprotinin (92.5mg/mL; Carl Roth; #A1624) and tranexamic acid (TA) (400 mM; Sigma; #857653), was added. 24 h and 48 h after casting, fibrin gel was detached from the silicon molds using a tooth hook. Within these 2 days, the cell/gel mix contracted, detached from the molds and was being held in place only at the two end attachment sites. Two days after casting, medium was switched to SkFM supplemented with aprotinin and TA. The medium was replaced every 2 days and BAMs were kept in culture for 7 days to allow myoblast fusion and differentiation to aligned myofibers.

7.5 CO-CULTURE BAM

Endothelial cells i) red fluorescent protein (RFP) labelled HUVEC or ii) mCherry labelled SkMVEC were cultured independently of myoblasts prior to 3D tissue engineering. Co-culture BAMs were made with either 600.000 HUVECs and 1.4 10^6 muscle cells or 100.000 SkMVECs and 1.9 10^6 muscle cells. The cells were harvested, centrifuged and resuspended in the thrombin solution (4 U/ml) as previously described and cast into silicone molds. Fibrinogen solution (2 mg/ml) was added to the mold and mixed with the cell-thrombin solution. After 3 hours of gelation, i) EGM-2 (for the co-culture using HUVECs) or EGM-MV (for the co-culture using SkMVEC) ii) M199-EGM ([M199-EGM]: Earl's Medium 199 (PAA; #E15-033), 10 % FCS, 1 % P/S, 1 % L-Glutamin (Gibco; #25030), 0.05 mg/ml ascorbic acid (Sigma; #A8960), 0.1 µg/ml rh-bFGF (ImmunoTools; #11343625) and 10 ng/ml FGF (Peprotech; #100-18B)) or iii) SkGM with a switch to SkFM after 2 days supplemented with fibrinolysis inhibitors, aprotinin

(92.5 µg/ml) and TA (400 µM) was added and replaced every 2 days. BAMs were kept in culture for 7 days before implantations or fixation for further analysis.

7.6 POLYMER SCAFFOLD PREPARATION, CELL SEEDING, AND CULTURE

Porous, chemically cross-linked elastomers polymerized from glycerol, xylitol, sebacic acid and citric acid were obtained in collaboration with prof. Wim Thielemans (KU Leuven Kulak). Poly(glycerol sebacate) (PGS) was prepared by reacting glycerol with sebacic acid in a 1:1 molar ratio. Poly(xylitol sebacate) (PXS) was prepared by reacting xylitol with sebacic acid, this in a 1:1, 1:1.25, 1:2 and 1:2.5 molar ratio. Prepolymers were formed under inert conditions at elevated temperature. Poly(glycerol sebacate citrate) (PGSC) 1:1 was prepared by addition of citric acid, in a 1:0.25 polyol to citric acid molar ratio, to the PGS 1:1 prepolymer following 3 hours polymerisation under vacuum. Poly(xylitol sebacate citrate) (PXSC) 1:1 and 1:2 was prepared by adding citric acid, in a 1:0.25 polyol to citric acid ratio, to PXS 1:1 and PXS 1:2 respectively following 3 hours polymerisation under vacuum. The prepolymers were cast and cured in a vacuum oven for further esterification. Prepolymers were additionally processed to introduce porosity by mixing the prepolymer with NaCl crystals. Polymer porosity was tuned by adding different salt weight percentages (1:6, 1:7, 1:8, 1:9 or 1:10 weight ratios of prepolymer and NaCl respectively). Scaffolds were manually cut to dimensions of approximately 1 cm. Prior to cell seeding these elastomeric scaffolds were incubated in 70% ethanol for 30 minutes as pre-wetting treatment and simultaneous sterilization step. Scaffolds were afterwards rinsed three times with PBS and submerged in SkGM for 15 minutes. Polymers were then air dried overnight prior to cell seeding. Polycarbonate polymers (SurpaPolix; Eindhoven; The Netherlands) were obtained in collaboration with prof. Jan Deprest (KU Leuven). Fibers of polycarbonate mesh were made by electro-spinning and are organized as a network-like structure with random in plane orientation. Fiber interspaces are in the order of a few microns and can be visualized in the blue channel based on auto-fluorescence. Polycarbonate mesh, with 400 µm thickness was cut into square pieces of 0.25 cm^2 using sterile scissors. Dimensions were measured using micrometre paper.

In general, polymers were transferred to silicon coated 6-well plates (Sylgard). Cells to be seeded onto the scaffolds were first resuspended in thrombin solution (4 U/ml) and mixed with fibrinogen (2 mg/ml) in an Eppendorf tube to attain a total fibrin ECM (1 mg/ml) volume of 1 ml. The cell/gel mix was seeded on top of the scaffolds at a density of i) 200.000 cells/ml gel mix per sample for the elastomeric scaffolds viability and alamar blue assay ii) 10 million

cells/ml gel mix for the elastomeric scaffolds and iii) 10 million cells/ml gel mix for the polycarbonate scaffolds to assess the impact on differentiation. Scaffolds were incubated at 37 °C and 5 % CO2 for 3 hours after seeding cells and flooded with 10 ml SkGM prior to returning to the incubator for 2 days. After 2 days in culture, myoblast fusion into postmitotic myofibers was again induced by switching the medium to differentiation medium (SkFM).

7.7 *IN VIVO* IMPLANTATION OF COCULTURE BAMS

To determine the optimal implantation site and animal model to obtain construct survival and host blood vessel ingrowth, co-culture BAMs were implanted for a period of 2 weeks in adult rats and mice under ethical approval (P099/2017). Briefly, constructs were subcutaneously implanted into 6-7 weeks old female wistar rats (Janvier) in the first model. Rats were divided into two groups with implantation of the constructs either onto the abdominal muscle (2 constructs per animal) or tibialis muscle. In the second model, constructs were implanted subcutaneously on the latissimus dorsi muscle of adult immunocompetent swiss mice (inbred strain; KU Leuven), immunodeficient *Foxn1nu* (Nu/Nu) mice and non-obese diabetic severe combined immunodeficiency (NOD/SCID) mice (Janvier)(each time 2 constructs per animal). All animals were anesthetized and maintained with isoflurane (0.5-2 %, 3-5 L/min) and oxygen. Rats and swiss mice receiving co-culture BAM implants were immunosuppressed with cyclosporine (10 mg/kg each day; Le Vet Pharma) and methylprednisolone (1.6 mg/kg each day; Solu Medrol®; Pfizer). After implantation, meloxicam (2 mg/kg; Meloxidyl CEVA) and buprenorphine (0.1 mg/kg; Vetergesic) were administered subcutaneously to avoid acute inflammation analgesia. Incisions were closed with 4-zero polyglecaprone suture (Monocryl; Ethicon) and implants were secured on both sides of the constructs to muscle fascia with 6-zero polypropylene suture (Ethicon). Animals were anesthetized two weeks later and 1.25 µg/g body mass Rhodamine-labelled ulex uropaeus agglutinine-I (UEA-I; Vectorlabs) was injected in the tailvein to determine whether anastomosis of tissue engineered endothelial networks with host blood vessels was established. In case constructs remained to be present upon explantation, construct and underlying host tissue was explanted. In case no constructs remained to be present, surrounding host tissue was explanted alone based on suture positions. Host muscle was explanted each time, which served as a negative control. Grafts were removed from the animals and immediately fixed using 4 % PFA solution (w/v) for 1 hour (with an added hour per additional millimetre thickness of the explant) and further operated as described below.

7.8 WHOLE MOUNT IMMUNOFLUORESCENCE STAINING AND CONFOCAL MICROSCOPY

BAMs were washed (3 times 5 minutes in PBS), and then fixed using 4 % PFA solution (w/v) in PBS for 1 hour. Scaffold-free BAMs were pinned on styrofoam to preserve their original shape while fixing. Prior to staining, constructs were additionally fixed in -20 °C methanol for 10 minutes. Fixed constructs were blocked and permeabilized in blocking buffer. Subsequently, BAMs were incubated overnight at 4 °C with a monoclonal mouse antibody against tropomyosin (Sigma; T9283; 1:100 in blocking buffer) or myosin heavy chain (MF20) (DSHB), recognizing all myosin heavy chain isoforms. After being washed three times with PBS for 5 minutes, BAMs were incubated with polyclonal rabbit anti-mouse antibody (Alexa Fluor 488; Invitrogen; A11059; 1:200 or Alexa Fluor 633; Invitrogen; 21063; 1:200) for 3 hours in the dark followed by incubation with DAPI (Life Technologies; 0.1 µg/ml in PBS) for 1 hour. BAMs were stored in PBS in the dark until visualized.

7.9 CONFOCAL IMAGING AND DATA ANALYSIS

Parameters characterizing the myofiber formation in engineered BAMs were attained from confocal imaging and were further analysed as described below. First, BAMs were placed on coverslips and visualized by confocal microscopy (Zeiss LSM710) within 48 hours. Per BAM, 3 z-stacks were acquired, each containing 20–40 images (depending on the intensity of the signal at various depths) every 5 mm towards the centre of the BAM. For myofiber analysis, each 20-mm z-projection (image grouping performed by the ImageJ software16) was manually analysed for different parameters of myofiber formation: myofiber alignment, length, and diameter, as well as number of myofibers per microscopic field. Myofiber alignment was determined by the standard deviation of the angles of the myofibers positions. A lower number indicated a better alignment. For endothelial network analysis, each 60-mm z-projection was automatically analysed by a customized version of the Angiogenesis Analyzer, an ImageJ plugin created by Gilles Carpentier (168). This tool quantifies endothelial networks in an objective manner by extracting characteristic information of the network. Parameters to define endothelial networks were junctions (group of joined nodes, pixels with at least three neighbours), branches (elements delimited by a junction and one extremity), isolated segments (binary lines, which are not branched), total length of endothelial network (interconnected segments, branches, and isolated segments), % branching length (length of interconnected

segments and branches divided by total network length), and meshes (areas enclosed by segments)(66).

7.10 *IN VIVO* GRAFT INTEGRATION ANALYSIS: INTRAVITAL IMAGES

For *in vivo* imaging at day 12 upon implantation, small skin incisions were performed at the implantation site of the adult swiss mice to insert the fibre-optic microprobe (SN PF 2294). Imaging on day 14 upon implantation was performed after opening the skin and was completed on each animal model except the wistar rats with implantation on the tibialis anterior muscle. Intravital imaging was performed by using a Cellvizio system (Mauna Kea Technologies; Paris) equipped with a confocal light path with an excitation wavelength of 488 nm and a collection bandwidth of 505–700 nm. Prior to imaging sessions, animals were anesthetized in an induction chamber using a mixture of isoflurane (0.5-2 %; 3-5 L/min) in 100 % oxygen. During imaging, anaesthesia was maintained with a mixture of ketamine (80 mg/kg) and xylazine (10 mg/kg).

7.11 VISUALIZATION OF CELL VIABILITY

The cell viability in 3D constructs was assessed by the LIVE/DEAD viability/Cytotoxicity assay kit (Invitrogen; #1030166). This two-colour fluorescence cell viability assay is based on a simultaneous determination of living and dead cells with two probes (i) calcein-AM for intracellular esterase activity indicative for living cells and (ii) ethidium homodimer-1 (EthD-1) for plasma membrane integrity indicative for dead cells. After washing with PBS, constructs were incubated in 2 µM calcein AM and 4 µM EthD-1 working solution (2 mM EthD-1 in dimethylsulfoxide (DMSO) [stock solution], further diluted in DPBS with addition of an aliquot of supplied 4 mM calcein AM solution in DMSO [stock solution]) for 45 minutes at RT. Cell viability was evaluated by determining the ratio of green (live) versus red (dead) cells using confocal microscopy (Zeiss LSM710).

7.12 DETERMINATION OF CELL PROLIFERATION

To assess quantitatively the proliferation of C2C12s seeded on chemically cross-linked elastomers, an alamar blue assay was performed. Briefly, cell metabolism was assed at timepoints 0, 2, 4 and 6 days after seeding by adding aseptically resazurin-based stock solution in an amount equal to 10 % of the culture volume ([work solution] 440 uM resazurin sodium salt (Sigma-Aldrich; #199303) in Hank's balanced salt solution (HBSS) without phenol red and serum (Invitrogen)). The cell constructs were incubated for 2 hours in the dark, then alamar blue reagent was transferred to a separate white 96-well microfluor plate (Roche;

#004729692001) and read fluorescently (GloMax-Multi Microplate Multimode Reader; Promega; ex: 560; em: 590). As a negative background control, a non-seeded scaffold control was included in the study design and the according fluorescence measures were subtracted from each sample reading. Negative values after subtraction were defined as zero.

7.13 STATISTICS

All statistics were performed using GraphPad Prism 5; n represents the number of analysed image stacks for microscopic analyses, number of replicates of cell-seeded scaffolds or number of replicates of BAMs. Before comparing data, each continuous variable was tested using the D'Agostino & Pearson omnibus and Shapiro-Wilk normality test to verify the normality of distribution of continuous variables. An unpaired Student t-test was used when two groups were compared. For comparing several normally distributed groups, a one-way analysis of variance (ANOVA) was used with a Bonferroni multiple comparison post-test. For groups that were not normally distributed and/or had unequal variances, a non-parametric Mann–Whitney test was used for comparison between two groups, while the Kruskal–Wallis test followed by Dunn's post-test was performed for multiple comparisons. Data are reported as the mean with standard deviation. Statistical significance was considered to be *$p < 0.05$, **$p < 0.01$, ***$p < 0.001$, NS=not significant.

8 RESULTS

8.1 CHARACTERIZATION OF ISOLATED HUMAN SKELETAL MUSCLE CELLS USING IMMUNOCYTOCHEMISTRY

Prior to all experiments using isolated human skeletal muscle cells, we first characterize the cells in terms of myoblast percentage and fusion capacity. For this thesis, all experiments were based on the same human skeletal muscle biopsy. We assessed by desmin staining that this heterogenous cell population had a myoblast percentage of 71.9 % ± 0.1 % ($n = 5$). This was higher than the requirement of 60 %, a threshold set by the lab (**Figure 7 panel A**). Prior to tropomyosin staining, myoblasts were differentiated to myofibers by exposure to low serum conditions. Myoblasts had a fusion index of 86.4 % ± 16.8 % ($n = 5$) as determined by tropomyosin, which again meets the minimal requirements of 60 % (**Figure 7 panel B**).

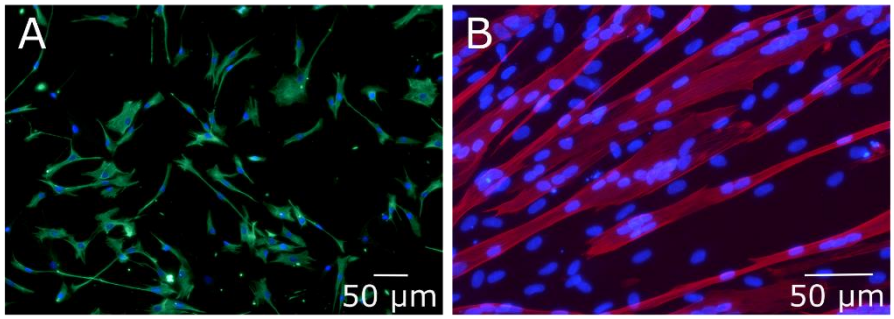

***Figure 7**. Fluorescence microscopy for cell characterization. (A) Myoblast stained for desmin (green). Nuclei stained with DAPI (blue). (B) Myofibers stained for tropomyosin (red). Nuclei stained with DAPI (blue).*

8.2 PRE-VASCULARIZATION OF TISSUE ENGINEERED SKELETAL MUSCLE

8.2.1 Tissue engineering of BAMs

From the aforementioned heterogenous cell population, we created BAMs (**Figure 8**). To make BAMs, a total of 2 million cells were mixed in a fibrin hydrogel (1 mg/ml), an ECM which allows cellular contraction. Standard BAMs composed of aligned myofibers only (**Figure 9 panel A**), are composed of the aforementioned heterogenous cell population. BAMS were cultured in growth medium (SkGM) for 2 days followed by differentiation in low serum

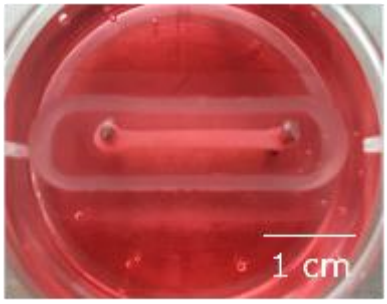

***Figure 8**. Macroscopic image of tissue engineered bio-artificial muscle (BAM) in mold with attachment posts.*

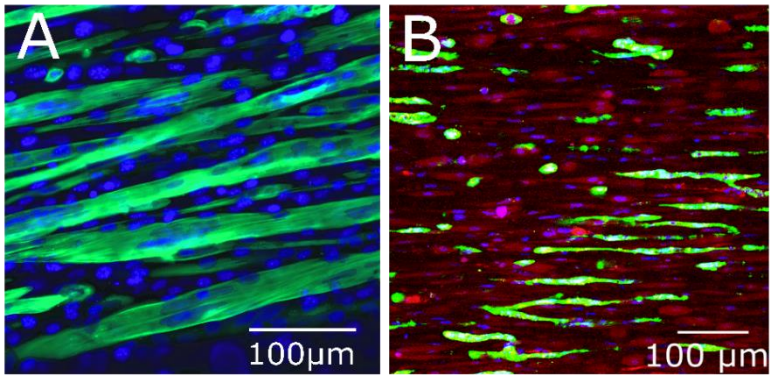

Figure 9. *Fluorescent confocal images of tissue engineered bio-artificial muscle (BAM). (A) Multinucleated myofibers (green) in BAM with 2 million muscle cells cultured in SkGM medium for 2 days followed by differentiation by switching to low serum conditions (SkFM) for an additional period of 5 days. (B) Co-culture BAM with 30 % human umbilical vein endothelial cells (HUVECs) and 70 % muscle cells cultured in EGM-2 for 7 days. Co-culture BAMs were composed of endothelial networks (green)between aligned myofibers (red). Nuclei stained with DAPI (blue).*

conditions (SkFM) for additional 5 days. The cell-ECM mix formed 2-cm-long tissue engineered muscle after contraction of the cell-ECM mix around the fixed attachment points (**Figure 8**). Whereas for co-culture BAMs, composed of endothelial networks and aligned myofibers (**Figure 9 panel B**), HUVECs and muscle cells were mixed in a 30:70 ratio in the same fibrin hydrogel as for the standard BAM. Culture conditions for these co-culture BAMs were adapated to EGM-2 based on earlier work performed in the Thorrez lab (66). Co-culture BAMs display an optimal endothelial network at 1 week after tissue engineering, thereafter degradation of the endothelial networks occurs. Standard BAMs can be maintained for longer periods without affecting myofiber morphology. In this thesis, all BAMs were maintained for 1 week.

8.2.2 *In vivo* graft evolution

To evaluate which implantation site and animal model is best to attain construct survival and host blood vessel ingrowth, co-culture BAMs (**Figure 9 panel B**) were implanted into the abdominal muscle and tibialis muscle of immunocompetent adult rats and into the latissimus dorsi muscle (further defined as the back) of adult immunocompetent Swiss mice, immunodeficient Nu/Nu mice and NOD/SCID mice (**Figure 10**). In order to capture the dynamics of the

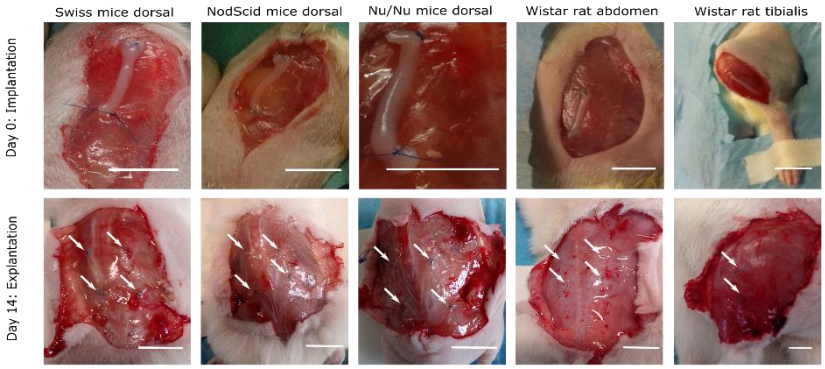

Figure 10. *Macroscopic images of different animal models and implantation sites with results 14 days post implantation. White arrows indicate suture positions of implanted co-culture BAMs. Constructs were present upon explantation only for the swiss mice model with implantation on the latissimus dorsi muscle. Scale bar represents 2cm.*

preformed vessel network, GFP-labelled HUVECs were used. In general, this pilot experiment further enabled us to capture preliminary data on host blood vessel ingrowth, anastomosis and construct survival.

12 days after implantation, small skin incisions were made in all three swiss mice to perform intravital microscopy. Intravital microscopy allowed direct visualization of our pre-established endothelial networks. After 12 days, considerable differences in endothelial network morphology and density were observed showing scattered vessel networks with little remaining GFP-labelled cells (**Figure 11**). The observed reduction in vessel density was present in all three mice, but we were only able to detect 4 out of 6 constructs.

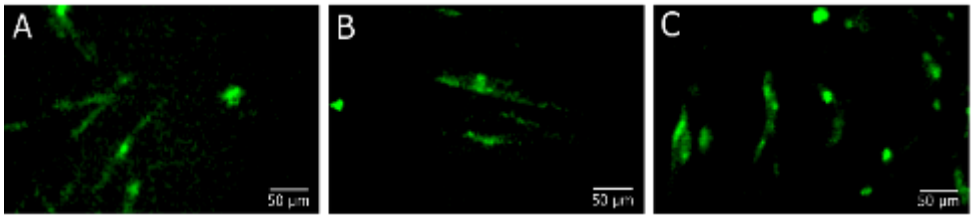

***Figure 11**. Intravital images of GFP-labelled HUVEC derived endothelial networks of co-culture grafts implanted on the latissimus dorsi muscle of adult swiss mice. Images were taken 12 days post implantation. Each panel represent a separate swiss mouse included in the study (n = 3).*

Prior to graft retrieval, at day 14 after implantation, intravital microscopy was performed in each animal model. Opening of the skin allowed us to better visualize the endothelial networks as suture positions could be used as a guidance. For all animal models, except the swiss mice, analysis post implantation was based on surrounding tissue since no grafts were remaining upon graft retrieval (**Figure 10**). *In vivo* morphology of graft microvessels differed between the different animal models (**Figure 12**). For the rat model, intravital images were taken of the surrounding tissue of the constructs because no macroscopic construct was visible. Images solitary showed single GFP-positive cells, indicating a degradation of the networks as observed prior to implantation (*see* **supplementary figure S1**). For the mouse model, we performed

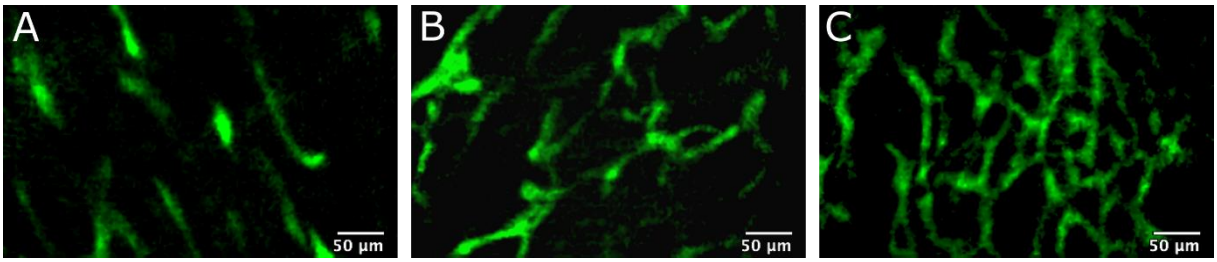

***Figure 12**. Intravital images of co-culture grafts implanted on the latissimus dorsi muscle of mice including GFP-labelled HUVEC derived endothelial network. Images taken 14 days post implantation. A) Swiss mouse model: scattered, little remaining GFP-labelled dots with no remaining interconnected networks. B) NOD/SCID mouse model: highly interconnected GFP-labelled networks. C) Nu/Nu mouse model: identical to the NOD/SCID model showing interconnected dense GFP-labelled networks.*

intravital microscopy on one animal for each mouse strain demonstrating clear differences in the morphology of the endothelial networks compared with the rat model. Although constructs were remaining for the swiss mice, GFP-labelled networks were clearly degraded as compared to the pre-implant since only single non-connected GFP-positive strands remained (**Figure 12 panel A**). Because no macroscopic remaining construct was visible, images from the NOD/SCID and Nu/Nu mice were based on surrounding tissue and both showed interconnected GFP-labelled networks (**Figure 12 panel B and C**).

Images obtained by intravital microscopy were further corroborated by confocal microscopy of explanted tissue. Morphology of these remaining networks were seen to be highly dependent on the animal model being used (**Figure 13**). Only in Swiss mice, 4 out of 6 implanted constructs could be retrieved. However, confocal imaging of the grafts exhibited only loose, scattered endothelial networks indicating a degradation of the networks as compared to pre-implant (**Figure 13 panel A**). Tissue surrounding the grafts implanted on the back, of Nu/Nu (**Figure 13 panel C**) and NOD/SCID mice (**Figure 13 panel B**) showed dense and highly interconnected endothelial networks in all explants of the NOD/SCID mice and in 2 out of 6 explants for the Nu/Nu mice. In rats, confocal imaging of the surrounding tissue of grafts implanted onto both the tibialis muscle and abdominal muscle showed no remnants of GFP-labelled cells (*see* **supplementary figure S2**).

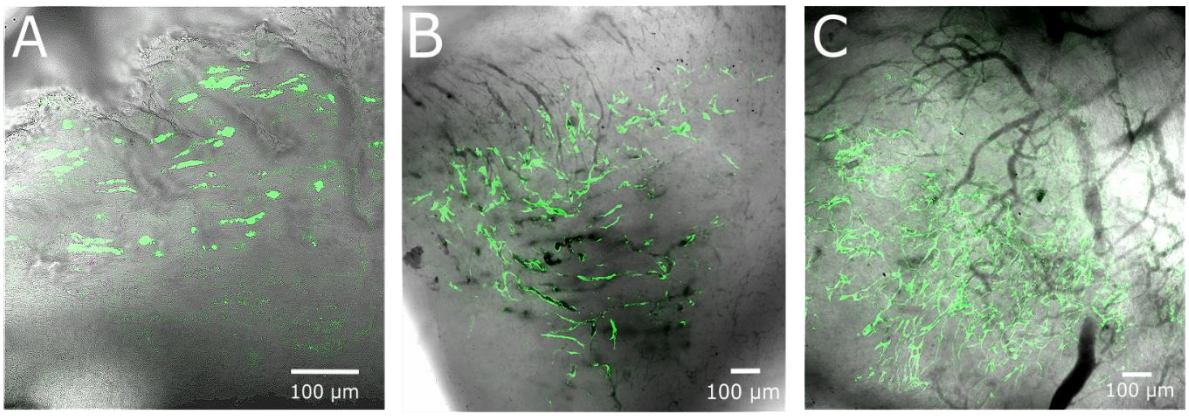

Figure 13*. Immunofluorescence microscopy overlayed with bright field microscopy. Bright field microscopic background allows visualization of host blood vessel presence (black). A) Construct retrieved 14 days post implantation on the back of a Swiss mice showing scattered remnants of GFP-labelled endothelial networks (green). B)Host muscle tissue of a NOD/SCID mouse originating from the location underlying the implantation site. Image shows interconnected GFP-labelled endothelial networks (green) . C) Host muscle tissue of Nu/Nu mice originating from the location underlying the implantation site. Image shows dense highly interconnected GFP-labelled endothelial networks (green).*

5 Minutes prior to sacrificing the mice, rhodamine labelled UEA-I lectin was injected into the tailvein of the host. This lectin specifically labels human endothelial cells which enables us to check for anastomosis. Confocal imaging demonstrated that 2 out of 6 grafts implanted into the NOD/SCID mice were viable, and connected to the host via microvessels as co-localization of the rhodamine and GFP were observed. (**Figure 14**). Furthermore, a number of microvessels

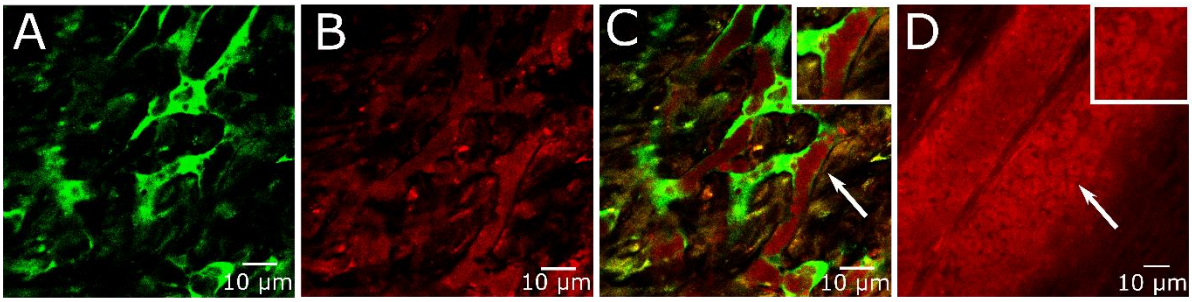

Figure 14. *Confocal images from NOD/SCID mice latissimus dorsi muscle underlying the implantation site of co-culture human BAM 14 days post implantation. (A) GFP-labelled HUVEC-derived endothelial networks (green). (B) Auto-fluorescent red blood cells (red). (C) Merged image of panel A and B demonstrating presence of red blood cells in GFP-labelled endothelial networks. (D) Perfused host blood vessel (red) of NOD/SCID mice present in control muscle apart from implantation site. White arrow indicates region within white square.*

containing red blood cells were observed in the HUVEC-derived vessels which further shows the perfusion of our preformed endothelial network (**Figure 15**). In contrast, no presence of rhodamine labelled UEA I was observed for the Nu/Nu mice despite the interconnected dense networks. Consistent with the morphology of the remaining networks, no proof of perfusion was found for the grafts implanted in the rat models or swiss mice.

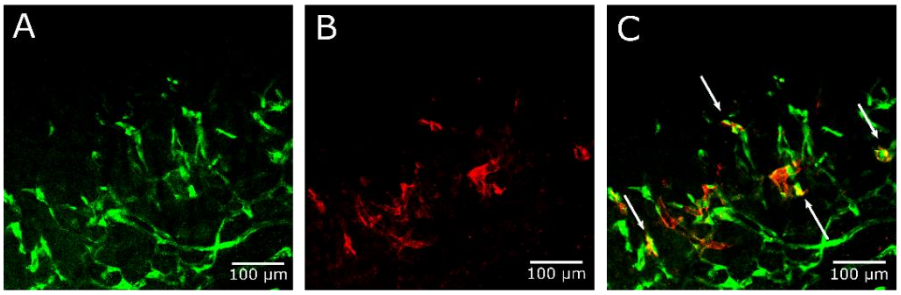

Figure 15*. Evidence for perfusion and connection with host microvessels of HUVEC networks in NOD/SCID mice. Confocal image from host tissue underlying implantation site of co-culture human BAM. (A) GFP-labelled HUVEC-derived endothelial networks 14 days post implantation (green). (B) Rhodamine labelled UEA-I staining of human endothelial cells (red). (C) Merged image of panel A and B. Co-localization of green and red staining is indicated by the white arrows.*

We examined myofiber survival within the explanted grafts present for the swiss mice through myosin heavy chain staining (MF20). While the initially implanted construct was composed of ordered and closely arranged myofibers, the explanted construct presented no indication of remaining human myofibers. For all other models, we were unable to differentiate

human myofibers from the host myofibers since antibodies specific for human myofibers do not exist. Staining of host tissue indicated the presence of only mature myofibers, likely all derived of the host, since human myofibers would display more embryonic features such as a smaller diameter and lack of cross striations.

8.2.3 Determining optimal endothelial cell type and medium conditions for the establishment of a pre-vascularized tissue engineered skeletal muscle

Aiming at the establishment of aligned myofibers with interspersed endothelial networks, a co-culture BAM containing HUVECs and muscle cells in a fibrin ECM was developed previously (66). We next aimed to enhance the co-culture conditions in this 3D tissue engineered muscle in terms of myofiber formation as well as endothelial network formation. Therefore, two approaches were explored simultaneously. First, we aimed to explore and compare 2 different endothelial cell (EC) types: HUVECs versus skeletal muscle microvascular endothelial cells (SkMVECs). Besides, we aimed to define an optimal medium which serves as an ideal trade-off for both cell types in the co-culture. Three types of media were compared (i) Ultroser based skeletal muscle growth medium (SkGM) with consecutive differentiation after 2 days in skeletal muscle fusion medium (SkFM), (ii) EGM-2 or EGM-MV both of which are the optimal culture medium for HUVECs and SkMVECs respectively or (iii) M199-EGM .

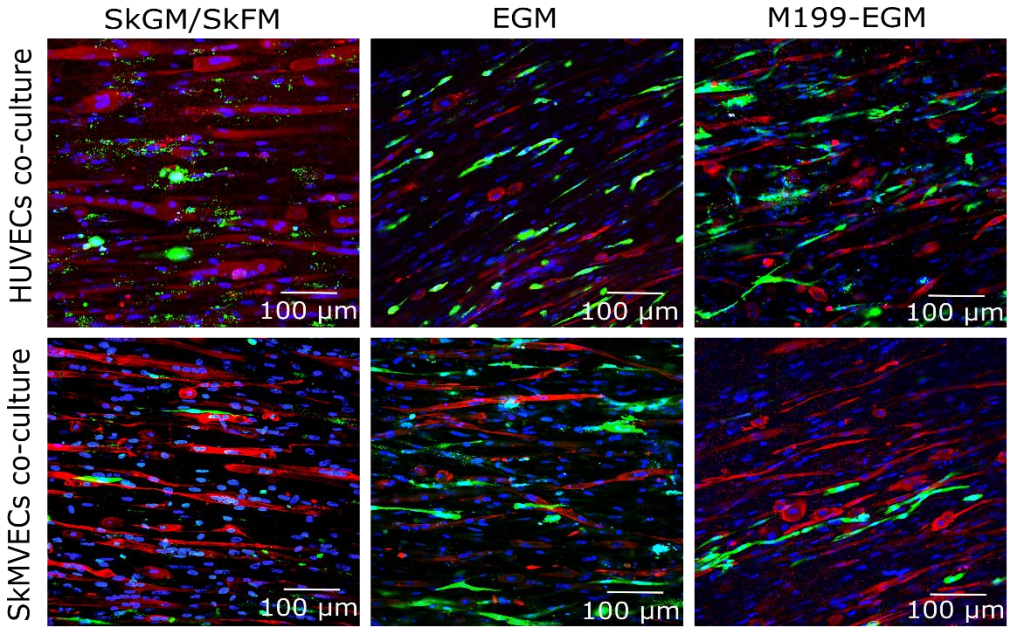

Figure 16. *Confocal imaging of BAMs cultured based on different co-culture conditions. GFP-labelled endothelial networks (green). Nuclei stained with DAPI (blue). Myofibers stained with tropomyosin (red). Replicates for each conditions was 3 (n = 3).*

Whole-mount tropomyosin staining was performed to visualize the extent of myofiber formation within the co-culture BAM (**Figure 16**). We first characterized the co-culture BAMs with 30% HUVECs. Myofiber formation in terms of length and density was found to be significantly better when cultured in the skeletal muscle medium. The number of myofibers was lowest when cultured in M199-EGM medium. However, the diameter of the formed myofibers

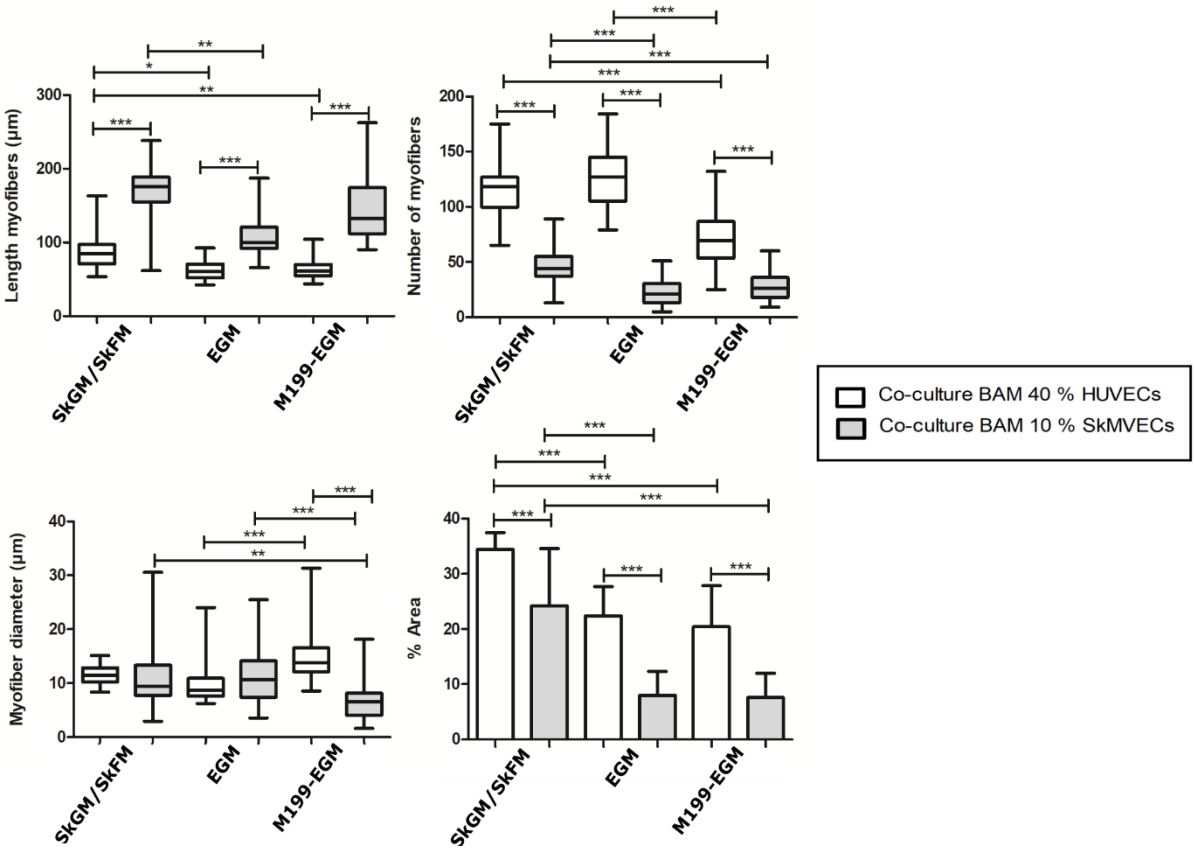

***Figure 17**. Media effect and endothelial cell type effect on myofiber formation. Comparison of myofiber parameters as measured in ImageJ. Myofiber formation characterized quantitatively by myofiber length, number of myofibers, myofiber diameter and myofiber density. Number of z-stacks analysed per conditions was (n = 3).*

was found to be significantly higher for the co-culture BAMs cultured in M199-EGM medium compared to EGM-2. In terms of length of myofibers and density of myofibers, EGM-2 and M199-EGM were found to be similar. Over the different myofiber formation parameters, culturing in skeletal muscle growth medium followed by skeletal muscle fusion medium was found to enable optimal myofiber formation (**Figure 17**).

The same parameters for myofiber differentiation were assessed in parallel for co-culture BAMs containing 10 % SkMVECs. Consistent with the data from the co-culture BAMs with 30 % HUVECs, the skeletal muscle growth and differentiation medium was seen to result in significantly longer myofibers which were packed significantly more dense compared to the

culture condition in EGM-MV medium. Also the number of myofibers per analysed microscopic field was found to differ significantly between the two aforementioned culture conditions, with a higher number when cultured in the skeletal muscle medium. Across all culture conditions, the skeletal muscle medium was found to result in significantly higher number of myofibers consistent with a higher density. Culturing in M199-EGM was found to perform equally well in terms of length, density and number of myofibers compared to the EGM-MV culturing condition. However, a significant difference in terms of diameter of the obtained myofibers was found, with significantly thicker myofibers when cultured in the EGM-MV compared to the skeletal muscle medium. This is in contrast with the results obtained from the co-culture BAMs consisting of 30 % HUVECs in which no significant differences in terms of diameter of the myofibers was found except for the culture conditions in EGM-2 versus M199-EGM (**Figure 17**).

In addition, an optimal medium would enhance the endothelial network formation as well (**Figure 16**). In the co-culture BAMs consisting of HUVECs and muscle cells, the EGM-2 and

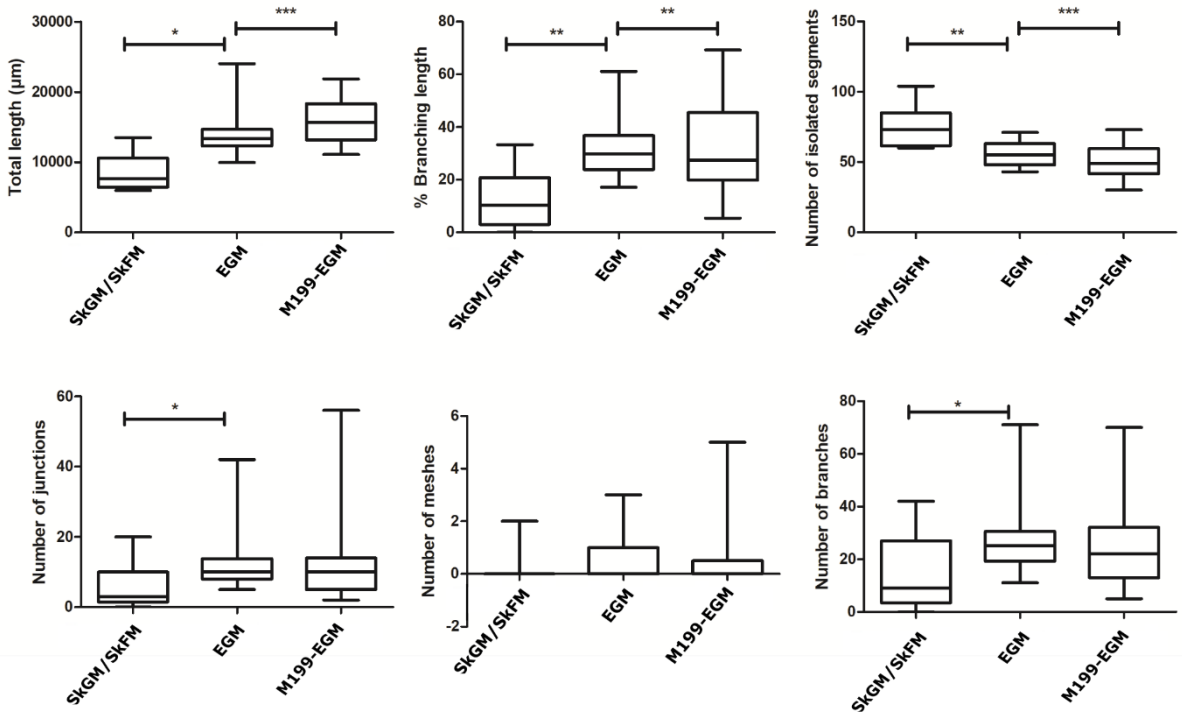

***Figure 18**. Media effect on endothelial network formation in fibrin (1mg/ml) co-culture BAMs with 30 % HUVECs. Comparison of endothelial network parameters as measured by a customized version of the Angiogenesis Analyzer, an ImageJ plugin created by Gilles Carpentier. Endothelial network formation characterized quantitatively by total length, percentage branching length, number of isolated segments, number of junctions, number of meshes and number of branches. Number of z-stack analysed per condition was 3 (n = 3).*

M199-EGM were found to perform equally well in terms of endothelial network formation. In these BAMs, the total length of the endothelial networks was significantly higher compared to the culture conditions using the skeletal muscle growth and fusion medium. Furthermore, endothelial networks were found to be highly interconnected which was reflected by significantly lower number of isolated segments throughout the BAM in comparison with the BAMs cultured in the skeletal muscle media. Also, the percentage branching length was significantly lower compared to the EGM-2 and M199-EGM culture conditions. This indicates again that endothelial network formation is enhanced when cultured in EGM-2 or M199-EGM. Significant differences compared to the skeletal muscle medium in terms of number of junctions and branches was additionally found for the culture medium EGM-2 but not for the M199-EGM (**Figure 18**). Quantitative data on the effect of different culture conditions on endothelial network formation for co-culture BAMs consisting of SkMVECs and muscle cells (collaboration with Gilles Carpentier) had not been received at the time of finalizing this thesis.

8.3 SCAFFOLD-BASED SKELETAL MUSCLE TISSUE ENGINEERING

8.3.1 Elastomeric scaffold-based skeletal muscle tissue engineering

8.3.1.1 Cell metabolism on chemically cross-linked elastomeric scaffolds

Biocompatibility of elastomeric scaffolds (*see* **supplementary figure S3**), polymerized from glycerol, xylitol, sebacic acid and citric acid was assessed over time. Therefore, C2C12 myoblasts suspended in a fibrin hydrogel were seeded in a porous scaffold based on these cross-linked elastomers. Prior to seeding pre-wetting treatment with 70 % ethanol was performed (*see* **supplementary figure S4**). Cellular metabolism was measured based on the alamar blue assay (**Figure 19 panel C**). In addition, cell survival was measured based on fluorescence microscopy analysis after live/dead staining at day 7. Living cells were stained green with membrane permeable calcein AM and dead cell were stained red by membrane impermeant ethidium homodimer-1. The percentage of live cells seeded on each elastomer further provides information on C2C12 viability (**Figure 19 panel A and B**). Because of the low cell proliferative capacity consistent with a low percentage of calcein AM-positive cells, poly(xylitol sebacate) (PXS) in a 1:1 molar polyol to sebacic acid ratio was excluded for further experiments. In contrast, fluorescence values obtained from cells seeded on PXS 1:1.25 showed that cells proliferated effectively. The morphology and cell viability were consistent with the observations for PXS 1:1.25 indicating no evidence of cytotoxicity. Higher molar ratios, PXS 1:2 and PXS 1:2.5, enabled a good initial proliferative capacity but seems to impart cytotoxicity

at 4-6 days in culture. Citric acid was mixed with PXS 1:1 and PXS 1:2 to obtain poly(xylitol sebacate citrate) (PXSC) 1:1 and PXSC 1:2 respectively. Metabolic activity was greater on PXSC 1:1, since PXSC 1:2 shows a decrease in metabolic activity although it initially shows a similar raise as seen for the PXSC 1:1.

The results from both the alamar blue and live/dead assay show that poly(glycerol sebacate) (PGS) 1:1 and poly(glycerol sebacate citrate) (PGSC) 1:1 scaffolds are able to maintain cell survival and metabolism of C2C12 myoblasts. For each scaffold the percentage of viable cells (in green) was very high and ranged between 90-95 % viability. Dead cells in the live/dead assay were shown as small dots stained in red but were negligible for both glycerol based elastomers. Based on the aforementioned results, following 4 elastomers were selected for

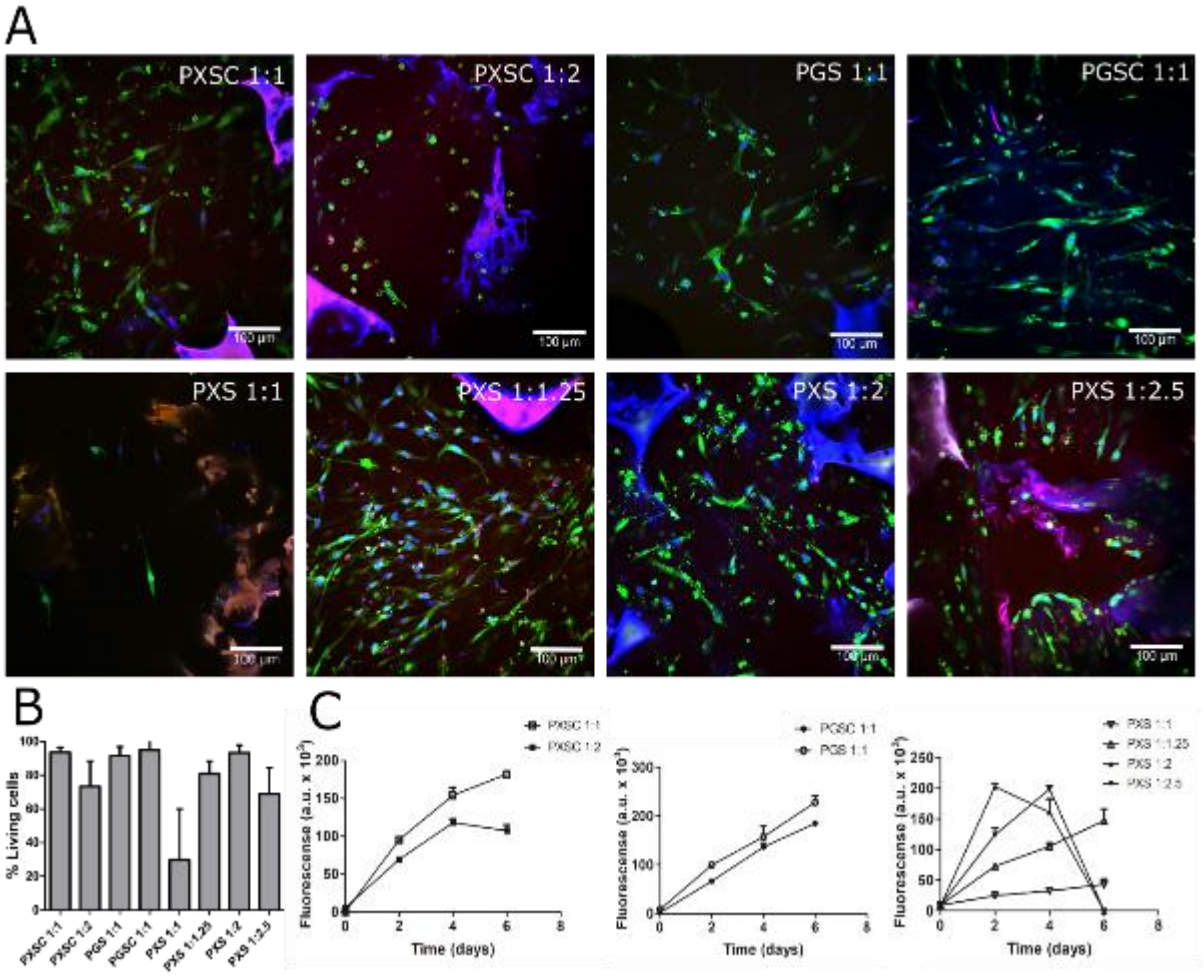

***Figure 19**. (A) The viability of C2C12 myoblasts, cast with a density of 200.000 cells per ml fibrin hydrogel on the different elastomer scaffolds, was observed by live (green)/dead (red) assay followed by confocal microscopy at day 7 post seeding. (B) Quantitative representation of the viability assay. Number of images analysed for each different elastomer scaffold was 5 (n = 5). (C) Alamar blue assay for cellular metabolism of C2C12 myoblasts measured at day 0, 2, 4 and 6. Results normalized to a non-seeded scaffold control which served as a negative background control. Negative values after subtraction were defined as zero. Number of replicates of seeded scaffold for each different elastomer scaffold was 3 (n = 3).*

further alamar blue and live/dead validation studies using a new batch of elastomers: PXS 1:1.25, PXSC 1:1, PGS 1:1 and PGSC 1:1.

8.3.1.2 Differentiation of human muscle cells on poly(glycerol sebacate) scaffolds in vitro

To assess the effect of elastomeric scaffold integration on myofiber formation, 5 x 10^6 human muscle cells were seeded on a 0.5 cm^3 scaffold. Prior to seeding, scaffolds were treated with 70 % ethanol. The aim of this experiment was to generate preliminary data on myoblast differentiation capacity when integrated in the scaffold. For this experiment, we selected the poly(glycerol sebacate) scaffold with a 1:1 acid-alcohol molar ratio and a porosity introduced by mixing the prepolymer with NaCl in a 1:7 weight ratio. Human muscle cells were first mixed with 125 µl fibrinogen (2 mg/ml) and 125 µl thrombin (4 U/ml) and quickly applied on top of the scaffolds which were positioned in a silicon coated well-plate. This method of cell seeding allowed for quick penetration of the cell-fibrin mix in the interconnected scaffold pores. After gelation, the cell-seeded scaffold was flooded with SkGM and maintained in this medium for 2 days. After 2 days, medium was changed to differentiation medium (SkFM) and maintained for an additional 5 days. We also evaluated cell seeding in the muscle growth medium (SkGM), without fibrin. Cells were resuspended every 30 minutes but this protocol resulted in precipitation of the cells on the bottom of the well.

From confocal imaging performed after staining for the differentiation marker tropomyosin, we observed efficient differentiation into myofibers throughout the scaffold. Seeded cells formed myofibers with an average diameter of 12.8 µm and length of 92.3 µm (**Table 1**).

Myofiber parameter	Values (n = 3)
Myofiber length (µm)	92.3 ± 22.9
Myofiber diameter (µm)	12.8 ± 7.0
% Area	9.7 ± 4.8
Misalignment factor	42.7 ± 7.2
Nuclei per myofiber	3.6 ± 0.5

Table 1. *Quantitative evaluation of myofiber formation within poly(glycerol sebacate) 1:1 scaffold as assessed with ImageJ. Myofiber formation parameters characterized by myofiber length, number of myofibers, misalignment factor, myofiber diameter, nuclei per myofiber and myofiber density. Number of z-stacks analysed was 3 (n = 3).*

Differentiation was further characterized by the number of nuclei per myofiber for which the average number was 3.6 nuclei. As expected based on the scaffold structure, resulting myofibers did not exhibit any specific directionality. With confocal microscopy we could image the top 100 µm of the scaffold. In this range, we examined fiber density in 5 volumes of 20 µm depth. Average fiber density was 9.7 %, but fiber density decreased from the surface layers to the deepest layers of the scaffold (**Figure 20**).

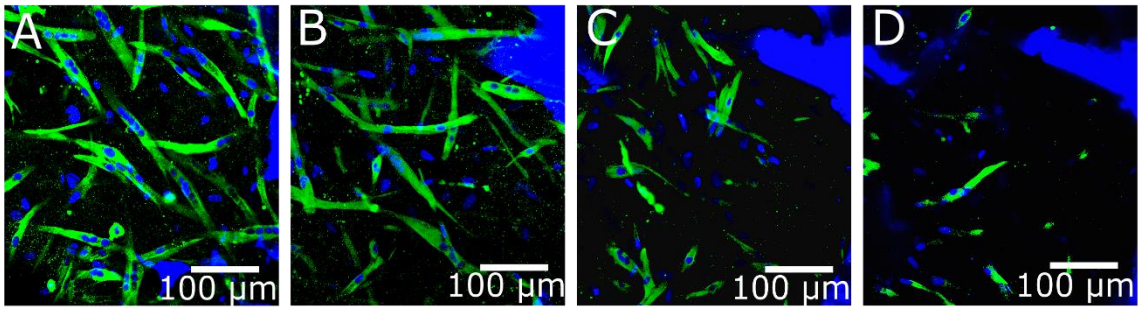

Figure 20. *Impact of poly(glycerol sebacate) 1:1 scaffold integration on myoblast differentiation into myofibers. (A-D) Serial confocal sections of tropomyosin stained myofibers (green) derived from human myoblasts within a fibrin hydrogel seeded on 0.5 cm^3 elastomeric PGS 1:1 scaffold. (A) Section at 5 µm depth. (B) Section at 35 µm depth. (C) Section at 65 µm depth. (D) Section at 95 µm depth. (A-D) Decreasing fiber density from surface layers to the deepest layers of the scaffold. Nuclei stained with DAPI (blue).*

8.3.2 Polycarbonate scaffold-based skeletal muscle tissue engineering

8.3.2.1 Differentiation of human muscle cells on polycarbonate scaffolds in vitro

To assess the impact of integration of the electrospun polycarbonate scaffold (*see* **supplementary figure S4**) in our standard scaffold-free BAM model, 2.5 x 10^6 cells were seeded on 0.25 cm^2 scaffolds positioned into silicon coated well-plates. Prior to seeding, cells were mixed with 125 µl fibrinogen (2 mg/ml) and 125 µl thrombin (4 U/ml) and quickly applied on top of the scaffolds. The hydrophobic nature of the scaffold resulted in a lack of penetration

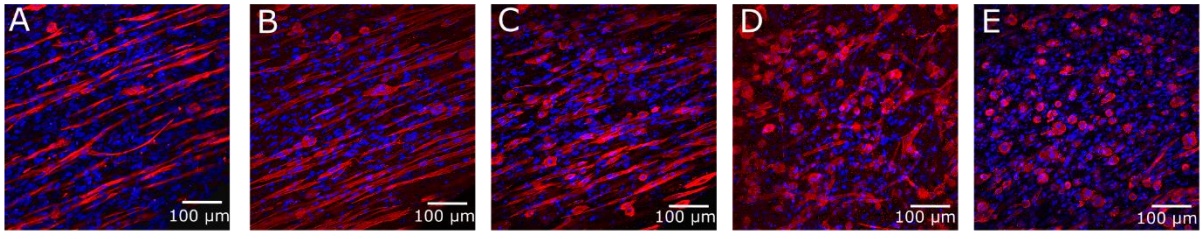

Figure 21*. Impact of polycarbonate scaffold integration on myoblast differentiation into myofibers. (A-E) Serial confocal sections of tropomyosin stained myofibers (red) derived from human myoblasts within, a fibrin hydrogel seeded on square pieces of 0.25 cm^2 polycarbonate scaffold. (A) Section at 5 µm depth. (B) Section at 15 µm depth. (C) Section at 25 µm depth. (D) Section at 35 µm depth. (E) Section at 45 µm depth reaching the polycarbonate scaffold layer. (A-C) Top layers of polycarbonate-based BAM are composed of long postmitotic muscle fibers positive for sarcomeric tropomyosin. (D-E) Range of 0-20 µm away from the scaffold primarily shows short myofibers with lower number of nuclei per myofiber compared to the top layers. Nuclei stained with DAPI (blue).*

of the cell-gel mix through the fibers leading to cell-mediated gel compaction only at one side of the scaffold. As the scaffold material had different topographical features at both sides (*see* **supplementary figure S5**), the experimental set-up was adapted to evaluate both sides. In subsequent experiments, scaffolds were positioned onto a droplet of the cell-gel mix (½ total volume) which was allowed 10-15 minutes to gel, before adding the remaining cell-ECM mix on top of the positioned scaffold. This approach resulted in a layer of cell-ECM mix at both sides of the scaffold (*see* **supplementary figure S6**). Scaffolds were incubated for 2 days in growth medium to allow proliferation of the seeded myoblasts before switching to differentiation medium for an additional 4 days, identical to the incubation of our standard scaffold-free BAM. With this technique, the formation of an approximately 50 µm thick layer of differentiated myoblasts within the fibrin ECM was obtained on the surface of the scaffold at both sides.

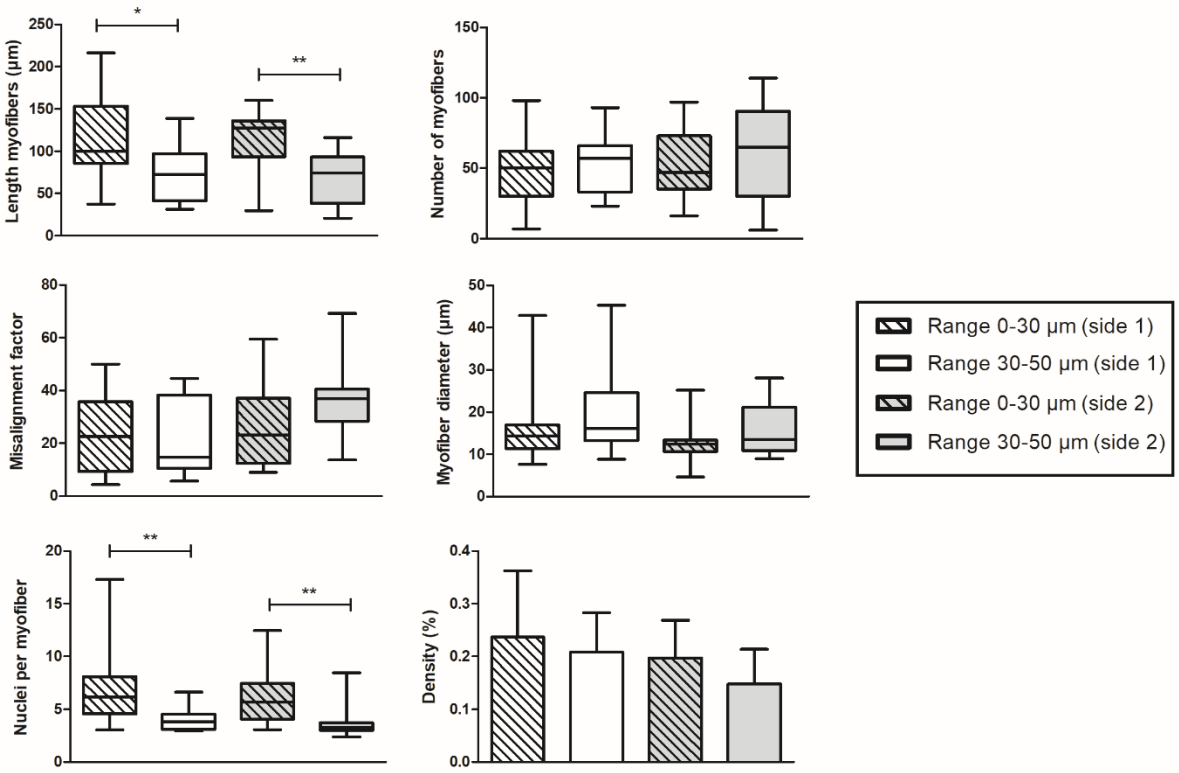

***Figure 22**. Effect of polycarbonate scaffold integration on myofiber formation. Quantitative evaluation of myofiber formation as assessed with ImageJ. Myofiber formation parameters characterized by myofiber length, number of myofibers, misalignment factor, myofiber diameter, nuclei per myofiber and myofiber density. The top layer (range 0-30 µm) contains significantly longer post mitotic muscle fibers compared to the 20 µm range close to the scaffold (range 30-50 µm). Myofiber differentiation, defined by nuclei per myofiber, also differ significantly between both ranges, with significantly higher number per myofiber for the 0-30 µm range. No significant differences in terms of myofiber formation were found between the two sides of the scaffold material. Number of z-stack analysed was 3 (n = 3) for each replicate (n = 3).*

Parallel with the 3D culture, a 2D fusion assay was performed to assess differentiation capacity into myofibers of the myoblasts being used (**Figure 7**). To determine the impact of scaffold integration on the myoblast differentiation into myofibers, immunostaining of the differentiation marker tropomyosin was monitored by confocal imaging (**Figure 21**). Top layers of the polycarbonate-based BAM primarily showed long post mitotic muscle fibers positive for sarcomeric tropomyosin with no significant difference between both sides of the scaffold (**Figure 22**). The myofibers were found to be aligned to a certain extent in some regions, whilst showing no specific directions in other regions at the same depth. This variability throughout different regions within the same BAM was seen for all replicates at both sides.

Fiber length decreased from the surface of the polycarbonate-based BAM towards the scaffold fibers itself with significantly shorter myofibers at 0-20 µm distance from the scaffold fibers compared to the top layers of the polycarbonate-based BAM. Myofiber differentiation was better at the top layers of the polycarbonate-based BAM as these myofibers contained a significantly higher number of nuclei per myofiber (6.72 ± 3.32 (side 1); 6.22 ± 2.70 (side 2), n =9) compared with those myofibers within 0-20 µm away from the scaffold (4.04 ± 1.06 (side 1); 3.64 ± 1.40 (side 2), n = 9). Further comparison of the myofiber formation between the top layers and the 20 µm range from the polycarbonate fibers in terms of diameter and number of formed myofibers showed no significant differences. In addition, myofiber alignment did not differ significantly between both ranges being compared (**Figure 22**).

8.3.2.2 Culture and compatibility on polycarbonate scaffolds

Favouring cell integration is a critical step when aiming to apply three-dimensional matrices into our tissue engineering method. From the confocal images, cells were observed within the polycarbonate fibers. These fibers can be visualized in the blue channel based on auto-fluorescence. This indicates proper scaffold integration in our BAM model despite the hydrophobicity of the scaffold material (**Figure 23**). Cells were embedded in a fibrin

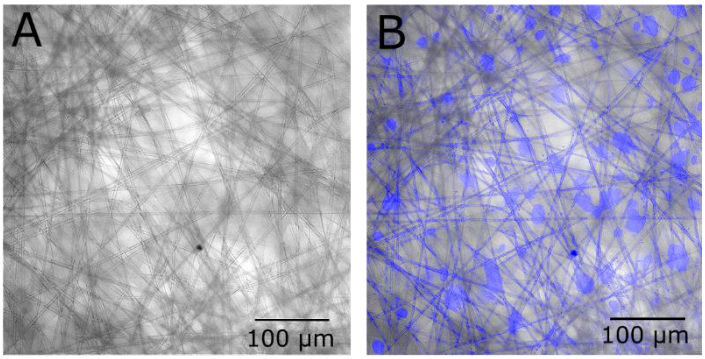

***Figure 23**. A) Light microscopic image of electrospun polycarbonate fibers. B) Confocal microscopic image of cell presence within the electrospun polycarbonate fibers (blue). Nuclei stained with DAPI as well as auto-fluorescent polycarbonate fibers (blue).*

hydrogel. Therefore, based on these images we can conclude that with our approach cells could reach all spaces including regions in between polycarbonate fibers.

In addition, cell survival and morphology was assessed using a live/dead assay to determine whether differences in survival and morphology contributed to the differences in differentiation. The percentage of living cells was assessed at various depths throughout the BAM with confocal microscopy (**Figure 24**). At the surface layers of the polycarbonate-based BAM, many living cells could be observed which is in accordance with the observed myofiber formation. At 30-50 µm depth, many dead cells were observed and between the polycarbonate fibers exclusively dead cells were seen.

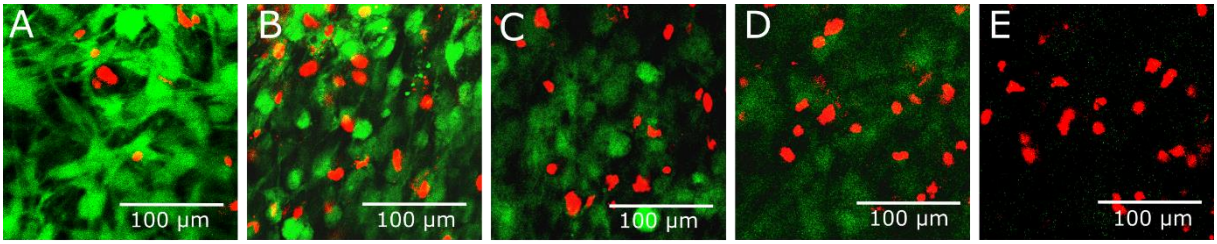

Figure 24. *Cell survival of human myoblasts seeded within fibrin hydrogel as assessed with live/dead assay. (A-E) Serial confocal sections of live (green) and dead (red) myoblasts. (A) Section at 5 µm depth. (B) Section at 15 µm depth. (C) Section at 25 µm depth. (D) Section at 35 µm depth. (E) Section at 45 µm depth between polycarbonate fibers. (A-C) The top layers of polycarbonate-based BAM show that the majority of cells was alive. (D-E) Range of 0-20 µm from the scaffold primarily shows dead cells.*

9 DISCUSSION

At present, the use of transplants to treat volumetric muscle loss has significant drawbacks. Tissue engineered skeletal muscle holds promise for an alternative treatment. In the Thorrez lab human bio-artificial muscles are created by a scaffold-free technology where myofibers self-organize resulting in a soft tissue (70,169). Still, many challenges towards clinical as well as *in vitro* testing applications remain. In this thesis, we explored several ways to tackle some of these challenges.

A first challenge is vascularization, needed for creation of larger tissue constructs. The current size limitation, due to the passive diffusion limit, impedes the potential for human muscle transplantation as well as physiologically relevant *in vitro* systems. Prevascularization is being explored as a method to allow *in vitro* perfusion and enhance *in vivo* survival of tissue-engineered constructs (170–172). In the Thorrez lab, networks of endothelial cells within the tissue-engineered muscle have been developed, resulting in aligned multinucleated myofibers with interspersed endothelial networks (66). However, data on maintenance and functionality of these networks were not known by the start of the present work. In this thesis, we investigated the evolution and potential anastomosis with host blood vessels of these endothelial networks through *in vivo* implantation studies.

We created *in vitro* co-culture BAMs composed of 30 % HUVECs. After 1 week *in vitro,* these BAMs were implanted for 2 weeks in adult immunodeficient NOD/SCID mice, immunodeficient Nu/Nu mice, immunosuppressed Swiss mice and immunosuppressed Wistar rats. In the NOD/SCID mouse model we provide evidence for connection of the HUVEC-derived networks with host vessels through two distinct microscopic observations. First, red blood cells were observed in HUVEC derived endothelial networks. Second, these networks were found positive for a human endothelial cell specific lectin which was administered to the host intravenously. These findings are in line with previous studies where a stable stacked cell sheet construct composed of HUVECs and human myoblasts was obtained through a 3D cell sheet manipulation system (65). In this study, anastomosis was observed by week 1 upon subcutaneous implantation on dorsal tissues of nude rats. However, constructs were only 5 cell layers thick and did not contain myofibers. In our work, both Nu/Nu and NOD/SCID mice showed similar highly interconnected endothelial network morphology. Although remaining endothelial networks in the Nu/Nu mice were more dense compared to the NOD/SCID mouse model, networks were only retrieved for 2 out of 6 explanted tissues.

In the rat model we found no macroscopic nor microscopic evidence of remaining human cells and construct. Based on these results we concluded that the rat is not a good animal model for our set-up. Two underlying mechanisms may explain this tissue loss. First, we cannot exclude a remaining immunological response against the xenogeneic human transplant, although immunosuppressant drugs were administered. Differences in NK cell response have been reported in mice versus rats so a more pronounced NK cell activity may have occurred in rats (173). Second, the rate of resorption *in vivo* of fibrin may differ between rats and mice.

Only the BAMs implanted in the Swiss mice could be macroscopically observed and retrieved after 14 days. However, in these mice, the endothelial networks were more degraded as compared to the other mouse models. Delay in mural cell recruitment from the host tissue might have resulted in the observed regression (174). Blood vessels composed of only endothelial lining regressed more rapidly as compared to the ones that are matured with a layer of pericytes or multiple smooth muscle cell layers (175). Therefore, optimizing the co-culture through addition of other cell populations such as pericytes opens perspectives towards stabilizing the endothelial networks (176,177).

Next to assessing potential anastomosis, the objective of the implantation experiments was to determine whether the myofibers of the prevascularized BAM remain viable *in vivo*. No evidence was found for any of the *in vivo* models for remaining human myofibers. Although we concluded from previous work that the presence of HUVECs does not impair the formation of myofibers we do see some limitations. While maturation of myofibers is enhanced upon culture duration of 2 weeks, HUVEC-derived endothelial networks start to degrade after 1 week *in vitro*. Also culture medium used in co-culture BAMs interferes with myofiber formation. From the *in vivo* pilot experiment we cannot exclude myofiber immaturity being the cause for the lack of myofiber maintenance. Therefore, follow-up experiments should be performed with myofiber only BAMs obtained after a prolonged culture of 2 weeks *in vitro* instead of 1 week. Additionally, we could also induce a necrotic stimulus upon scratching the fascia, since a necrotic stimulus was found to increase myogenesis (178).

Degradation of the BAM occurred rapidly. Still, fibrin-based materials remain attractive as ECM of choice since both *in vivo* (179) and *in vitro* (180) studies have shown a positive effect in stimulating vascularization. Further, optimizing our hydrogel-based muscle constructs by varying matrix protein composition and concentration may address this limitation. Hinds et al. defined 4 mg/ml fibrin with 40 % Matrigel as the optimal matrix composition for myofiber function (125). Adapting our 1 mg/ml fibrin hydrogel to these findings might help to prolong the presence of fibrin. However, it remains to be seen whether this would interfere with the

endothelial network formation and mural cell recruitment. In previous work of the lab, addition of Matrigel did not enhance myofiber nor endothelial network formation (66).

Regarding the rapid degradation, reinforcement with synthetic polymers has been explored. Composite hydrogels may indeed add value to our current approach by promoting vascularization with fibrin while delaying degradation. PEG-based hydrogels have been investigated for a number of tissue engineering applications and can be used to generate a fibrin loaded porous PEG hydrogel. These composite materials showed delayed fibrin breakdown while supporting tissue invasion and vascular network formation *in vivo* (181). Another strategy to prolong the life of fibrin matrices is the addition of protease inhibitors such as aprotinin. To avoid rapid diffusion out of the fibrin matrices, an engineered aprotinin variant that covalently binds to fibrin during gel formation has been developed (182). This approach might be of use for our setup as aprotinin-protected fibrin matrices were still detectable *in vivo* at day 24 while fibrin was no longer detectable by day 10 when using no protease inhibitor. We observed construct degradation by 14 days, which is in line with these findings.

Based on the preliminary data obtained from the *in vivo* studies, optimization studies were performed to further define an optimal co-culture condition in terms of medium composition and EC type to enhance both endothelial and myofiber formation. Interactions between ECs and myogenic precursor cells have been discussed by many researchers (183,184). Inversely, also myogenic cells have been linked to proangiogenic activity, for which VEGF seems to play an important role (185). But, combining different cell types presents a challenge regarding culture conditions underscoring the need for further defining optimal co-culture conditions (186).

Our data from co-cultures containing both muscle cells and endothelial cells further underscored the difficulties in defining the optimal trade-off for both cell types. As expected, skeletal muscle growth and differentiation media enable optimal myofiber formation, but these culture conditions strongly interfere with endothelial network formation. Current culture conditions rely on EGM-2 as it enabled endothelial network formation while still allowing myofiber formation (66). However, we reported an impaired myofiber formation when compared to culturing in SkGM/SkFM (66), supported by others who found that EGM allowed only 2% of muscle cells to express myogenin (170). Addition of embryonic fibroblasts promoted vascularization of the engineered muscle (170). These findings can explain why EGM-2 culture conditions in our approach did not impair myoblast formation as much as we start from a heterogenous cell population containing fibroblasts. Still, optimizing the fibroblast

ratios in our co-culture condition may be useful as well as further defining optimal co-culture conditions (187).

Since myofiber information was still suboptimal compared to standard BAMs, we explored the use of a medium which had never been tested in this context and which we defined as M199-EGM. In HUVEC myoblast co-cultures, M199-EGM was found to result in a larger myofiber diameter. Further experiments can be conducted to evaluate the number of nuclei per myofiber. Also for endothelial network formation, M199-EGM was better than EGM-2 and both were found to be superior to skeletal muscle medium.

Although HUVECs are widely used as endothelial cells for research, the endothelial cells which are present in native muscle are skeletal muscle microvascular endothelial cells (SkMVECs). Therefore we additionally assessed endothelial networks and myofiber formation in co-culture BAMs using SkMVECs. For all culture conditions, myofiber differentiation was improved when using SkMVECs as compared to HUVECs. The relative ratio of endothelial cells versus myoblasts was different (10% SkMVEC vs 30% HUVEC) to obtain optimal endothelial network formation, based on earlier work in our lab. Therefore, myofiber density and number of myofibers per microscopic field could not be directly compared. Future experiments should be conducted with similar ratios to properly compare both cell types. Also the differences observed in density could be linked to the extent of contraction of the cell-fibrin hydrogel to ensure that differences found in density are not due to altered contraction.

Skeletal muscle tissue engineering approaches should take the hierarchical structure of native skeletal muscle tissue with all its different components (188) into account. We focussed in this thesis on the vasculogenesis of constructs. We simulated vascular growth *in vitro* without scaffolds, permitting unimpeded growth of endothelial vascular networks within a fibrin hydrogel. Nonetheless, scaffolds have been used to obtain networks as well, showing particular promise for scaffolds with uniform geometry such as interconnected pores in facilitating the vascularization process (170). Scaffolds can be used instead of (or in parallel with) hydrogels, to provide a spatially organized template and initial mechanical strength to the construct. However, scaffold architecture often interferes with appropriate myofiber formation. Indeed, the organisation of myoblasts into muscle fibres must occur in an ordered way to obtain myofibers oriented in parallel to each other to generate sufficient force for contraction (189). Several attempts have been made so far and succeeded indeed in driving myofiber formation in an oriented way (190,191). However, these reports were largely based on work with the murine C2C12 myoblast cell line, while our work is based on human myoblasts (191). When human satellite cells were used, the polynucleated myotubes were myosin negative (190). Furthermore,

many scaffolds explored in the field of tissue engineering suffer from disadvantages such as inappropriate degradation rates, release of acidic by-products or high tensile modulus (192,193).

Our tissue engineering approach is distinct from most other muscle tissue engineering methods, as we obtain parallel oriented myofibers in a scaffold-free approach, whereas many other approaches obtain randomly oriented myotubes especially when scaffolds are introduced. Therefore, it was not entirely clear whether scaffolds would be of benefit in our SMTE approach. Because of desirable characteristics of scaffolds mainly related to mechanical strength, we explored the use of scaffolds in our model and determined the impact of this integration on myofiber differentiation and alignment. In addition, the use of scaffolds with predefined pores might be beneficial to allow for medium perfusion as an alternative for our vasculogenesis strategy.

A first scaffold we explored was a biodegradable polycarbonate scaffold with randomly oriented fibers obtained through electrospinning. This scaffold was obtained from collaborators who were extensively studying meshes made from this polycarbonate for potential application in the context of prolapse treatment. Their initial findings identified the polymer material as being biocompatible. Furthermore, their *in vivo* experiments were based on an abdominal wall defect model which is a valuable model for our research aims as well (194). Based on the similarity in terms of experimental set-ups and their initial findings on biocompatibility, we evaluated this biomaterial in the context of SMTE.

Although this type of electrospun scaffold had a hydrophobic nature, we were successful in proper integration with the fibrin hydrogel. However, when we analyzed myofiber differentiation and alignment, both quantitative and qualitative data clearly illustrated the decreasing differentiation in the region close to and in between the scaffold fibers. Also, cell survival data suggested cell survival increasing in function of the distance to the scaffold. The discrepancy between our findings and those of our collaborators in terms of biocompatibility is not clear and may warrant further investigation.

A second class of scaffolds we explored for skeletal muscle tissue engineering was encompassing different elastomers composed of glycerol, xylitol, sebacic acid and citric acid. These chemically crosslinked elastomers were promising based on their reported consistent degradation rates and predictable decline in mechanical properties (108). Its biocompatibility has been demonstrated with cardiomyocytes and *in vivo* data over a period of 2 weeks with PGS patches, sutured over the left ventricle of rats, did not find any deleterious effects (195). We assessed biocompatibility of 8 different scaffold compositions (obtained in collaboration with

the group of prof. W. Thielemans) through an alamar blue and live/dead assay. Some of the scaffold compositions indicated moderate to low cell survival. However, 4 elastomer compositions were selected based on their excellent support of cell survival and cell metabolism: PGS 1:1, PGSC 1:1, PXS 1:1.25 and PXSC 1:1. Preliminary data on myoblast differentiation indicated that the PGS 1:1 elastomer was suitable since we observed differentiated myofibers. With an average length of 92.3 µm, an average diameter of 12.8 µm and an average number of nuclei per fiber of 3.6, differentiation of myofibers was supported on the PGS 1:1 scaffolds. Still, values are below those observed for the standard scaffold-free BAMs (66). Further experiments should be conducted to evaluate the other elastomer compositions. Scaffold design may be further improved by modifying parameters such as pore size and structural orientation of the polymers. As for the lack of alignment, adapting the structure of the elastomeric scaffolds to better mimick the honeycomb structure of the ECM of native skeletal muscle should be explored. Such honeycomb microstructures of 250 µm thick, made of poly(glycerol sebacate), have been studied in the field of cardiac tissue engineering (196). It remains to be seen if thicker structures can be created and are of use for myofiber differentiation. Furthermore, using collagen instead of fibrin as an ECM might also be suggested for further optimization since gelation time of collagen is significantly longer which might result in deeper penetration of the cells through the scaffold (169). Also, different cell densities during seeding might enhance myofiber differentiation.

10 CONCLUSION

Through tissue engineering approaches, 3D constructs composed of human aligned myofibers can be generated. Reconstruction of human skeletal muscle *in vitro* has potential application in regenerative medicine, drug screening and disease modelling. However, several differences with real skeletal muscle still limit these applications. These include a lack of vascularization and a limited mechanical strength. Therefore, we investigated in parallel approaches to overcome these limitations.

This thesis provides an initial *in vivo* evaluation of the functionality of HUVEC derived endothelial networks introduced *in vitro* in our fibrin ECM based human BAM. The observed anastomosis of these HUVEC networks in our BAM model after 2 weeks of implantation marks the potential of the prevascularization strategy to assist in perfusion by the host. These results indicate the potential of this co-culture technique for proper prevascularization of our tissue engineered muscle, which may ultimately enhance its survival *in vivo.* As for the human myofiber maintenance, we found better myofiber formation by using skeletal muscle microvascular endothelial cells instead of of HUVECs. For HUVEC based co-culture BAMs, M199-EGM was found to result in better myofiber and endothelial network formation compared to the EGM-2 which is currently used. In terms of myofiber formation, EGM-MV was defined as the best medium composition when using SkMVECs in co-culture BAMs.

We demonstrated the limited potential of the tested electrospun polycarbonate scaffold in SMTE, as survival of human myoblasts was found to be decreased in the proximity of the scaffold and thus no myofibers were found. We also show the previously unreported property of poly(glycerol sebacate) to support myoblast differentiation into post-mitotic myofibers. In addition to these properties, the microporous structure of the poly(glycerol sebacate) makes it of particular interest in the context of prevascularization, which further provides perspectives to finetune the features of this scaffold material for skeletal muscle tissue engineering.

11 DUTCH SUMMARY

Skeletspieren onderscheiden zich van de meeste andere organen door hun intrinsiek herstelmechanisme. Dit herstelmechanisme berust op weefsel specifieke volwassen stamcellen, de satelliet cellen. Deze stamcellen zijn onder normale omstandigheden rustend. Ze bevinden zich onder de basale lamina van de spiervezels en hebben myogene differentiatie capaciteit. Volgend op spierschade geïnduceerd door sport, ziekte of trauma worden satelliet cellen geactiveerd tot actieve myoblasten. Deze kunnen op hun beurt fuseren met elkaar ter vorming van een nieuwe spiervezel of fuseren met beschadigde spiervezels. Echter, wanneer een spierdefect te groot is, zoals bijvoorbeeld bij spiertrauma door ongeval, oorlogsverwondingen, sommige oncologisch-chirurgische ingrepen,…wordt dit intrinsiek herstelmechanisme overrompeld en spreken we over volumetrisch spierverlies.

Ondanks de geassocieerde economische en sociale lasten van volumetrisch spierverlies, bestaan hier momenteel geen klinisch relevante producten voor. De huidige behandeling is gebaseerd op autologe en allogene spiergreffes, maar beide opties hebben intrinsieke nadelen. Tissue engineering van skeletspierweefsel kan mogelijks deze onbeantwoorde medische vraag tegemoetkomen. Dit interdisciplinair veld richt zich op de aanmaak van biologisch weefsel *in vitro.* In ons labo worden skeletspieren aangemaakt met een technologie gebaseerd op een fibrine hydrogel die resulteert in spiervezels die tijdens de differentiatie parallel georganiseren worden en een zacht weefsel vormen. Ondanks de vooruitgang geboekt in dit veld, zijn er blijvende uitdagingen die klinische applicaties in de weg staan. Deze omvatten, maar zijn niet beperkt tot, (i) de identificatie van een gepast draagmateriaal, (ii) de vascularisatie van het aangemaakt weefsel en (iii) de overgang van laboratorium schaal naar klinische schaal productie. Mogelijke oplossingen van enkele van de huidige tekortkomingen werden verder bestudeerd in deze thesis.

Skeletspieren worden gekenmerkt door een hiërarchische structuur opgebouwd uit verschillende componenten. Een succesvolle aanpak van skeletspierweefsel engineering zou elk van deze elementen in rekening moeten brengen. Wij focusten in deze thesis op de vasculatuur van constructen. Het opzetten van een efficiënte vascularisatie is cruciaal als we de huidige limitatie in grootte van de constructen willen aanpakken. In deze thesis werd verder gebouwd op een bio-artificiële spier (BAM) opgebouwd uit gealigneerde spiervezels met tussenliggende endotheliale netwerken. Deze netwerken werden bekomen door een co-cultuur

systeem te ontwikkelen opgebouwd uit 30 % endotheelcellen afgeleid van humane navelstrengen (HUVEC). De overige 70 % bestaat uit skeletspiercellen die geïsoleerd werden uit humane skeletspierbiopten. De bekomen HUVEC afgeleide endotheel netwerken vormden zich *in vitro* door middel van een proces genaamd vasculogenesis.

Een eerste objectief van de thesis was het *in vivo* evalueren in termen van behoud en evolutie van deze co-cultuur BAMs over een periode van 2 weken. Hiervoor diende eerst een optimaal diermodel bepaal te worden. We evalueerden in parallel zowel ratmodellen als muizenmodellen en verder werd ook gekeken naar de beste implantatie site. Een week oude co-cultuur BAMs bestaande uit 30 % HUVECs werden geïmplanteerd op de latissimus dorsi spier van volwassen (i) immunocompetente Swiss muizen behandeld met immuunsuppressiva, (ii) niet-obees diabetische ernstig gecombineerde immuundeficiënte (NOD/SCID) muizen en (iii) immuundeficiënte *Foxn1nu* (Nu/Nu) muizen. Het ratmodel werd qua implantatie site opgedeeld in 2 groepen met implantatie op (i) de tibialis spier of (ii) de abdominale spier van volwassen Wistar ratten. Verder kon uit deze implantatie studie ook preliminaire data gehaald worden omtrent potentiële connectie van de HUVEC afgeleide endotheel netwerken met de gastheer vasculatuur.

Om de dynamiek van de HUVEC afgeleide endotheel netwerken te kunnen volgen, werd gebruik gemaakt van groen fluorescent gelabelde cellen. Beeldanalyses waren gebaseerd op intravitale en confocale microscopie waarbij sterke verschillen in endotheel netwerk morfologie werden waargenomen tussen de verschillende modellen. Intravitale microscopie werd uitgevoerd op 12 en 14 dagen na implantatie. Van de intravitale beelden voor de Swiss muis werd afgeleid dat de endotheel netwerken sterke degradatie ondergaan hadden tijdens de periode van implantatie. Dit werd verder bevestigd door de beelden opgenomen na 14 dagen en de confocale beelden. Echter, in dit diermodel, anders dan voor alle andere, waren constructen nog aanwezig op het moment van explantatie. Daarom werden de analyses voor de andere diermodellen uitgevoerd op omgevend gastheerweefsel dat geëxplanteerd werd op basis van de posities van de chirurgische draadjes waarmee de BAM werd ingehecht. Voor de immuundeficiënte muizen toonden intravitale en confocale beelden de aanwezigheid van geïnterconnecteerde HUVEC-afgeleide endotheel netwerken aan. Deze waren dens voor de Nu/Nu muis, maar konden slechts waargenomen worden in 2 van de 6 explanten. In de NOD/SCID muis konden HUVEC-afgeleide endotheel netwerken teruggevonden worden in 4 van de 6 explanten. Verder kon door middel van intraveneuze injectie van een rhodamine gemerkt lectine evidentie voor connectie met de gastheer vasculatuur aangetoond worden in 2

van de 6 explanten. Dit lectine is afgeleid van ulex europaeus agglutinine-I en bindt specifiek op humane endotheelcellen. Deze connectie werd verder bevestigd door aanwezigheid van rode bloedcellen in de HUVEC-afgeleide endotheel netwerken. Uit observaties voor beide ratmodellen werd besloten dat dit diermodel een suboptimale setting biedt voor onze objectieven daar noch constructen, noch endotheel netwerken noch humaan afgeleide spiervezels konden worden geobserveerd. Dit zou mogelijks verklaard kunnen worden door een sterkere NK cel activiteit in ratten in vergelijking met muizen. Ook is het mogelijk dat ratten een snellere resorptie van de fibrine matrix induceren.

In geen enkele conditie werden humane spiervezels teruggevonden. Enkel mature spiervezels konden worden waargenomen, waarschijnlijk allemaal afkomstig van de gastheer want humane spiervels zouden embryonale eigenschappen vertonen. Op basis van deze bevindingen konden echter weinig conclusies getrokken worden in termen van spiervezel behoud. Want vanuit deze experimentele setup kon niet worden geconcludeerd of immaturiteit van de geïmplanteerde humane spiervezels een reden van snelle degradatie was. Daarom is het uitvoeren van een vervolg experiment met BAMs opgebouwd uit humane spiervezels alleen een aangewezen volgende stap. Deze BAMs kunnen door de afwezigheid van endotheel netwerken langer in cultuur gehouden worden wat op zijn beurt resulteert in meer mature spiervezels.

Daarnaast kan het verder optimaliseren van de co-cultuur condities *in vitro* ook helpen bij het behoud van zowel spiervezels als endotheel netwerken. Het opstellen van deze co-cultuur condities betreft een uitdaging op zich waarin een afweging moet gemaakt worden tussen beide cel types bij het bepalen van optimale cultuurcondities. Daarom was een volgend objectief het verder exploreren van verschillende media (i) skeletspier groeimedium (SkGM) met opeenvolgend differentiatie na 2 dagen in skeletspier fusiemedium (SkFM), (ii) EGM-2 wat een optimaal cultuur medium is voor endotheelcellen of (iii) M199-EGM. Daarnaast kan het exploreren van andere endotheel cel types ook waardevol zijn in het optimaliseren van de co-cultuur condities. In deze context werden co-cultuur BAMs geëxploreerd met 10 % skeletspier microvasculaire endotheelcellen (SkMVECs). Deze cel ratio's werden voordien geoptimaliseerd in ons labo. Het skeletspier differentiatiemedium is voor myoblast differentiatie capaciteit superieur ten opzichte van EGM-2 en M199-EGM. Terwijl de laatstgenoemde sterk gelijkend bevonden werden. De hogere diameter van spiervezels bekomen wanneer gecultiveerd in M199-EGM voor de co-cultuur BAMs met 30 % HUVECs wees echter in de richting van een meer optimale conditie in termen van spiervezel vorming. Dit dient verder

bekeken te worden om na te gaan of dit ook resulteert in meer nuclei per spiervezel. Voor de conditie met 10 % SkMVECs werden contradictorische bevindingen gevonden met een grotere diameter van de spiervezels wanneer gecultiveerd in EGM-MV in plaats van M199-EGM. In termen van endotheel netwerk vorming werd, voor HUVEC-myoblast co-cultuur, M199-EGM beter bevonden in termen van totale lengte van het endotheel netwerk, % vertakkingslengte en aantal geïsoleerde segmenten ten opzichte van EGM-2. Cultiveren in skeletspier media vertoonde geen endotheelnetwerk vorming; in deze conditie werden enkel losse endotheelcellen gevonden. Data voor de endotheel netwerk vorming voor co-cultuur BAMs met 10 % SkMVECs (samenwerking met Gilles Carpentier) waren nog niet beschikbaar op het moment van finaliseren van deze thesis.

Een laatste objectief is gedreven door de huidige tendens binnen het veld van tissue engineering. Allerhande draagmaterialen (synthetische en/of natuurlijke) worden sterk geëxploreerd en tonen veelbelovende resultaten bij het reconstrueren van de myoblastfusie in een gealigneerde organisatie van skeletspiervezels. Met onze skeletspier tissue engineering technologie worden gealigneerde spiervezels bekomen zonder gebruik van deze draagmaterialen. Een mogelijk voordeel van draagmaterialen in ons model in termen van spiervezel differentiatie en aligneren diende echter nog bekeken te worden. Verder worden draagmaterialen ook in de context van endotheliale netwerken onderzocht. Hierbij zijn vooral draagmaterialen met een uniforme geometrie zoals geïnterconnecteerde poriën interessant voor het faciliteren van het vascularisatie proces.

Binnen de context van synthetische draagmaterialen werden 2 verschillende materialen geëxploreerd. Het eerste synthetische polymeer dat werd bekeken is een polycarbonaat materiaal bekomen via electrospinning. Electrospinning is een techniek waarbij een netwerk aan vezels met tussenruimtes van een paar micrometers wordt bekomen. Deze materialen werden bekomen door collaboratie met de groep van prof. Jan Deprest. Humane spiercellen werden geïntegreerd in de fibrine hydrogel, die standaard is voor onze BAM, en aangebracht op de polycarbonaat draagstructuur. Op basis van confocale beelden van de polycarbonaat vezels kon worden waargenomen dat deze techniek goede integratie toeliet. Differentiatie na integratie van deze synthetische draagstructuur in ons model werd kwantitatief en kwalitatief geëvalueerd na een periode van 7 dagen. Een sterke afname van lengte van de spiervezels en aantal nuclei per spiervezel werden waargenomen in de nabijheid van de draagstructuur in vergelijking met de toplagen waar goede spiervezel vorming werd waargenomen. Verdere evaluatie toonde aan dat dit verschil in differentiatie te wijten is aan een hogere celdood in de

nabijheid van de draagstructuur. Deze observaties verschillen van de bio-compatibiliteit in het ratmodel van de collaborerende groep clinici, maar onderstreept het belang van *in vitro* cel studies. Daarnaast kan ook verschil in compatibiliteit tussen verschillende celtypes een reden zijn voor verschillende observaties in termen van biocompatibiliteit. De hoge celdood die we observeerden, beperkt verdere toepassingen van deze polycarbonaat draagstructuur.

Een tweede type draagmateriaal dat werd geëvalueerd betreft een groep van elastomeren opgebouwd uit xylitol, glycerol, sebacaat en citroenzuur. Deze elastomeren worden gekenmerkt door hun gunstige mechanische eigenschappen. Elasticiteit van deze elastomeren wordt aanzien als een belangrijk aspect in de context van dynamische weefsels zoals spieren. Daarom bieden deze structuren een goed uitgangspunt om als draagmateriaal te dienen voor onze BAM. Eerst werd een selectie gemaakt gebaseerd op een alamar blue assay en live/dead assay om een idee te krijgen van respectievelijk cel metabolisme en cel overleving na het aanbrengen van C2C12 muis myoblasten ingebed in een fibrine hydrogel. Hieruit werden 4 elastomeersamenstelling geselecteerd voor verder onderzoek: poly(glycerol sebacaat) 1:1, poly(glycerol sebacaat citraat) 1:1, poly(xylitol sebacaat) 1:1.25 en poly(xylitol sebacaat citraat) 1:1 (waarbij de waardes de molaire ratio's weergeven van de suiker en alcohol respectievelijk). Preliminaire data rond humane myoblast differentiatie capaciteit na integratie in de elastomere draagstructuur werd verder bekeken voor de poly(glycerol sebacaat) 1:1 draagstructuren. De humane spiercellen werden ingebed in een fibrine hydrogel en op het polymeer aangebracht voor gelatie kon optreden. Deze aanpak is in overeenstemming met de aanmaak van standaard BAMs en laat ons toe deze in parallel te evalueren. Echter directe vergelijkingen worden bemoeilijkt doordat celgemedieerde contractie verschilt wanneer draagstructuren al dan niet aanwezig zijn, zodat celdensiteit verschillend is. Confocale beeldanalyse na immunocytochemische kleuring voor de differentiatiemerker tropomyosine toonde efficiënte differentiatie in spiervezels aan met een gemiddelde diameter van 12.8 µm en lengte van 92.3 µm. Verder werd ook gekeken naar alignering, maar zoals verwacht, laat de elastomeer structuur weinig tot geen alignering in een specifieke richting toe. Het verder ontwikkelen van de elastomeer naar een structuur meer gelijkend op de natieve spier lijkt dan ook een interessante volgende stap. Eerdere rapporteringen van honinggraatstructuren in deze elastomeren toont aan dat dit een haalbare kaart zou moeten zijn.

12 REFERENCES

1. Pallua N, Suschek C V. Tissue Engineering. Pallua N, Suscheck C V., editors. Tissue Engineering: From Lab to Clinic. Berlin, Heidelberg: Springer Berlin Heidelberg; 2011. 1-634 p.
2. Organ Donation Statistics: Why be an Organ Donor? [Internet]. organdonor. 2015 [cited 2018 Feb 1]. Available from: https://www.organdonor.gov/statistics-stories/statistics.html
3. Hrsa. OPTN : Organ Procurement and Transplantation Network. U. S. Department of Health and Human Services 1999 p. 23.
4. Frontera WR, Ochala J. Skeletal Muscle: A Brief Review of Structure and Function. Calcif Tissue Int. 2015;96(3):183–95.
5. Järvinen TAH, Järvinen TLN, Kääriäinen M, Kalimo H, Järvinen M. Muscle Injuries. Am J Sports Med. 2005;33(5):745–64.
6. Lieber RL, Ward SR. Skeletal muscle design to meet functional demands. Philos Trans R Soc B Biol Sci. 2011;366(1570):1466–76.
7. Gillies AR, Lieber RL. Structure and function of the skeletal muscle extracellular matrix. Muscle Nerve. 2011;44(3):318–31.
8. Musarò A. The Basis of Muscle Regeneration. Adv Biol. 2014;2014:1–16.
9. Mauro A. Satellite cell of skeletal muscle fibers. J Cell Biol. 1961;9(2):493–5.
10. Seale P, Sabourin LA, Girgis-Gabardo A, Mansouri A, Gruss P, Rudnicki MA. Pax7 Is Required for the Specification of Myogenic Satellite Cells. Cell. 2000;102(6):777–86.
11. Sherwood RI, Christensen JL, Conboy IM, Conboy MJ, Rando TA, Weissman IL, et al. Isolation of Adult Mouse Myogenic Progenitors. Cell. 2004;119(4):543–54.
12. Hawke TJ, Garry DJ. Myogenic satellite cells: physiology to molecular biology. J Appl Physiol. 2001;91(8750–7587; 0161–7567; 2):534–51.
13. Lepper C, Partridge TA, Fan C-MC-M. An absolute requirement for Pax7-positive satellite cells in acute injury-induced skeletal muscle regeneration. Development. 2011;138(17):3639–46.
14. Gal-Levi R, Leshem Y, Aoki S, Nakamura T, Halevy O. Hepatocyte growth factor plays a dual role in regulating skeletal muscle satellite cell proliferation and differentiation. Biochim Biophys Acta - Mol Cell Res. 1998;1402(1):39–51.
15. Lu H, Huang D, Saederup N, Charo IF, Ransohoff RM, Zhou L. Macrophages recruited via CCR2 produce insulin-like growth factor-1 to repair acute skeletal muscle injury. FASEB J. 2011;25(1):358–69.

16. Camargo FD, Green R, Capetenaki Y, Jackson KA, Goodell MA. Single hematopoietic stem cells generate skeletal muscle through myeloid intermediates. Nat Med. 2003;9(12):1520–7.

17. Chazaud B, Sonnet C, Lafuste P, Bassez G, Rimaniol A-C, Poron F, et al. Satellite cells attract monocytes and use macrophages as a support to escape apoptosis and enhance muscle growth. J Cell Biol. 2003;163(5):1133–43.

18. Grefte S, Kuijpers-Jagtman AM, Torensma R, Von den Hoff JW. Skeletal Muscle Development and Regeneration. Stem Cells Dev. 2007;16(5):857–68.

19. Wagers AJ, Conboy IM. Cellular and Molecular Signatures of Muscle Regeneration: Current Concepts and Controversies in Adult Myogenesis. Cell. 2005;122(5):659–67.

20. Hernández-Hernández JM, García-González EG, Brun CE, Rudnicki MA. The myogenic regulatory factors, determinants of muscle development, cell identity and regeneration. Semin Cell Dev Biol. 2017;72:10–8.

21. Chal J, Pourquié O. Making muscle: skeletal myogenesis in vivo and in vitro. Development. 2017;144(12):2104–22.

22. Wang YX, Rudnicki MA. Satellite cells, the engines of muscle repair. Nat Rev Mol Cell Biol. 2012;13(2):127–33.

23. Bischoff R. Proliferation of muscle satellite cells on intact myofibers in culture. Dev Biol. 1986;115(1):129–39.

24. Jonah D Lee BCS, Lisa M Larkin KWV. Isolation and Purification of Satellite Cells for Skeletal Muscle Tissue Engineering. J Regen Med. 2015;3(2).

25. Zammit PS, Partridge TA, Yablonka-Reuveni Z. The Skeletal Muscle Satellite Cell: The Stem Cell That Came in From the Cold. J Histochem Cytochem. 2006;54(11):1177–91.

26. Post MJ. Cultured meat from stem cells: Challenges and prospects. Meat Sci. 2012;92(3):297–301.

27. Bisson A, Le Corre S, Joly-Helas G, Chambon P, Demoulins L, Jean L, et al. Chromosomal Instability but Lack of Transformation in Human Myoblast Preparations. Cell Transplant. 2014;23(12):1475–87.

28. Zuk PA. Human Adipose Tissue Is a Source of Multipotent Stem Cells. Mol Biol Cell. 2002;13(12):4279–95.

29. Lin C-S, Lin G, Lue TF. Allogeneic and Xenogeneic Transplantation of Adipose-Derived Stem Cells in Immunocompetent Recipients Without Immunosuppressants. Stem Cells Dev. 2012;21(15):2770–8.

30. Ma T, Sun J, Zhao Z, Lei W, Chen Y, Wang X, et al. A brief review: adipose-derived stem cells and their therapeutic potential in cardiovascular diseases. Stem Cell Res Ther. 2017;8(1):124.

31. Di Rocco G, Iachininoto MG, Tritarelli A, Straino S, Zacheo A, Germani A, et al. Myogenic potential of adipose-tissue-derived cells. J Cell Sci. 2006;119(14):2945–52.

32. Yilgor Huri P, Cook CA, Hutton DL, Goh BC, Gimble JM, DiGirolamo DJ, et al. Biophysical cues enhance myogenesis of human adipose derived stem/stromal cells. Biochem Biophys Res Commun. 2013;438(1):180–5.

33. Goudenege S, Pisani DF, Wdziekonski B, Di Santo JP, Bagnis C, Dani C, et al. Enhancement of Myogenic and Muscle Repair Capacities of Human Adipose–derived Stem Cells With Forced Expression of MyoD. Mol Ther. 2009;17(6):1064–72.

34. LaBarge MA, Blau HM. Biological progression from adult bone marrow to mononucleate muscle stem cell to multinucelate muscle fibers in response to injury. Cell. 2002;111:589–601.

35. Bayati V, Hashemitabar M, Gazor R, Nejatbakhsh R, Bijannejad D. Expression of surface markers and myogenic potential of rat bone marrow- and adipose-derived stem cells: a comparative study. Anat Cell Biol. 2013;46(2):113.

36. Natsu K, Ochi M, Mochizuki Y, Hachisuka H, Yanada S, Yasunaga Y. Allogeneic Bone Marrow-Derived Mesenchymal Stromal Cells Promote the Regeneration of Injured Skeletal Muscle without Differentiation into Myofibers. Tissue Eng. 2004;10(7–8):1093–112.

37. Merritt EK, Cannon M V, Hammers DW, Le LN, Gokhale R, Sarathy A, et al. Repair of Traumatic Skeletal Muscle Injury with Bone-Marrow-Derived Mesenchymal Stem Cells Seeded on Extracellular Matrix. Tissue Eng Part A. 2010;16(9):2871–81.

38. Helal MAM, Shaheen NEM, Abu Zahra FA. Immunomodulatory capacity of the local mesenchymal stem cells transplantation after severe skeletal muscle injury in female rats. Immunopharmacol Immunotoxicol. 2016;38(6):414–22.

39. Cho PS, Messina DJ, Hirsh EL, Chi N, Goldman SN, Lo DP, et al. Immunogenicity of umbilical cord tissue derived cells. Blood. 2008;111(1):430–8.

40. Zucconi E, Vieira NM, Bueno CR, Secco M, Jazedje T, Costa Valadares M, et al. Preclinical Studies with Umbilical Cord Mesenchymal Stromal Cells in Different Animal Models for Muscular Dystrophy. J Biomed Biotechnol. 2011;2011:1–9.

41. Nunes VA, Cavaçana N, Canovas M, Strauss BE, Zatz M. Stem cells from umbilical cord blood differentiate into myotubes and express dystrophin in vitro only after exposure to in vivo muscle environment. Biol Cell. 2007;99(4):185–96.

42. Gang EJ, Jeong JA, Hong SH, Hwang SH, Kom SW, Yang IH, et al. Skeletal Myogenic Differentiation of Mesenchymal Stem Cells Isolated from Human Umbelical Cord Blood. 2004;580–9.

43. Kocaefe Ç, Balcı D, Balcı Hayta B, Can A. Reprogramming of Human Umbilical Cord Stromal Mesenchymal Stem Cells for Myogenic Differentiation and Muscle Repair.

Stem Cell Rev Reports. 2010;6(4):512–22.

44. Bautch VL. Stem cells and the vasculature. Nat Med. 2011;17(11):1437–43.

45. Sá da Bandeira D, Casamitjana J, Crisan M. Pericytes, integral components of adult hematopoietic stem cell niches. Pharmacol Ther. 2017;171:104–13.

46. Dellavalle A, Maroli G, Covarello D, Azzoni E, Innocenzi A, Perani L, et al. Pericytes resident in postnatal skeletal muscle differentiate into muscle fibres and generate satellite cells. Nat Commun. 2011;2:499.

47. Dellavalle A, Sampaolesi M, Tonlorenzi R, Tagliafico E, Sacchetti B, Perani L, et al. Pericytes of human skeletal muscle are myogenic precursors distinct from satellite cells. Nat Cell Biol. 2007;9(3):255–67.

48. Fuoco C, Sangalli E, Vono R, Testa S, Sacchetti B, Latronico MVG, et al. 3D hydrogel environment rejuvenates aged pericytes for skeletal muscle tissue engineering. Front Physiol. 2014;5:203.

49. Amit M, Carpenter MK, Inokuma MS, Chiu C-P, Harris CP, Waknitz MA, et al. Clonally Derived Human Embryonic Stem Cell Lines Maintain Pluripotency and Proliferative Potential for Prolonged Periods of Culture. Dev Biol. 2000;227(2):271–8.

50. Bryja V, Bonilla S, Čajánek L, Parish CL, Schwartz CM, Luo Y, et al. An Efficient Method for the Derivation of Mouse Embryonic Stem Cells. Stem Cells. 2006;24(4):844–9.

51. Robertson JA. Embryo Stem Cell Research: Ten Years of Controversy. J Law, Med Ethics. 2010;38(2):191–203.

52. Lewis MP, Mudera V, Cheema U, Shah R. Muscle tissue engineering. In: Fundamentals of Tissue Engineering and Regenerative Medicine. 2009. p. 243–53.

53. Bhartiya D, Nagvenkar P, Sriraman K, Shaikh A. An Overview of Pluripotent Stem Cells. In: Pluripotent Stem Cells. InTech; 2013. p. 1–23.

54. Li M, Dickinson CE, Finkelstein EB, Neville CM, Sundback CA. The Role of Fibroblasts in Self-Assembled Skeletal Muscle. Tissue Eng Part A. 2011;17(21–22):2641–50.

55. Rao N, Evans S, Stewart D, Spencer KH, Sheikh F, Hui EE, et al. Fibroblasts influence muscle progenitor differentiation and alignment in contact independent and dependent manners in organized co-culture devices. Biomed Microdevices. 2013;15(1):161–9.

56. Risau W, Flamme I. Vasculogenesis. Annu Rev Cell Dev Biol. 1995;11(1):73–91.

57. Davis GE, Camarillo CW. An alpha2beta1 Integrin-Dependent Pinocytic Mechanism Involving Intracellular Vacuole Formation and Coalescence Regulates Capillary Lumen and Tube Formation in Three-Dimensional Collagen Matrix. Exp Cell Res. 1996;224(1):39–51.

58. Stratman AN, Davis MJ, Davis GE. VEGF and FGF prime vascular tube morphogenesis

and sprouting directed by hematopoietic stem cell cytokines. Blood. 2011;117(14):3709–19.

59. Morin KT, Tranquillo RT. Guided sprouting from endothelial spheroids in fibrin gels aligned by magnetic fields and cell-induced gel compaction. Biomaterials. 2011;32(26):6111–8.

60. Waters JP, Kluger MS, Graham M, Chang WG, Bradley JR, Pober JS. In vitro Self-Assembly of Human Pericyte-Supported Endothelial Microvessels in Three-Dimensional Coculture: A Simple Model for Interrogating Endothelial-Pericyte Interactions. J Vasc Res. 2013;50(4):324–31.

61. Kim J, Chung M, Kim S, Jo DH, Kim JH, Jeon NL. Engineering of a Biomimetic Pericyte-Covered 3D Microvascular Network. Lee JW, editor. PLoS One. 2015;10(7):e0133880.

62. Stratman AN, Davis GE. Endothelial Cell-Pericyte Interactions Stimulate Basement Membrane Matrix Assembly: Influence on Vascular Tube Remodeling, Maturation, and Stabilization. Microsc Microanal. 2012;18(1):68–80.

63. Wang X, Phan DTT, Sobrino A, George SC, Hughes CCW, Lee AP. Engineering anastomosis between living capillary networks and endothelial cell-lined microfluidic channels. Lab Chip. 2016;16(2):282–90.

64. Moya ML, Hsu Y-H, Lee AP, Hughes CCW, George SC. In Vitro Perfused Human Capillary Networks. Tissue Eng Part C Methods. 2013;19(9):730–7.

65. Sasagawa T, Shimizu T, Sekiya S, Haraguchi Y, Yamato M, Sawa Y, et al. Design of prevascularized three-dimensional cell-dense tissues using a cell sheet stacking manipulation technology. Biomaterials. 2010;31(7):1646–54.

66. Gholobova D, Decroix L, Van Muylder V, Desender L, Gerard M, Carpentier G, et al. Endothelial Network Formation Within Human Tissue-Engineered Skeletal Muscle. Tissue Eng Part A. 2015;21(19–20):2548–58.

67. Koffler J, Kaufman-Francis K, Yulia S, Dana E, Daria AP, Landesberg A, et al. Improved vascular organization enhances functional integration of engineered skeletal muscle grafts. Proc Natl Acad Sci. 2011;36108108(10).

68. Jiang JXS, Choi RCY, Siow NL, Lee HHC, Wan DCC, Tsim KWK. Muscle induces neuronal expression of acetylcholinesterase in neuron-muscle co-culture: transcriptional regulation mediated by cAMP-dependent signaling. J Biol Chem. 2003;278(46):45435–44.

69. Williams ML, Kostrominova TY, Arruda EM, Larkin LM. Effect of implantation on engineered skeletal muscle constructs. J Tissue Eng Regen Med. 2013;7(6):434–42.

70. Thorrez L, Vandenburgh H, Callewaert N, Mertens N, Shansky J, Wang L, et al. Angiogenesis Enhances Factor IX Delivery and Persistence from Retrievable Human

Bioengineered Muscle Implants. Mol Ther. 2006;14(3):442–51.

71. Martin NRW, Passey SL, Player DJ, Khodabukus A, Ferguson RA, Sharples AP, et al. Factors affecting the structure and maturation of human tissue engineered skeletal muscle. Biomaterials. 2013;34(23):5759–65.

72. Chapple CR, Raz S, Brubaker L, Zimmern PE. Mesh Sling in an Era of Uncertainty: Lessons Learned and the Way Forward. Eur Urol. 2013;64(4):525–9.

73. Ryan AJ, O'Brien FJ. Insoluble elastin reduces collagen scaffold stiffness, improves viscoelastic properties, and induces a contractile phenotype in smooth muscle cells. Biomaterials. 2015;73:296–307.

74. Liu X, Won Y, Ma PX. Porogen-induced surface modification of nano-fibrous poly(l-lactic acid) scaffolds for tissue engineering. Biomaterials. 2006;27(21):3980–7.

75. Wilkinson AE, McCormick AM, Leipzig ND. Central Nervous System Tissue Engineering: Current Considerations and Strategies. Synth Lect Tissue Eng. 2011;3(2):1–120.

76. Osses N, Brandan E. ECM is required for skeletal muscle differentiation independently of muscle regulatory factor expression. Am J Physiol Physiol. 2002;282(2):C383–94.

77. Nishimura T. The role of intramuscular connective tissue in meat texture. Anim Sci J. 2010;81(1):21–7.

78. Chattopadhyay S, Raines RT. Review collagen-based biomaterials for wound healing. Glick GD, editor. Biopolymers. 2014;101(8):821–33.

79. Pallua N, Suschek C V. Tissue Engineering: From Lab to clinic. Vol. 1. 2011.

80. Mazaki T, Shiozaki Y, Yamane K, Yoshida A, Nakamura M, Yoshida Y, et al. A novel, visible light-induced, rapidly cross-linkable gelatin scaffold for osteochondral tissue engineering. Sci Rep. 2015;4(1):4457.

81. Xia Y, Mei F, Duan Y, Gao Y, Xiong Z, Zhang T, et al. Bone tissue engineering using bone marrow stromal cells and an injectable sodium alginate/gelatin scaffold. J Biomed Mater Res Part A. 2012;100A(4):1044–50.

82. Bendall JR. The elastin content of various muscles of beef animals. J Sci Food Agric. 1967;18(12):553–8.

83. Chow JP, Simionescu DT, Carter AL, Simionescu A. Immunomodulatory effects of adipose tissue-derived stem cells on elastin scaffold remodeling in diabetes. Tissue Eng Regen Med. 2016;13(6):701–12.

84. Hafemann B, Ensslen S, Erdmann C, Niedballa R, Zühlke A, Ghofrani K, et al. Use of a collagen/elastin-membrane for the tissue engineering of dermis. Burns. 1999;25(5):373–84.

85. Vasconcelos DM, Gonçalves RM, Almeida CR, Pereira IO, Oliveira MI, Neves N, et al.

Fibrinogen scaffolds with immunomodulatory properties promote in vivo bone regeneration. Biomaterials. 2016;111:163–78.

86. Sell SA, Francis MP, Garg K, McClure MJ, Simpson DG, Bowlin GL. Cross-linking methods of electrospun fibrinogen scaffolds for tissue engineering applications. Biomed Mater. 2008;3(4):45001.

87. McManus M, Boland E, Sell S, Bowen W, Koo H, Simpson D, et al. Electrospun nanofibre fibrinogen for urinary tract tissue reconstruction. Biomed Mater. 2007;2(4):257–62.

88. Kim DW, Lee OJ, Kim S-W, Ki CS, Chao JR, Yoo H, et al. Novel fabrication of fluorescent silk utilized in biotechnological and medical applications. Biomaterials. 2015;70:48–56.

89. Altman GH, Diaz F, Jakuba C, Calabro T, Horan RL, Chen J, et al. Silk-based biomaterials. Biomaterials. 2003;24(3):401–16.

90. Haupt J, García-López JM, Chope K. Use of a novel silk mesh for ventral midline hernioplasty in a mare. BMC Vet Res. 2015;11(1):58.

91. Seth A, Chung YG, Gil ES, Tu D, Franck D, Di Vizio D, et al. The performance of silk scaffolds in a rat model of augmentation cystoplasty. Biomaterials. 2013;34(20):4758–65.

92. Frazza EJ, Schmitt EE. A new absorbable suture. J Biomed Mater Res. 1971;5(2):43–58.

93. Takeuchi J, Suzuki H, Murata M, Kakei Y, Ri S, Umeda M, et al. Clinical evaluation of application of polyglycolic acid sheet and fibrin glue spray for partial glossectomy. J Oral Maxillofac Surg. 2013;71(2):e126–31.

94. Mundinger GS, Prucz RB, Rozen SM, Tufaro AP. Reconstruction of the Inferior Alveolar Nerve with Bioabsorbable Polyglycolic Acid Nerve Conduits. Plast Reconstr Surg. 2012;129(1):110e–117e.

95. Zambon JP, de Sá Barretto LS, Nakamura ANS e, Duailibi S, Leite K, Magalhaes RS, et al. Histological changes induced by Polyglycolic-Acid (PGA) scaffolds seeded with autologous adipose or muscle-derived stem cells when implanted on rabbit bladder. Organogenesis. 2014;10(2):278–88.

96. You Q, Wang F, Duan L, Du X, Xiao M, Shen Z. Construction of small-caliber, polydiaxanone cyclohexanone vascular stents. Cell Biochem Biophys. 2010;57(1):35–43.

97. Higgins SP, Solan AK, Niklason LE. Effects of polyglycolic acid on porcine smooth muscle cell growth and differentiation. J Biomed Mater Res. 2003;67A(1):295–302.

98. Zambon JP, De Sá Barretto LS, Sawaki E Nakamura AN, Duailibi S, Leite K, Magalhaes

RS, et al. Histological changes induced by Polyglycolic-Acid (PGA) scaffolds seeded with autologous adipose or muscle-derived stem cells when implanted on rabbit bladder. Organogenesis. 2014;10(2):278–88.

99. Roman S, Urbánková I, Callewaert G, Lesage F, Hillary C, Osman NI, et al. Evaluating Alternative Materials for the Treatment of Stress Urinary Incontinence and Pelvic Organ Prolapse: A Comparison of the In Vivo Response to Meshes Implanted in Rabbits. J Urol. 2016;196(1):261–9.

100. Kakinoki S, Yamaoka T. Stable modification of poly(lactic acid) surface with neurite outgrowth-promoting peptides via hydrophobic collagen-like sequence. Acta Biomater. 2010;6(6):1925–30.

101. Lopes MS, Jardini AL, Filho RM. Poly (Lactic Acid) Production for Tissue Engineering Applications. Procedia Eng. 2012;42:1402–13.

102. Park BH, Zhou L, Jang KY, Park HS, Lim JM, Yoon SJ, et al. Enhancement of tibial regeneration in a rat model by adipose-derived stromal cells in a PLGA scaffold. Bone. 2012;51(3):313–23.

103. Kim M, Choi YS, Yang SH, Hong H-N, Cho S-W, Cha SM, et al. Muscle regeneration by adipose tissue-derived adult stem cells attached to injectable PLGA spheres. Biochem Biophys Res Commun. 2006;348(2):386–92.

104. Ko HJ, Suh JH, Choi SY, Choi JY, Moon HJ, Lee JW, et al. Two cases of upper lip correction using multipolydioxanone scaffold. Dermatol Ther. 2016;29(1):10–2.

105. Ko HJ, Choi JY, Moon HJ, Lee JW, Jang SI, Bae I-H, et al. Multi-polydioxanone (PDO) scaffold for forehead wrinkle correction: A pilot study. J Cosmet Laser Ther. 2016;18(7):405–8.

106. Alfaro De Prá MA, Ribeiro-do-Valle RM, Maraschin M, Veleirinho B. Effect of collector design on the morphological properties of polycaprolactone electrospun fibers. Mater Lett. 2017;193:154–7.

107. Williams JM, Adewunmi A, Schek RM, Flanagan CL, Krebsbach PH, Feinberg SE, et al. Bone tissue engineering using polycaprolactone scaffolds fabricated via selective laser sintering. Biomaterials. 2005;26(23):4817–27.

108. Chen Q, Liang S, Thouas GA. Elastomeric biomaterials for tissue engineering. Prog Polym Sci. 2013;38:584–671.

109. Wang Y, Ameer GA, Sheppard BJ, Langer R. A tough biodegradable elastomer. Nat Biotechnol. 2002;20(6):602–6.

110. Oh SJ, Woo JO, Park J-E, Son K. Thermal, mechanical, and morphological properties of polyol-based poly(ester amide) elastomers. Mater Lett. 2015;143:219–22.

111. Bruggeman JP, Bettinger CJ, Langer R. Biodegradable xylitol-based elastomers: In vivo

behavior and biocompatibility. 2010;(1):92–104.

112. Wang Y, Kim YM, Langer R. In vivo degradation characteristics of poly(glycerol sebacate). J Biomed Mater Res. 2003;66A(1):192–7.

113. Chen Q, Yang X, Li Y. A comparative study on in vitro enzymatic degradation of poly(glycerol sebacate) and poly(xylitol sebacate). RSC Adv. 2012;2(10):4125.

114. Ifkovits JL, Padera RF, Burdick JA. Biodegradable and radically polymerized elastomers with enhanced processing capabilities. Biomed Mater. 2008;3(3):34104.

115. Nair LS, Laurencin CT. Biodegradable polymers as biomaterials. Vol. 32, Progress in Polymer Science (Oxford). Pergamon; 2007. p. 762–98.

116. Pomerantseva I, Krebs N, Hart A, Neville CM, Huang AY, Sundback CA. Degradation behavior of poly(glycerol sebacate). J Biomed Mater Res Part A. 2009;91A(4):1038–47.

117. Liu Q, Tan T, Weng J, Zhang L. Study on the control of the compositions and properties of a biodegradable polyester elastomer. Biomed Mater. 2009;4(2):25015.

118. Blanquer SBG, Gebraad AWH, Miettinen S, Poot AA, Grijpma DW, Haimi SP. Differentiation of adipose stem cells seeded towards annulus fibrosus cells on a designed poly(trimethylene carbonate) scaffold prepared by stereolithography. J Tissue Eng Regen Med. 2017;11(10):2752–62.

119. Zhang Z, Kuijer R, Bulstra SK, Grijpma DW, Feijen J. The in vivo and in vitro degradation behavior of poly(trimethylene carbonate). Biomaterials. 2006;27(9):1741–8.

120. Zhang C, Subramanian H, Grailer JJ, Tiwari A, Pilla S, Steeber DA, et al. Fabrication of biodegradable poly(trimethylene carbonate) networks for potential tissue engineering scaffold applications. Polym Adv Technol. 2009;20(9):742–7.

121. Encalada-Diaz I, Cole BJ, MacGillivray JD, Ruiz-Suarez M, Kercher JS, Friel NA, et al. Rotator cuff repair augmentation using a novel polycarbonate polyurethane patch: preliminary results at 12 months' follow-up. J Shoulder Elb Surg. 2011;20(5):788–94.

122. Chen S, Nakamoto T, Kawazoe N, Chen G. Engineering multi-layered skeletal muscle tissue by using 3D microgrooved collagen scaffolds. Biomaterials. 2015;73:23–31.

123. Palma E, Inghilleri M, Conti L, Deflorio C, Frasca V, Manteca A, et al. Physiological characterization of human muscle acetylcholine receptors from ALS patients. Proc Natl Acad Sci. 2011;108(50):20184–8.

124. Kalman B, Monge C, Bigot A, Mouly V, Picart C, Boudou T. Engineering human 3D micromuscles with co-culture of fibroblasts and myoblasts. Comput Methods Biomech Biomed Engin. 2015;18(sup1):1960–1.

125. Hinds S, Bian W, Dennis RG, Bursac N. The role of extracellular matrix composition in structure and function of bioengineered skeletal muscle. Biomaterials.

2011;32(14):3575–83.

126. Roskelley C. A hierarchy of ECM-mediated signalling regulates tissue-specific gene expression. Curr Opin Cell Biol. 1995;7(5):736–47.

127. Watt FM, Jordan PW, O'Neill CH. Cell shape controls terminal differentiation of human epidermal keratinocytes. Proc Natl Acad Sci. 1988;85(15):5576–80.

128. Discher DE. Tissue Cells Feel and Respond to the Stiffness of Their Substrate. Science (80-). 2005;310(5751):1139–43.

129. Dove A. Screening for content—the evolution of high throughput. Nat Biotechnol. 2003;21(8):859–64.

130. Madden L, Juhas M, Kraus WE, Truskey GA, Bursac N. Bioengineered human myobundles mimic clinical responses of skeletal muscle to drugs. Elife. 2015;4.

131. Vandenburgh H, Shansky J, Benesch-Lee F, Barbata V, Reid J, Thorrez L, et al. Drug-screening platform based on the contractility of tissue-engineered muscle. Muscle Nerve. 2008;37(4):438–47.

132. Vandenburgh H, Shansky J, Benesch-Lee F, Skelly K, Spinazzola JM, Saponjian Y, et al. Automated drug screening with contractile muscle tissue engineered from dystrophic myoblasts. FASEB J. 2009;23(10):3325–34.

133. Newswire PR, York N, York N. Intramuscular Drug Delivery Market & Pipeline Insight. 2017;1–3.

134. Lydia O, Eva W, Francesco T, Martin H. Advancing agricultural greenhouse gas quantification. Environ Res Lett. 2013;8(1):11002.

135. Post MJ. Cultured beef: medical technology to produce food. J Sci Food Agric. 2014;94(6):1039–41.

136. Cezar CA, Mooney DJ. Biomaterial-based delivery for skeletal muscle repair. Adv Drug Deliv Rev. 2015;84:188–97.

137. Rahaman MN, Mao JJ. Stem cell-based composite tissue constructs for regenerative medicine. Biotechnol Bioeng. 2005;91(3):261–84.

138. Dutt V, Gupta S, Dabur R, Injeti E, Mittal A. Skeletal muscle atrophy: Potential therapeutic agents and their mechanisms of action. Pharmacol Res. 2015;99:86–100.

139. LeRoith D. Non-islet cell hypoglycemia. Ann Endocrinol (Paris). 2004;65(1):99–103.

140. Fan Y, Maley M, Beilharz M, Grounds M. Rapid death of injected myoblasts in myoblast transfer therapy. Muscle Nerve. 1996;19(7):853–60.

141. Vandenburgh H, Tatto M Del, Shansky J, Goldstein L, Russell K, Genes N, et al. Attenuation of Skeletal Muscle Wasting with Recombinant Human Growth Hormone Secreted from a Tissue-Engineered Bioartificial Muscle. Hum Gene Ther.

1998;9(17):2555–64.

142. VandenDriessche T. Lentiviral vectors containing the human immunodeficiency virus type-1 central polypurine tract can efficiently transduce nondividing hepatocytes and antigen-presenting cells in vivo. Blood. 2002;100(3):813–22.

143. Hadjizadeh A, Doillon CJ. Directional migration of endothelial cells towards angiogenesis using polymer fibres in a 3D co-culture system. J Tissue Eng Regen Med. 2010;4(7):524–31.

144. Rangarajan S, Madden L, Bursac N. Use of Flow, Electrical, and Mechanical Stimulation to Promote Engineering of Striated Muscles. Ann Biomed Eng. 2014;42(7):1391–405.

145. Spitters TWGM, Leijten JCH, Deus FD, Costa IBF, van Apeldoorn AA, van Blitterswijk CA, et al. A Dual Flow Bioreactor with Controlled Mechanical Stimulation for Cartilage Tissue Engineering. Tissue Eng Part C Methods. 2013;19(10):774–83.

146. Liaw NY, Zimmermann W-H. Mechanical stimulation in the engineering of heart muscle. Adv Drug Deliv Rev. 2016;96:156–60.

147. Vandenburgh HH. Motion into mass: how does tension stimulate muscle growth? Med Sci Sports Exerc. 1987;19(5 Suppl):S142-9.

148. Moon DG, Christ G, Stitzel JD, Atala A, Yoo JJ. Cyclic mechanical preconditioning improves engineered muscle contraction. Tissue Eng Part A. 2008;14(4):473–82.

149. Handschin C, Mortezavi A, Plock J, Eberli D. External physical and biochemical stimulation to enhance skeletal muscle bioengineering. Adv Drug Deliv Rev. 2015;82–83:168–75.

150. Hornberger TA, Armstrong DD, Koh TJ, Burkholder TJ, Esser KA. Intracellular signaling specificity in response to uniaxial vs. multiaxial stretch: implications for mechanotransduction. Am J Physiol Physiol. 2005;288(1):C185–94.

151. Van der Schaft DWJ, van Spreeuwel ACC, Van Assen HC, Baaijens FPT. Mechanoregulation of Vascularization in Aligned Tissue-Engineered Muscle: A Role for Vascular Endothelial Growth Factor. Tissue Eng Part A. 2011;17(21–22):2857–65.

152. McCaig CD, Rajnicek AM, Song B, Zhao M. Controlling Cell Behavior Electrically: Current Views and Future Potential. Physiol Rev. 2005;85(3):943–78.

153. Hamid S, Hayek R. Role of electrical stimulation for rehabilitation and regeneration after spinal cord injury: An overview. Eur Spine J. 2008;17(9):1256–69.

154. Graupe D. An overview of the state of the art of noninvasive FES for independent ambulation by thoracic level paraplegics. Neurol Res. 2002;24(5):431–42.

155. Ikeda K, Ito A, Sato M, Kawabe Y, Kamihira M. Improved contractile force generation of tissue-engineered skeletal muscle constructs by IGF-I and Bcl-2 gene transfer with electrical pulse stimulation. Regen Ther. 2016;3:38–44.

156. Langelaan MLP, Boonen KJM, Rosaria-Chak KY, van der Schaft DWJ, Post MJ, Baaijens FPT. Advanced maturation by electrical stimulation: Differences in response between C2C12 and primary muscle progenitor cells. J Tissue Eng Regen Med. 2011;5(7):529–39.

157. Neville CM, Schmidt M, Schmidt J. Response of myogenic determination factors to cessation and resumption of electrical activity in skeletal muscle: a possible role for myogenin in denervation supersensitivity. Cell Mol Neurobiol. 1992;12(6):511–27.

158. Yu F, Li R, Jen N, Chi N, Lien C-L, Hsiai T. Canonical Wnt/β-catenin Signaling Pathway mediates Shear Stress-Activated Angiopoeitin-2 expression and vasculogenesis. FASEB J. 2013;27(1 Supplement):526.6-526.6.

159. Obi S, Masuda H, Shizuno T, Sato A, Yamamoto K, Ando J, et al. Fluid shear stress induces differentiation of circulating phenotype endothelial progenitor cells. Am J Physiol Physiol. 2012;303(6):C595–606.

160. Li R, Beebe T, Jen N, Yu F, Takabe W, Harrison M, et al. Shear Stress-Activated Wnt-Angiopoietin-2 Signaling Recapitulates Vascular Repair in Zebrafish Embryos. Arterioscler Thromb Vasc Biol. 2014;34(10):2268–75.

161. Lucitti JL, Jones EA V., Huang C, Chen J, Fraser SE, Dickinson ME. Vascular remodeling of the mouse yolk sac requires hemodynamic force. Development. 2007;134(18):3317–26.

162. Meeson A, Palmer M, Calfon M, Lang R. A relationship between apoptosis and flow during programmed capillary regression is revealed by vital analysis. Development. 1996;122(12):3929–38.

163. Kochhan E, Lenard A, Ellertsdottir E, Herwig L, Affolter M, Belting H-G, et al. Blood Flow Changes Coincide with Cellular Rearrangements during Blood Vessel Pruning in Zebrafish Embryos. Hogan B, editor. PLoS One. 2013;8(10):e75060.

164. Ott M, Ballermann B. Shear stress-conditioned, endothelial cell-seeded vascular grafts: Improved cell adherence in response to in vitro shear stress. Surgery. 1995;117(3):334–9.

165. Inoguchi H, Tanaka T, Maehara Y, Matsuda T. The effect of gradually graded shear stress on the morphological integrity of a huvec-seeded compliant small-diameter vascular graft. Biomaterials. 2007;28(3):486–95.

166. Noria S, Cowan DB, Gotlieb AI, Langille BL. Transient and Steady-State Effects of Shear Stress on Endothelial Cell Adherens Junctions. Circ Res. 1999;85(6):504–14.

167. Cimetta E, Flaibani M, Mella M, Serena E, Boldrin L, De Coppi P, et al. Enhancement of Viability of Muscle Precursor Cells on 3D Scaffold in a Perfusion Bioreactor. Int J Artif Organs. 2007;30(5):415–28.

168. Gilles Carpentier research web site: computer image analysis [Internet]. [cited 2018 May 14]. Available from: http://image.bio.methods.free.fr/ImageJ/?lang=en

169. Thorrez L, Shansky J, Wang L, Fast L, Vandendriessche T, Chuah M, et al. Growth, differentiation, transplantation and survival of human skeletal myofibers on biodegradable scaffolds. Biomaterials. 2008;29(1):75–84.

170. Levenberg S, Rouwkema J, Macdonald M, Garfein ES, Kohane DS, Darland DC, et al. Engineering vascularized skeletal muscle tissue. Nat Biotechnol. 2005;23(7):879–84.

171. Lesman A, Habib M, Caspi O, Gepstein A, Arbel G, Levenberg S, et al. Transplantation of a Tissue-Engineered Human Vascularized Cardiac Muscle. Tissue Eng Part A. 2010;16(1):115–25.

172. Pedersen TO, Blois AL, Xing Z, Xue Y, Sun Y, Finne-Wistrand A, et al. Endothelial microvascular networks affect gene-expression profiles and osteogenic potential of tissue-engineered constructs. Stem Cell Res Ther. 2013;4(3):52.

173. Cook JL, Lewis AM. Immunological surveillance against DNA-virus-transformed cells: correlations between natural killer cell cytolytic competence and tumor susceptibility of athymic rodents. J Virol. 1987;61(7):2155–61.

174. Koike N, Fukumura D, Gralla O, Au P, Schechner JS, Jain RK. Creation of long-lasting blood vessels. Nature. 2004;428(6979):138–9.

175. Hellström M, Gerhardt H, Kalén M, Li X, Eriksson U, Wolburg H, et al. Lack of pericytes leads to endothelial hyperplasia and abnormal vascular morphogenesis. J Cell Biol. 2001;152(3):543–53.

176. Sampaolesi M, Blot S, D'Antona G, Granger N, Tonlorenzi R, Innocenzi A, et al. Mesoangioblast stem cells ameliorate muscle function in dystrophic dogs. Nature. 2006;444(7119):574–9.

177. Abou-Khalil R, Mounier R, Chazaud B. Regulation of myogenic stem cell behaviour by vessel cells: The "ménage à trois" of satellite cells, periendothelial cells and endothelial cells. Cell Cycle. 2010;9(5):892–6.

178. Kuraitis D, Berardinelli MG, Suuronen EJ, Musaro A. A necrotic stimulus is required to maximize matrix-mediated myogenesis in mice. Dis Model Mech. 2013;6(3):793–801.

179. Atrick CHWP. Three-Dimensional , Quantitative Analysis of Desmin and Smooth Muscle Alpha Actin Expression during Angiogenesis. Ann Biomed Eng. 2004;32(8):1100–7.

180. Urech L, Bittermann AG, Hubbell JA, Hall H. Mechanical properties, proteolytic degradability and biological modifications affect angiogenic process extension into native and modified fibrin matrices in vitro. Biomaterials. 2005;26(12):1369–79.

181. Jiang B, Waller TM, Larson JC, Appel AA, Brey EM. Fibrin-Loaded Porous Poly(Ethylene Glycol) Hydrogels as Scaffold Materials for Vascularized Tissue

Formation. Tissue Eng Part A. 2013;19(1–2):224–34.

182. Lorentz KM, Kontos S, Frey P, Hubbell JA. Engineered aprotinin for improved stability of fibrin biomaterials. Biomaterials. 2011;32(2):430–8.

183. Latroche C, Weiss-Gayet M, Muller L, Gitiaux C, Leblanc P, Liot S, et al. Coupling between Myogenesis and Angiogenesis during Skeletal Muscle Regeneration Is Stimulated by Restorative Macrophages. Stem Cell Reports. 2017;9(6):2018–33.

184. Cleaver O, Melton DA. Endothelial signaling during development. Nat Med. 2003;9(6):661–8.

185. Rhoads RP, Johnson RM, Rathbone CR, Liu X, Temm-Grove C, Sheehan SM, et al. Satellite cell-mediated angiogenesis in vitro coincides with a functional hypoxia-inducible factor pathway. Am J Physiol Physiol. 2009;296(6):C1321–8.

186. Baldwin J, Antille M, Bonda U, De-Juan-Pardo EM, Khosrotehrani K, Ivanovski S, et al. In vitro pre-vascularisation of tissue-engineered constructs A co-culture perspective. Vasc Cell. 2014;6(1):13.

187. Kunz-Schughart LA, Schroeder JA, Wondrak M, van Rey F, Lehle K, Hofstaedter F, et al. Potential of fibroblasts to regulate the formation of three-dimensional vessel-like structures from endothelial cells in vitro. Am J Physiol Physiol. 2006;290(5):C1385–98.

188. Cittadella Vigodarzere G, Mantero S. Skeletal muscle tissue engineering: strategies for volumetric constructs. Front Physiol. 2014;5(September):362.

189. Vandenburgh HH. Functional Assessment and Tissue Design of Skeletal Muscle. Ann N Y Acad Sci. 2002;961(1):201–2.

190. Riboldi SA, Sampaolesi M, Neuenschwander P, Cossu G, Mantero S. Electrospun degradable polyesterurethane membranes: potential scaffolds for skeletal muscle tissue engineering. Biomaterials. 2005;26(22):4606–15.

191. Huang NF, Patel S, Thakar RG, Wu J, Hsiao BS, Chu B, et al. Myotube Assembly on Nanofibrous and Micropatterned Polymers. Nano Lett. 2006;6(3):537–42.

192. Agrawal CM, Ray RB. Biodegradable polymeric scaffolds for musculoskeletal tissue engineering. J Biomed Mater Res. 2001;55(2):141–50.

193. Gunatillake P. Biodegradable synthetic polymers for tissue engineering. Eur Cells Mater. 2003;5:1–16.

194. Hympanova L, Mori da Cunha MGMC, Rynkevic R, Zündel M, Gallego MR, Vange J, et al. Physiologic musculofascial compliance following reinforcement with electrospun polycaprolactone-ureidopyrimidinone mesh in a rat model. J Mech Behav Biomed Mater. 2017;74(March):349–57.

195. Chen Q-Z, Ishii H, Thouas GA, Lyon AR, Wright JS, Blaker JJ, et al. An elastomeric patch derived from poly(glycerol sebacate) for delivery of embryonic stem cells to the

heart. Biomaterials. 2010;31(14):3885–93.

196. Engelmayr GC, Cheng M, Bettinger CJ, Borenstein JT, Langer R, Freed LE. Accordion-like honeycombs for tissue engineering of cardiac anisotropy. Nat Mater. 2008;7(12):1003–10.

197. Gallik Stephen. Microscopic Study of Skeketal Muscle [Internet]. [cited 2018 May 12]. Available from: http://histologyolm.stevegallik.org/node/145

198. Cervelli M, Leonetti A, Duranti G, Sabatini S, Ceci R, Mariottini P. Skeletal Muscle Pathophysiology: The Emerging Role of Spermine Oxidase and Spermidine. Med Sci. 2018;6(1):14.

13 APPENDIX I: [SUPPLEMENTARY FIGURES]

13.1 S1: RAT INTRAVITAL IMAGE 14 DAYS POST IMPLANTATION OF 1-WEEK OLD CO-CULTURE BAM

Supplementary figure S2. Intravital image of wistar rat with co-culture BAM implanted onto the abdominal muscle for a period of 2 weeks. Image was taken 14 days post implantation, prior to explantation. Scattered remnants of GFP-labelled HUVEC-derived endothelial networks were observed suggesting a high degradative state.

13.2 S2: CONFOCAL IMAGE OF SURROUNDING HOST MUSCLE TISSUE OF ADULT WISTAR RAT 14 DAYS POST IMPLANATION OF 1-WEEK OLD CO-CULTURE BAM

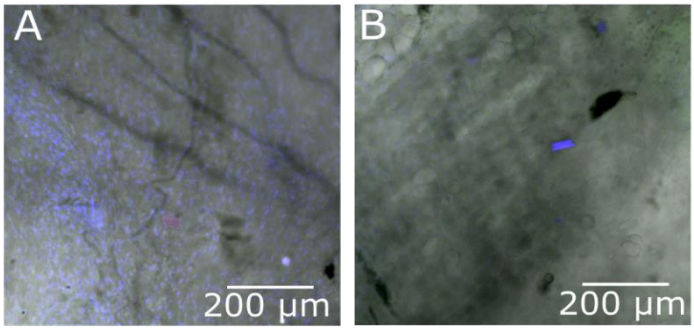

Supplementary figure S2. *Confocal image of surrounding host muscle tissue explanted based on suture positions 14 days post implantation of co-culture BAM containing 30 % HUVECs on (A) tibialis muscle of Wistar rats or (B) abdominal muscle of Wistar rats. No indication for remaining GFP-labelled endothelial networks or human myofibers.*

13.3 S3: MACROSCOPIC AND MICROSCOPIC IMAGE OF ELASTOMERIC SCAFFOLD

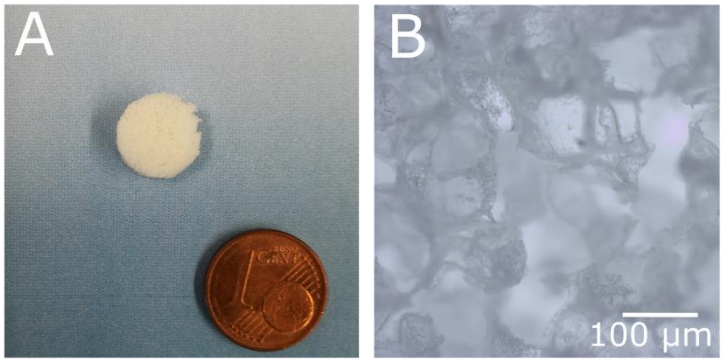

***Supplementary figure S3**. Macroscopic and microscopic image of PGS 1:1. (A) Macroscopic image showing PGS 1:1 with average dimensions of 1 cm^3. (B) Light microscopic image of porous structure of PGS 1:1 obtained through salt leaching techniques. Prepolymer was mixed with natriumchloride in a 1:7 weight ratio.*

13.4 S4: PRE-TREATMENT WITH 70 % ETHANOL OF ELASTOMERIC SCAFFOLD TO REDUCE HYDROPHOBICITY PRIOR TO CELL SEEDING

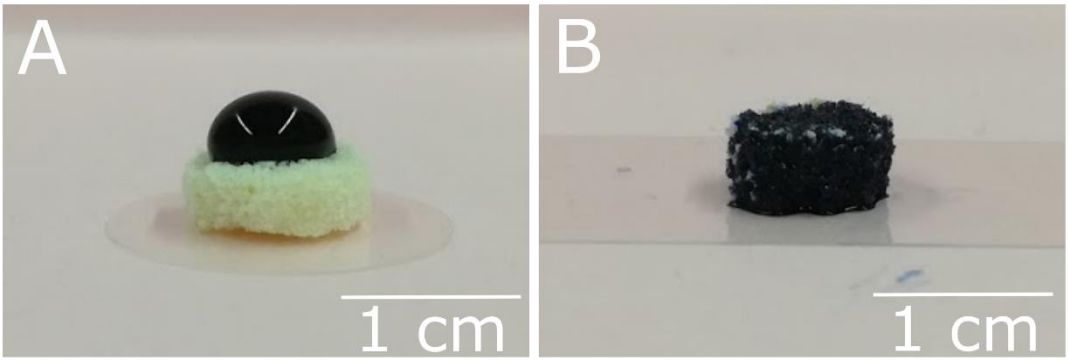

***Supplementary figure S4**. Macroscopic image of poly(xylitol sebacate citrate) 1:1 before and after pre-treatment with 70 % ethanol for 30 minutes. (A) Macroscopic image showing PXSC 1:1 prior to pre-treatment illustrating its hydrophobicity. (B) Macroscopic image of PXSC 1:1 after pre-treatment with 70 % ethanol for 30 minutes demonstration proper penetration of the trypan blue dye.*

13.5 S5: MACROSCOPIC AND MICROSCOPIC IMAGE OF POLYCARBONATE SCAFFOLD WITH DIFFERENT TOPOGRAPHICAL FEATURES AT BOTH SIDES

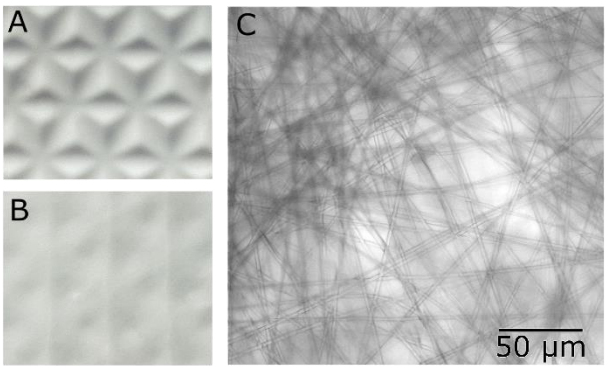

Supplementary figure S5. *Macroscopic and microscopic image of polycarbonate scaffold. (A-B) Different topographical features at both sides, macroscopic image. (C) Microscopic image of polycarbonate fiber network.*

13.6 S6: CELL-ECM ON POLYCARBONATE SCAFFOLD 2 DAYS AFTER SEEDING

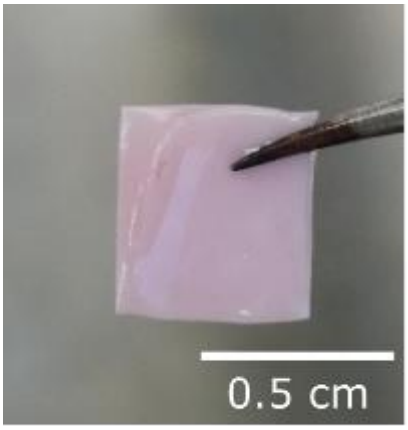

Supplementary figure S6. *Formation of approximate 50 µm thick cell-ECM layer 2 days after adding cell-ECM suspension on top of the polycarbonate scaffold positioned in a silicon coated 6-well plate.*